

FRIEDRICH-SCHILLER-UNIVERSITÄT JENA
PHYSIKALISCH-ASTRONOMISCHE FAKULTÄT



seit 1558

On the Effects of Variable Leg-Spring Properties during Hopping

DISSERTATION

zur Erlangung des Akademischen Grades
Doctor Rerum Naturalium (Dr. rer. nat.)

vorgelegt dem Rat der Physikalisch-Astronomischen Fakultät
der Friedrich-Schiller-Universität Jena

von Dipl.-Phys. SEBASTIAN RIESE,
geboren am 10.06.1982 in Stralsund

1. Gutachter: Prof. Dr. B. Brüggemann
2. Gutachter: Prof. Dr. R. Blickhan
3. Gutachter: Prof. Dr. P. van der Smagt
4. Gutachter: Prof. Dr. M. Rettenmayr
5. Gutachter: Prof. Dr. A. Seyfarth

Tag der Disputation: 2. Juli 2013

Contents

Zusammenfassung	1
Abstract	3
1. Introduction	5
1.1. The Spring-Loaded Inverted Pendulum	5
1.2. Natural Variability	7
1.3. Contributions of the Thesis	9
2. The Variable-Leg-Spring Concept	12
2.1. Theoretical Considerations	12
2.1.1. Equation of Motion	12
2.1.2. Landing-Takeoff Asymmetry	16
2.1.3. Periodicity	17
2.1.4. Stability	17
2.1.5. Robustness	21
2.1.6. Energy Efficiency	22
2.2. Simulation Protocol	24
2.3. Effects on Hopping	25
2.3.1. Periodic Solutions	25
2.3.2. Landing-Takeoff Asymmetry	29
2.3.3. Leg Softening and Stretching Ensure Stable Hopping	31
2.3.4. Additional Damping Is Beneficial for Stable Hopping	32
2.3.5. Trading Stability for Robustness	38
2.3.6. Trading Stability for Efficiency	39
2.4. Application for Robotics	39
3. The Variable-Leg-Spring Model with Velocity-Dependent Stiffness	45
3.1. Modification of the VLS Model	45
3.1.1. Velocity-Dependent Stiffness	45
3.1.2. Landing-Takeoff Asymmetry	47
3.1.3. Energy Efficiency	47
3.1.4. A Template Muscle-Model	48
3.2. Effects on Hopping	52
3.2.1. Basic Stability Properties are Inherited	52

3.2.2.	Flight Control is Beneficial for Stable Hopping	55
3.2.3.	Muscle-like Properties are Beneficial for Stable Hopping	57
3.2.4.	Comparison with a Template Muscle-Model	62
4.	Variable Leg-Spring Properties in Human Hopping	66
4.1.	Extraction of Leg-Spring Properties from the Data	66
4.1.1.	Experimental Setup	66
4.1.2.	Kinematics and Kinetics	67
4.1.3.	Estimation of stiffness and rest length	67
4.2.	Results	69
4.2.1.	Measured data	69
4.2.2.	Estimation results	72
4.3.	Variable Leg-Spring Properties	74
4.4.	Non-linear Parameters vs. Linear Dynamics	76
4.5.	Frequency-dependent Control	78
5.	Conclusion and Outlook	80
5.1.	Conclusion	80
5.2.	Future Work	81
	Literature	84
	Danksagung	92
	Ehrenwörtliche Erklärung	93
	Lebenslauf	94

Zusammenfassung

Das Federmassemodell, auch spring-loaded inverted pendulum (SLIP), beschreibt die Schwerpunktsbewegung biologischer Laufsysteme. Dieses Modell bildet die Beine als lineare Federn mit konstanten Parametern ab. In biologischen Systemen können sich federartige Eigenschaften der Gliedmaßen jedoch zeitlich ändern. Daher wurde in der vorliegenden Arbeit untersucht, inwieweit Variationen der Federparameter während des Bodenkontaktes die Dynamik des Federmassemodells beeinflussen.

Bei anfänglicher Vernachlässigung zusätzlicher Dämpfung konnte stabiles Hüpfen nur für Steifigkeitsabsenkung bei gleichzeitiger Ruhelängenerhöhung im Kontakt generiert werden. Mit zusätzlicher Dämpfung konnte stabiles Hüpfen für einen größeren Bereich von Steifigkeits- und Ruhelängenvariationen erzeugt werden. Dabei konnten nun auch Steifigkeitserhöhungen oder Ruhelängenabsenkungen stabiles Hüpfen ermöglichen. Innerhalb des vorgeschlagenen Kontrollraumes für stabiles Hüpfen besteht keine Notwendigkeit für präzise Parametereinstellungen.

Weiterhin wurde die Robustheit der stabilen Hüpflösungen untersucht. Dazu wurde das Einzugsgebiet der stabilen Fixpunkte bestimmt. Die Ergebnisse zeigen einen Kompromiss zwischen maximaler Stabilität und maximaler Robustheit. Zusätzliche Dämpfung erhöhte die Robustheit nur geringfügig. Dafür vergrößerte sich das Gebiet des jeweiligen Robustheitsgrades.

Als drittes Kriterium für erfolgreiche Bewegung wurde neben Stabilität und Robustheit die Energieeffizienz betrachtet. Dazu wurden eine auf der im System verrichteten mechanischen Arbeit basierende Kostenfunktion, sowie das Verhältnis von

elastischer und Gesamtarbeit berechnet. Bei zusätzlicher Dämpfung vergrößerten sich die Gebiete für robustes Hüpfen. Gleichzeitig erhöhte sich das Maximum der Bewegungskosten nur geringfügig. Allerdings sank dabei das Verhältnis von elastischer und Gesamtarbeit dramatisch, d.h. es wurde weniger Arbeit passiv von der Feder geleistet, wodurch das Hüpfen weniger effizient wurde.

Im Nachfolgenden wurde das Modell modifiziert, indem die Anpassung der Beinsteifigkeit in Abhängigkeit der Geschwindigkeit erfolgte. Die Einbeziehung solcher muskelartigen Eigenschaften erhöhte die Stabilität in hohem Maße. Auch bezüglich der Robustheit war dieser Modellansatz von Vorteil. Anders als im Modell mit zeitabhängiger Beinsteifigkeit waren nun Hüpfösungen mit maximaler Robustheit schon bei niedrigen bis mittleren Bewegungskosten möglich. Außerdem existieren für das modifizierte Modell Lösungen mit optimaler Stabilität und Robustheit. Durch Einbeziehung von Steifigkeitsanpassungen in der Flugphase wurde der Kontrollraum erheblich erweitert.

Schließlich wurde untersucht, wieviel Variation der Beinfederparameter beim Hüpfen auf der Stelle auftritt. Dazu wurden, ausgehend von gemessenen Bodenreaktionkräften und Schwerpunktsbewegungen, die Ruhelängen- und Steifigkeitsprofile abgeschätzt. Die Versuche beinhalteten fünf Hüpfrequenzen im Bereich von 1,2 bis 3,6 Hz. Die Ergebnisse zeigen, dass obwohl Beinsteifigkeit und Ruhelänge während des Bodenkontaktes nicht konstant sind, für die meisten Frequenzen die Schwerpunktsdynamik in guter Näherung der des linearen Federmassemodells ähnelt. Die Ruhelängen- und Steifigkeitsprofile für langsames und schnelles Hüpfen weichen deutlich voneinander ab. Außerdem existieren für 1,2 Hz zwei unterschiedliche Kontrollstrategien, die jeweils von einer Hälfte der Probanden angewendet wurden.

Da Hüpfen eine spezielle Form des Rennens im Sinne von Rennen mit verschwindender horizontaler Komponente ist, können diese Erkenntnisse helfen, leistungs- und anpassungsfähigere Laufsysteme und Beinprothesen durch Ausnutzung der zugrundeliegenden Systemmechanik zu entwickeln.

Abstract

The spring-loaded inverted pendulum (SLIP) describes the planar center-of-mass dynamics of legged locomotion. This model features linear springs with constant parameters as legs. In biological systems however, spring-like properties of limbs can change over time. Therefore, in this thesis it is asked how variation of spring parameters during ground contact would affect the dynamics of the spring-mass model.

Neglecting damping initially, it is found that decreasing leg stiffness and increasing rest length of the leg during stance phase are required for orbitally stable hopping. With damping, stable hopping is found for a larger region of rest-length rates and leg-stiffness rates. Here also increasing leg stiffness and decreasing rest length can result in stable hopping. Within the predicted range of leg parameter variations for stable hopping there is no need for precise parameter tuning.

Furthermore, robustness of the stable hopping solutions is addressed. For this, the basin of attraction of the stable fixed points is determined. Results show a trade-off between maximum stability and maximum robustness. Additional velocity-dependent damping only slightly increases robustness. However, the areas of a given robustness level are enlarged.

As a third criterion for successful motion energy efficiency is investigated. To do so, the work-based cost of movement as well as the work ratio between elastic and total work are estimated. Similarly to robustness, the areas of a given maximum cost of movement grow for increasing additional damping. At the same time the

maximum cost of transport only slightly increases. However, the work ratio decreases drastically, i.e. less work is done passively by the spring and hopping becomes less efficient.

The model is also modified to include velocity-dependent leg stiffness. Incorporating this muscle-like property, considerably improves stability. Unlike in the model with time-dependent leg stiffness, the tradeoff between robustness and cost of movement is less pronounced. Hopping solutions with maximum robustness may be achieved at low to medium cost of movement. Furthermore, in the modified model there are sweet spots with optimal stability and robustness. If flight control is included, the accessible control space is spread substantially.

Finally, it was investigated how much variation of leg-spring parameters is present during vertical human hopping. In order to do so, rest-length and leg-stiffness profiles were estimated from ground-reaction forces and center-of-mass dynamics apprehended in human hopping experiments. Trials included five hopping frequencies ranging from 1.2 to 3.6 Hz. The results show that, even though leg stiffness and rest length vary during stance, for most frequencies the center-of-mass dynamics still resemble those of a linear spring-mass hopper. Rest-length and leg-stiffness profiles differ for slow and fast hopping. Furthermore, at 1.2 Hz two distinct control schemes were observed.

As hopping gaits form a subset of the running gait (with vanishing horizontal velocity), these results may help to improve leg design in robots and prostheses.

1. Introduction

1.1. The Spring-Loaded Inverted Pendulum

Judging by our everyday experience legged locomotion appears a rather simple task. We walk and run without thinking about it. However, if studied in more detail legged locomotion turns out to be somewhat contradictory. On the one hand, due to its complexity the full interaction of the skeletal system, muscles, tendons and nerves necessary to generate locomotion is not fully understood. On the other hand, global leg behavior is surprisingly spring-like (Alexander, 1984).

So far, it is unclear where the global spring-like behavior of the leg originates. Some studies, e.g. Brown and Loeb (1997), suggest that non-linear visco-elastic properties of the muscle-tendon complex, so-called “preflexes”, are the main contributor, especially during fast movements. Others, e.g. Bobbert and Casius (2011), argue that muscle activation determines global leg behavior. Also, combinations of reflexes and feed-forward patterns have been suggested (Cham et al., 2000).

In any case, the spring-like leg behavior motivated an elastic model of legged locomotion, the spring-loaded inverted pendulum or SLIP model (Blickhan, 1989; McMahon and Cheng, 1990; Geyer et al., 2006). In the SLIP model the body is represented by a point mass m and the legs are described by linear springs with stiffness k , rest length l_0 and angle of attack α_0 , see Figure 1.1. This approach is supported by the force-length function of the leg found experimentally, i.e. the relationship between ground-reaction force and momentary leg length (Farley, 1991;

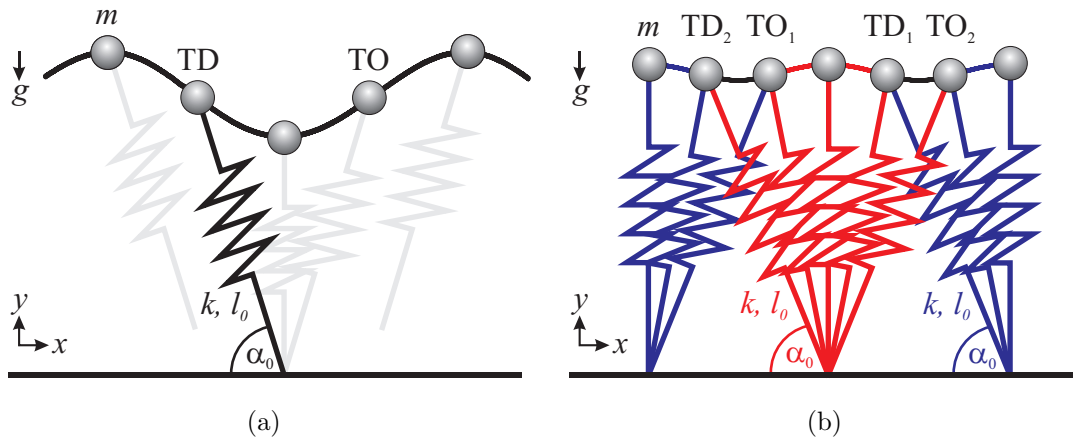


Figure 1.1.: SLIP model for (a) running and (b) walking. The model consists of a point mass m and attached massless leg springs (with rest length l_0 , stiffness k and angle of attack α_0). TD and TO denote touchdown and takeoff, respectively. For the bipedal SLIP model, center-of-mass trajectory during double support phases is color-coded black, while single support is represented by the color of the supporting leg.

Blickhan and Full, 1993). The SLIP model can be considered as a “template model” (Full and Koditschek, 1999) as it is a highly reduced model still presenting the key characteristics for the center-of-mass dynamics of human gaits.

Furthermore, the SLIP model describes fundamental parameter dependencies in legged locomotion, e.g. Seyfarth et al. (2002). An important criterion for locomotion is orbital stability, i.e. the notion, how fast small perturbations are compensated and periodic motion is re-established (Strogatz, 1994; Dingwell et al., 2007). As shown by Seyfarth et al. (2002), the SLIP model for running exhibits mechanical self-stability for an appropriate choice of initial velocity, leg stiffness and angle of attack. Small deviations from a periodic solution converge back to the periodic solution. The work of Daley (2009) and Rummel et al. (2010) complements the notion of orbital stability with the notion of robustness, i.e. which magnitude of perturbations may be compensated. For SLIP walking, a trade-off between stability and robustness was found (Rummel et al., 2010).

As the SLIP model represents a considerable reduction of complexity with respect to real legs, its predictions have to be put under careful scrutiny. For instance, the SLIP model is energy-conservative. Thus, it only exhibits neutral stability with respect to energy perturbations, i.e. if a perturbation is encountered the system transitions from the original periodic solution to a new periodic solution (Holmes et al., 2006; Maus et al., 2010). Biological systems however show the ability to compensate various energy losses or perturbations. Also, questions regarding energy efficiency and cost of transport (Srinivasa and Ruina, 2006) of biological and artificial legged systems may not be addressed with this model.

1.2. Natural Variability

Real legs deviate from the perfect spring. In fact, muscles clearly have visco-elastic properties. This visco-elasticity may explain the landing-takeoff asymmetry observed in running (Cavagna, 2006; Lipfert, 2010) and hopping (Farley, 1991; Kuitunen et al., 2011), that cannot be described by the conservative SLIP model with fixed leg parameters. In Cavagna and Legramandi (2009) it is hypothesized that due to the force-velocity function of muscles greater ground-reaction forces are generated during compression than during decompression. This may be interpreted as a change in leg stiffness or as a variable joint stiffness as found in human running (Guenther and Blickhan, 2002; Peter et al., 2009) and in simulation (Rapoport, 2003). The global force-length functions for human hopping and running also indicate that leg stiffness changes during ground contact (Farley, 1991; Lipfert, 2010). In addition, experimental data for hopping and running, e.g. Lipfert (2010) and Kuitunen et al. (2011), show that leg length, i.e. distance between center of mass and center of pressure, is larger at takeoff than at touchdown.

Leg compliance and its adaptation in response to changing environmental conditions are hypothesized to be crucial for successful locomotion, e.g. Grimmer et al.

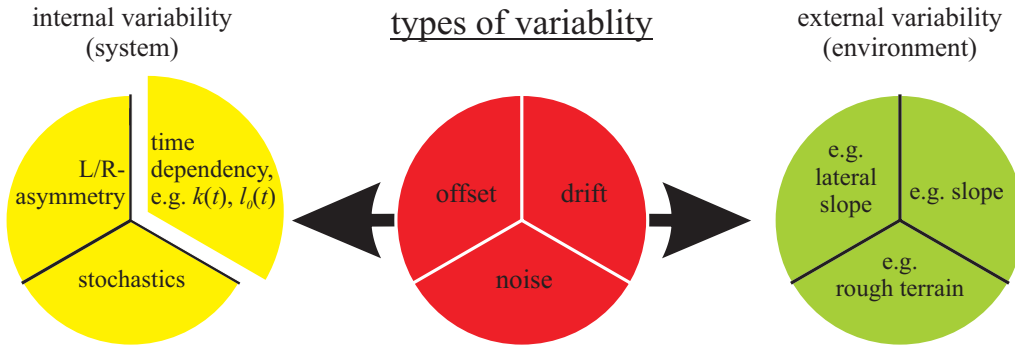


Figure 1.2.: Forms of variability. This thesis is focussed on time-varying parameters.

(2008). Thus, recent developments in robotics reflect the concept of variable compliance; for an excellent overview discussing different design strategies see Van Ham et al. (2009) or the introduction of Schuy et al. (2012). As tunable compliant actuators, in contrast to serial-elastic actuators (SEA), allow to change stiffness on-the-fly, i.e. at high speed, it was argued by Hurst et al. (2004) that this concept “could result in an effective actuation method for highly dynamic legged locomotion”.

Following this argument, it may be beneficial to consider the natural variability of human gait as a fundamental system property, rather than trying to develop more and more precise, yet complex systems and control schemes. In order to do so, biomechanical models may be modified to incorporate the parameter variations found experimentally, i.e. internal variability.

Internal variability encompasses recurring, in contrast to temporary or one-time, variations of system parameters, see Figure 1.2, which may be classified as

- offset, e.g. left-right asymmetry of the leg parameters (angle of attack $\alpha_1 \neq \alpha_2$, leg stiffness $k_1 \neq k_2$, rest length $l_1 \neq l_2$; Merker et al. 2011),
- drift, e.g. time variability of the leg parameters during ground contact (rest length $l_0(t)$, leg stiffness $k(t)$ or $k(v)$; **the focus of this thesis**) or
- noise, e.g. stochastical step-to-step variations of the leg parameters.

1.3. Contributions of the Thesis

A common approach to improve explanatory and predictive power of the SLIP model is to increase its structural complexity, following the template-anchor concept of Full and Koditschek (1999), e.g. by adding a trunk (Maus et al., 2010) or a foot (Maykranz et al., 2009). Additional structures, however, complicate analysis and therefore, fundamental insights might be overlooked. In the present thesis the SLIP remains structurally unchanged, but leg parameters (rest length, leg stiffness) are assumed to be variable during ground contact, see Chapter 2.

There are already studies considering spring-mass models with either variable rest-length (Cham and Cutkosky, 2003; Schmitt and Clark, 2009) or variable stiffness (Koditschek and Buehler, 1991; Komsuoglu, 2004; Kalveram et al., 2010) during contact, but so far there was no systematic investigation addressing the interaction of the two. Most importantly, simultaneous variation of rest length and leg stiffness during contact presents a simple approach to manipulate spring energy and thus system energy during contact, while maintaining periodic solutions. Positive parameter rates correspond to energy input, i.e. actuation, negative ones to energy withdrawal, i.e. (functional) damping. Thus, for appropriate choices of parameter rates (and initial conditions) system energy at touchdown and takeoff will be the same. Hence, the motion will be periodic, even though the system is non-conservative during stance. For that reason, changing rest length and leg stiffness simultaneously during contact allows to model visco-elastic muscle properties without the need to introduce additional damping. In the following, this approach is also referred to as the variable-leg-spring (VLS) concept.

In order to simplify analysis as much as possible, the system is reduced to vertical hopping, which can be considered as running without horizontal velocity. The leg operation is reduced to changes in leg shortening and extension. Hence, no rotational movements like swinging the leg forth and back are taken into account.

Within this approach it is hypothesized that the landing-takeoff asymmetry observed in bouncing gaits can be understood as a requirement for stable hopping. For this, appropriate leg parameter variations during ground contact resulting in orbitally stable hopping cycles are investigated. Additional damping is expected to be beneficial, but contrary to the findings of Komsuoglu (2004) not necessary for stable hopping. Such supportive leg adjustments could provide the basis for more functional locomotory systems operating at a variety of speeds and gaits.

Following Daley (2009) and Rummel et al. (2010), the work presented here combines the notion of orbital stability with the concept of robustness. Similarly to the results for walking (Rummel et al., 2010), a trade-off between stability and robustness is expected for hopping. Additional damping is expected to further increase robustness, as damping increases the tolerance for perturbations in apex height and thus, the size of the basin of attraction. Moreover, damping is expected to enlarge the area of a given level of robustness.

To further compare functional damping via leg softening on the one hand and additional velocity-dependent damping on the other, energy efficiency for increasing damping coefficient is investigated. In order to do so, a work-based cost of movement inspired by Srinivasa and Ruina (2006) and Rummel et al. (2010) as well as the ratio between elastic and total work are calculated. As additional damping increases the non-elastic properties of the hopper for a given parameter setup, less efficient hopping for increasing damping is expected.

Non-linearities in the variation of leg parameters will most likely be beneficial. Schmitt and Clark (2009) were able to show that a sinusoidal rest-length variation along with an appropriate leg-placement protocol results in stable and robust running. Following a recent study regarding the force-velocity function of muscles during hopping (Haeufle et al., 2010), a velocity-dependent stiffness protocol may also be considered as an appropriate approach. In Haeufle et al. (2010) the time-dependency of leg properties during ground contact was not explicitly prescribed but

an outcome of the muscle dynamics. Therefore, in Chapter 3 leg-stiffness variation is considered to be velocity-dependent, i.e. reactive. Incorporating this muscle-like property to the VLS model is assumed to further increase stability.

Two hopping models are investigated. In the first model, leg stiffness is allowed to vary only during ground contact and held constant otherwise. However, for running the domain of stable solutions can be enlarged by introducing swing leg control (Blum et al., 2010). In this control scheme, variation of leg parameters prior to touchdown compensates perturbations of ground level and thus, allows to access previously unstable periodic solutions and even further stabilize already stable solutions. Thus, the second model incorporates a modified swing-leg control, as it is assumed to further improve hopping stability.

By adapting the VLS concept to experimental data, it is the aim of Chapter 4 to investigate the behavior of leg stiffness and rest length in vertical human hopping. It is assumed that the spring-like leg function in human hopping results from the interaction of non-linear leg properties: Leg stiffness and rest length may be non-constant, nevertheless generating a linear force-length function on leg level. Furthermore, hopping below the preferred frequency is assumed to exhibit different rest-length and leg-stiffness profiles than hopping with frequencies above the preferred one, as suggested by Farley (1991).

2. The Variable-Leg-Spring Concept

The following chapter is based on Riese and Seyfarth (2012a,b). The analyses and results in this chapter are the contribution of the author of this thesis. Discussions with A. Seyfarth, S. Grimmer and F. Peuker were appreciated.

2.1. Theoretical Considerations

2.1.1. Equation of Motion

The spring-mass model consists of a point mass m on top of a massless spring with rest length l_0 and stiffness k (Blickhan, 1989; McMahon and Cheng, 1990), see Figure 2.1. The spring contributes to the system dynamics only during ground contact, in the one-dimensional case for center-of-mass position $y \leq l_0$. Additional to the original model, velocity-dependent damping is included during stance. Thus, during flight phase the model is subjected solely to gravitational force. With gravity opposing the spring force during contact phase, the equation of motion is

$$m\ddot{y} = \begin{cases} -mg, & y > l_0, \\ k(l_0 - y) - \delta\dot{y} - mg, & y \leq l_0, \end{cases} \quad (2.1)$$

where $\dot{\cdot} := d/dt$ denotes the time derivative.

As a first-order approximation for variable leg-spring parameters, rest length and leg stiffness are allowed to change linearly with time t between touchdown (TD) and

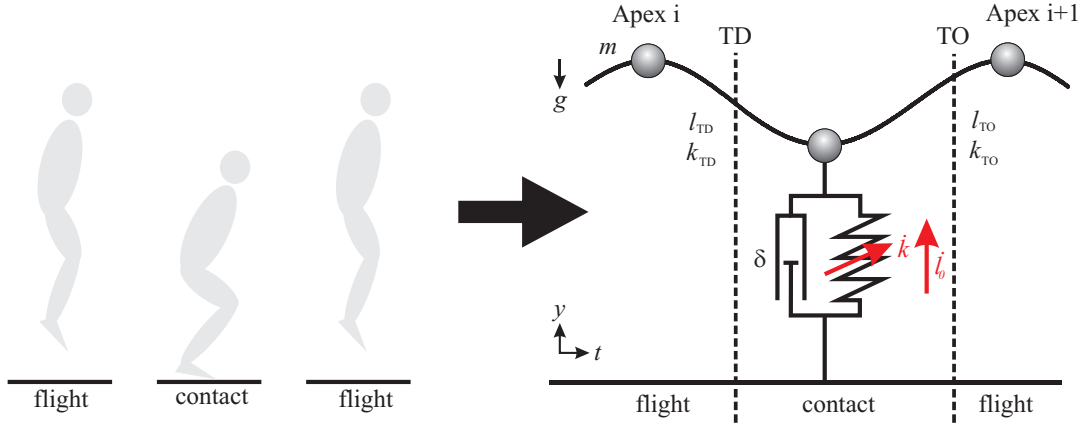


Figure 2.1.: Variable-leg-spring (VLS) hopper. The model consists of a point mass with an attached massless leg and a parallel damper. Leg-spring parameters, rest length l_0 and leg stiffness k , change linearly with time during contact phase, Equation 2.2, and are held constant during flight phases. Reset of spring parameters to their respective touchdown value, l_{TD} and k_{TD} , takes place at apex, i.e. the highest point of center-of-mass trajectory.

takeoff (TO),

$$l_0(t) = l_{TD} + \dot{l}_0(t - t_{TD}), \quad (2.2a)$$

$$k(t) = k_{TD} + \dot{k}(t - t_{TD}). \quad (2.2b)$$

During flight phases, rest length and leg stiffness are kept constant and are reset at each apex to l_{TD} and k_{TD} , respectively. The linear dependency in Equation 2.2 was chosen, because the ideal timing and shape of actuation is still under debate (see Chapter 1). This approach is a considerable simplification but will nevertheless describe the fundamental behavior of a spring-mass system with variable leg-spring parameters during stance.

In order to evaluate the system's capacity to cope with additional, continuous energy losses during contact and to better understand the effect of active energy removal via leg adaptation, viscous damping was included for part of the simulations.

Parameter	
gravitational acceleration	g
mass	m
rest length	l_{TD}
leg stiffness	k_{TD}
rest-length rate	\dot{l}_0
stiffness rate	\dot{k}
damping coefficient	δ

Table 2.1.: Parameters of the VLS model.

Impacts are neglected in this thesis. Incorporating a more realistic ground-contact model and leg masses would undoubtedly change the dynamics of the model. However, no or only small impacts are observed in human hopping, indicating a minor contribution to hopping dynamics (Farley, 1991; Kuitunen et al., 2011).

In total, the system is described by seven parameters, see Table 2.1. This number can be reduced to four dimensionless parameters using a uniquely defined normalization with respect to g , m and l_{TD} , see Table 2.2. Accordingly, dimensionless vertical position $Y = y/l_{\text{TD}}$ and dimensionless time $\tau = \sqrt{g/l_{\text{TD}}}(t - t_{\text{TD}})$ are introduced. The dimensionless equation of motion during stance now reads

$$Y'' = (K + K'\tau)(1 + L'_0\tau - Y) - DY' - 1, \quad (2.3)$$

where $'$ denotes the time derivative with respect to τ . If not mentioned otherwise, dimensionless quantities are used from now on.

Parameter	
(dimensionless) leg stiffness	$K = k_{\text{TD}} l_{\text{TD}} (m g)^{-1}$
(dimensionless) stiffness rate	$K' = \dot{k} (l_{\text{TD}}/g)^{3/2} m^{-1}$
(dimensionless) rest-length rate	$L'_0 = \dot{l}_0 (g l_{\text{TD}})^{-1/2}$
(dimensionless) damping coefficient	$D = \delta (l_{\text{TD}}/g)^{1/2} m^{-1}$

Table 2.2.: Normalized parameters of the VLS model.

By introducing the coordinate system co-moving with the instantaneous rest length,

$$X := Y - 1 - L'_0\tau, \quad (2.4)$$

and by omitting damping for the time being, the equation of motion during stance may be further simplified to

$$X'' = -(K + K'\tau)X - 1. \quad (2.5)$$

This choice also is of advantage because it holds that $X_{\text{TD}} = X_{\text{TO}} \equiv 0$, thus simplifying the conditions for the phase transitions between flight and stance.

The simplified equation of motion is a special case of the RICCATI differential equation, which is not generally solvable. However, the solution of Equation 2.5 could be computed directly, using MATHEMATICA (v7.0, Wolfram Research Inc., Champaign, IL, USA),

$$\begin{aligned} X(\tau) = & \frac{K + K'\tau}{K'} X'_{\text{TD}} {}_0F_1\left(\left;\frac{4}{3}; -\frac{(K + K'\tau)^3}{9K'^2}\right.\right) {}_0F_1\left(\left;\frac{2}{3}; -\frac{K^3}{9K'^2}\right.\right) \\ & - \frac{K}{K'} X'_{\text{TD}} {}_0F_1\left(\left;\frac{4}{3}; -\frac{K^3}{9K'^2}\right.\right) {}_0F_1\left(\left;\frac{2}{3}; -\frac{(K + K'\tau)^3}{9K'^2}\right.\right) \\ & - \frac{K + K'\tau}{K'^2} {}_0F_1\left(\left;\frac{4}{3}; -\frac{(K + K'\tau)^3}{9K'^2}\right.\right) \\ & \times \left[(K + K'\tau) {}_1F_2\left(\frac{1}{3}; \frac{2}{3}, \frac{4}{3}; -\frac{(K + K'\tau)^3}{9K'^2}\right) - K {}_1F_2\left(\frac{1}{3}; \frac{2}{3}, \frac{4}{3}; -\frac{K^3}{9K'^2}\right) \right] \\ & + \frac{1}{2K'^2} {}_0F_1\left(\left;\frac{2}{3}; -\frac{(K + K'\tau)^3}{9K'^2}\right.\right) \\ & \times \left[(K + K'\tau)^2 {}_1F_2\left(\frac{2}{3}; \frac{4}{3}, \frac{5}{3}; -\frac{(K + K'\tau)^3}{9K'^2}\right) - K^2 {}_1F_2\left(\frac{2}{3}; \frac{4}{3}, \frac{5}{3}; -\frac{K^3}{9K'^2}\right) \right], \end{aligned} \quad (2.6)$$

with

$${}_pF_q(a_1, \dots, a_p; b_1, \dots, b_q; z) := \sum_{i=1}^{\infty} \prod_{j=1}^p \frac{\Gamma(j + a_j)}{\Gamma(a_j)} \prod_{k=1}^q \frac{\Gamma(b_k)}{\Gamma(k + b_k)} \frac{z^i}{i!} \quad (2.7)$$

being the generalized hypergeometric function.

2.1.2. Landing-Takeoff Asymmetry

The variation in rest-length influences the asymmetry of touchdown and takeoff height, $Y_{\text{TO}} = Y_{\text{TD}} + L'_0 \tau_{\text{st}}$ with stance time τ_{st} , as well as the asymmetry of touchdown and takeoff velocity. However, the variation in rest length has no influence on the asymmetry of the ground-reaction force, because the variation is linear in time. In the coordinate system co-moving with the instantaneous rest length, Equation 2.4, only the leg-stiffness variation affects the ground-reaction force, see Equation 2.5. As $Y'' = X''$, this also holds in the resting coordinate system, the only difference being an offset between touchdown velocities, $X'_{\text{TD}} = Y'_{\text{TD}} - L'_0$.

Equation 2.5 allows to interpret the system as a sequence of spring-mass systems with instantaneous leg stiffness $K(\tau) = K + K'\tau$. Thus, according to Geyer et al. (2006), instantaneous stance time $\tau_{\text{st}}(\tau)$ is

$$\tau_{\text{st}}(\tau) = \frac{2}{\sqrt{K(\tau)}} \left[\pi + \arctan \left(\sqrt{K(\tau)} X'_{\text{TD}} \right) \right]. \quad (2.8)$$

As $X'_{\text{TD}} < 0$ is fixed, instantaneous stance time decreases for increasing leg stiffness and vice versa.

The result of this stiffness dependency becomes clear if one imagines a switch of leg stiffness at the instant of maximum leg compression. The compression phase with stiffness K_1 will last for $\tau_{\text{st},1}/2$, whereas the decompression phase with stiffness K_2 will last for $\tau_{\text{st},2}/2$. If stiffness decreases, $K_1 > K_2$, then according to Equation 2.8 decompression will take longer than compression, $\tau_{\text{st},1} < \tau_{\text{st},2}$. Therefore, the system

exhibits the expected landing-takeoff asymmetry. Maximum force will appear in the first half of total stance time, $\tau_{\text{st}} = (\tau_{\text{st},1} + \tau_{\text{st},2})/2$. Accordingly, for increasing stiffness maximum force will appear in the second half of total stance time.

This reasoning holds for any monotonic variation of leg stiffness during stance. If leg stiffness decreases, any displacement during compression will take less time than the corresponding displacement during decompression. Thus, for monotonically decreasing leg stiffness maximum force will appear in the first half of stance time.

2.1.3. Periodicity

Variations of rest length and leg stiffness during contact present a simple approach to manipulate spring energy, and thus system energy during contact, while maintaining periodic solutions. Positive parameter rates correspond to energy input, i.e. actuation, negative ones to energy withdrawal, i.e. (functional) damping, see Section 2.1.6. Hence, for appropriate choices of parameter rates (and initial conditions), system energy at touchdown and takeoff will be the same. Thus, the motion will be periodic, even though the system is non-conservative during stance.

As the differential equation is of second order, two initial conditions are required. Choosing instant of apex with $\dot{Y} \equiv 0$ as a POINCARÉ section, only one free initial condition, initial apex height Y_0 , remains. Thus, analysis reduces to a one-step POINCARÉ map of hopping height, with mapping function $Y_{0,i+1} = f(Y_{0,i})$. A periodic solution then is equivalent to a fixed point Y^* , with $Y^* = f(Y^*)$.

2.1.4. Stability

The slope of the POINCARÉ map at the fixed point, i.e. the eigenvalue λ of the JACOBIAN matrix of the periodic solution, is direct measure for orbital stability: If $|\lambda| = |dY_{0,i+1}/dY_{0,i}(Y^*)| < 1$ is satisfied, the solution is orbitally stable, i.e. slightly perturbed apex heights converge to the fixed point (Strogatz, 1994), see Figure 2.2.

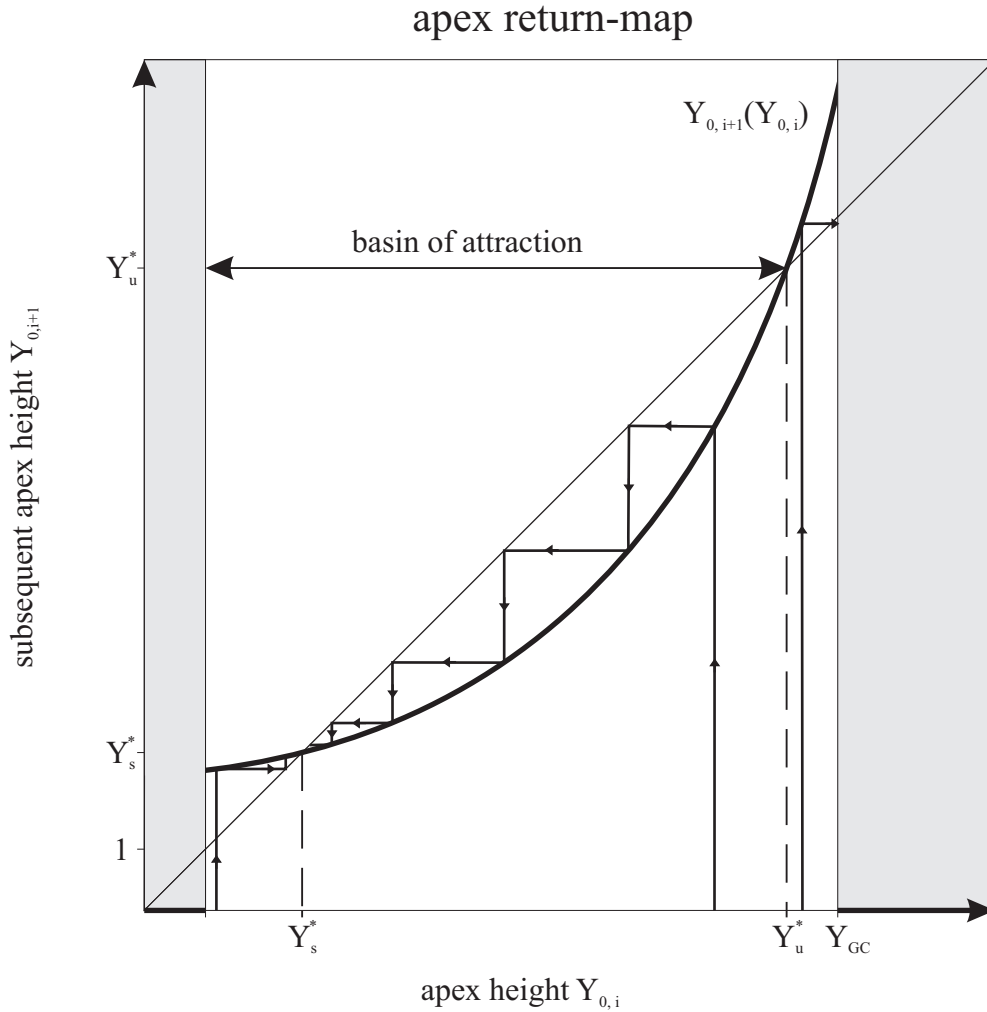


Figure 2.2.: Apex return map. Stable and unstable fixed points are shown, Y_s^* and Y_u^* respectively. Initial conditions with $1 < Y_{0,i} < Y_u^*$ converge towards Y_s^* . Within the areas shaded gray the point mass hits the ground, i.e. $Y_{0,i+1} \equiv 0$.

Subsequently, stability always refers to orbital stability as defined here.

The mapping function $Y_{0,i+1} = f(Y_{0,i})$ required to proof orbital stability is a composition of three maps, $f = f_3 \circ f_2 \circ f_1$. This is due to the phase transitions at touchdown and takeoff (sequence of flight phase, stance phase and again flight phase, see Figure 2.1).

The map f_1 describes the free fall until touchdown. As $Y'_{0,i} \equiv 0$ (choice of POINCARÉ section) and $Y_{\text{TD}} \equiv 1$ (normalization of Y), f_1 simply reads

$$Y'_{\text{TD}} = f_1(Y_{0,i}) = \sqrt{2(Y_{0,i} - 1)}. \quad (2.9)$$

Similarly, the map f_3 for the flight phase between takeoff and apex $i + 1$ is based on conservation of energy during flight phase,

$$Y_{0,i+1} = f_3(Y_{\text{TO}}, Y'_{\text{TO}}) = Y_{\text{TO}} + \frac{1}{2} Y'^2_{\text{TO}}. \quad (2.10)$$

The non-trivial part of constructing f is deriving the stance-phase map f_2 ,

$$f_2 : Y'_{\text{TD}} \mapsto (Y_{\text{TO}}, Y'_{\text{TO}}), \quad (2.11)$$

or in the co-moving coordinate system, with $X_{\text{TD}} = X_{\text{TO}} \equiv 0$,

$$\tilde{f}_2 : X'_{\text{TD}} \mapsto X'_{\text{TO}} \quad (2.12)$$

For this, the solution of the equation of motion, given by Equation 2.6, is required. However, the result is so complex that $X(\tau) = 0$ may only be solved for the trivial case $\tau = 0$. Thus, stance time τ_{st} , with $X(\tau_{\text{st}}) = 0$, cannot be derived. Therefore, X'_{TO} (or $Y_{\text{TO}} = 1 + L'_0 \tau_{\text{st}}$ and $Y'_{\text{TO}} = X'(\tau_{\text{st}}) + L'_0$) cannot be computed, i.e. the return map cannot be constructed analytically.

Nevertheless, to support the numerical findings in Section 2.3, a simplified problem may be investigated as proof of concept. In this simplified problem, leg stiffness and rest length are constant, but change instantaneously at the instant of maximum leg compression, Y_{min} . Then, the return map reads

$$Y_{0,i+1} = Y_{\text{min}} + \frac{1}{2}(K + \Delta K)(1 + \Delta L_0 - Y_{\text{min}})^2, \quad (2.13)$$

where Y_{\min} satisfies the conditions

$$Y'(Y_{\min}) = 0, \quad (2.14a)$$

$$0 < Y_{\min} < 1, \quad (2.14b)$$

$$Y_{0,i} = Y_{\min} + \frac{1}{2}K(1 - Y_{\min})^2. \quad (2.14c)$$

The last condition follows from the conservation of total energy, which during stance reads $E_{\text{tot}} = Y_0 = Y + \frac{1}{2}Y'^2 + \frac{1}{2}K(1 - Y)^2$. Furthermore, $K + \Delta K > 0$ and $1 + \Delta L_0 > Y_{\min}$ have to be satisfied. Otherwise, leg stiffness vanishes during stance or the new rest length would be smaller than Y_{\min} , respectively. Thus, in both cases the mass point would hit the ground.

An additional condition is imposed by the constraint of periodic hopping, $Y_{0,i+1} = Y_{0,i}$, which may also be written as

$$\frac{K}{(K + \Delta K)} = \frac{(1 + \Delta L_0 - Y_{\min})^2}{(1 - Y_{\min})^2}. \quad (2.15)$$

This condition can be used to fix ΔK . Then, the derivative of the return map at the fixed point Y^* reads

$$\lambda := \frac{dY_{0,i+1}}{dY_{0,i}}(Y^*) = \frac{z^2 + z - K\Delta L_0}{z^2 + z + zK\Delta L_0}, \quad (2.16)$$

where $z := \sqrt{1 + 2K(Y^* - 1)}$ was introduced for notational ease.

λ has a pole of order 1 for $\Delta L_0 = -(1 + z)/K$. Here, only small variations of rest length, $\Delta L_0 \ll 1$, are considered and λ simplifies to

$$\lambda = 1 - \Delta L_0 \frac{K}{z}. \quad (2.17)$$

Stable hopping requires $|\lambda| < 1$. With $K > 0$ and $z > 0$, this condition only is satisfied for $\Delta L_0 > 0$. According to Equation 2.15 this leads to $\Delta K < 0$. Thus,

stable hopping with an instantaneous change in rest length and leg stiffness at the instance of maximum leg compression requires an increase in rest length and a decrease of leg stiffness.

The dynamics described by this simplified model are likely to differ from the dynamics with linear-in-time leg-spring parameters. However, for ever decreasing intervals (in which the spring parameters are kept constant) and ever decreasing parameter changes, the models merge into each other. Thus, it is likely that the stability requirement (increasing rest length and decreasing leg stiffness) is preserved and also valid for linear-in-time variations of the leg-spring parameters.

2.1.5. Robustness

Robustness is defined here as the largest step the model could either take up or down while maintaining the hopping movement. Within the basin of attraction initial conditions will converge towards a periodic solution, see Figure 2.2. Thus, robustness ΔY is the minimum distance from the fixed point to the boundaries of the effective basin of attraction, Y_{\min} and Y_{\max} respectively,

$$\Delta Y = \min(Y_{\max} - Y^*, Y^* - Y_{\min}). \quad (2.18)$$

In principle, the basin of attraction is confined between the touchdown condition, $Y_0 > 1$, and the unstable fixed point. For initial apex heights $Y_0 \leq 1$ the leg will not be initialized and the mass point follows a free-fall trajectory until ground contact, whereas beyond the unstable fixed point Y_u^* all initial conditions diverge.

However, two effects may cause the hopper to fall down, i.e. the point mass to hit the ground, before encountering the theoretical boundaries of the basin of attraction. Damping, whether functional or velocity-dependent, may prevent take-off for sufficiently small initial apex heights and a given choice of L'_0 , as the energy withdrawal may be not compensable with this actuation. For sufficiently large initial

apex heights the model may hit the upper falling-down barrier Y_{GC} . Beyond Y_{GC} the spring cannot store sufficient initial energy and thus, properly support the point mass, resulting in total leg compression and ground contact (GC) of the point mass.

For a linear spring with fixed parameters the maximum apex height is easily calculated. The system is energy-conservative, so system energy satisfies

$$E = Y_0 = Y + \frac{1}{2}Y'^2 + \frac{1}{2}K(1 - Y)^2. \quad (2.19)$$

For the minimum apex height resulting in falling down, Y_{GC} , ground contact $Y = 0$ is reached with zero velocity, $Y' = 0$. Thus, for successful hopping with a constant linear spring initial values have to satisfy

$$Y_0 < Y_{GC} = \frac{1}{2}K. \quad (2.20)$$

As the decreasing effect of leg softening exceeds the increasing effect of leg lengthening regarding the spring's capacity to store energy, variable-leg-spring hoppers with rest length and leg stiffness rates lying in the region of stable hopping also observe this limit.

The limit for the maximum apex height may also be calculated for a constant linear spring with additional velocity-dependent damping. However, as the calculation is lengthy, the starting interval for the bisection procedure to identify the maximum apex height was simply chosen as $[Y_s^*; K]$, see Section 2.2. Here, all simulations resulted in maximum apex heights well below $Y_0 = K$.

2.1.6. Energy Efficiency

Two notions of energy efficiency are used in this thesis: (a) the work-based cost of movement, C_{Y_0} , and (b) the ratio of elastic and total work, η . The first notion describes hopping performance with respect to hopping height, whereas the second

notion is a measure for the relation between elastic and non-elastic properties of the hopper.

The calculation of the work done by spring and damper is straight-forward using Equation 2.3. To determine the total mechanical work performed by the system due to variable leg-spring parameters, the time derivative of system energy

$$E(\tau) = Y + \frac{1}{2}Y'^2 + \frac{1}{2}(K + K'\tau)(1 + L'_0\tau - Y)^2. \quad (2.21)$$

is required. Using Equation 2.3 for simplification the time derivative yields

$$E' = \frac{1}{2}(1 + L'_0\tau - Y)^2 K' + (K + K'\tau)(1 + L'_0\tau - Y) L'_0. \quad (2.22)$$

Thus, positive and negative contributions to the work due to variable leg-spring parameters are solely determined by the signs of the parameter rates, L'_0 and K' , as during ground contact the conditions $K > K'\tau$ and $Y \leq 1 + L'_0\tau$ have to be satisfied.

Following Srinivasa and Ruina (2006); Rummel et al. (2010), but simplifying the notation used therein, the work-based cost of movement is defined as

$$C_{Y_0} := \frac{1}{Y_0} \int_0^{\tau_s} (|P_{\text{spring}}| + |P_{\text{damp}}| + |P_{L'_0}| + |P_{K'}|) d\tau, \quad (2.23)$$

where because of Equations 2.3 and 2.22 the individual contributions are given by

$$P_{\text{spring}} = (K_{\text{TD}} + K'\tau)(1 + L'_0\tau - Y) Y', \quad (2.24a)$$

$$P_{\text{damp}} = -DY'^2 \quad (2.24b)$$

$$P_{L'_0} = (K_{\text{TD}} + K'\tau)(1 + L'_0\tau - Y) L'_0, \quad (2.24c)$$

$$P_{K'} = \frac{1}{2}(1 + L'_0\tau - Y)^2 K'. \quad (2.24d)$$

Similarly, the work ratio of elastic and total work is defined as

$$\eta := \frac{W_{\text{spring}}}{W_{\text{total}}} = \frac{\int_0^{\tau_s} |P_{\text{spring}}| \, d\tau}{\int_0^{\tau_s} (|P_{\text{spring}}| + |P_{L'_0}| + |P_{K'}| + |P_{\text{damp}}|) \, d\tau}. \quad (2.25)$$

2.2. Simulation Protocol

As the analytical result is too complex to be of actual use, numerical integration of the VLS hopper is done numerically in MATLAB (R2010a, The MathWorks Inc., Natick, MA, USA). Because of the tenfold smaller runtime, the built-in SIMULINK toolbox is employed rather than integrating the equation of motion directly in MATLAB, see Figure 2.3. As the implemented RUNGE-KUTTA variable-step integrator (ode45) is used, Equation 2.3, which is of second order, is decomposed into two equations of first order. A maximum time-step size of 10^{-2} and relative and absolute tolerance $\leq 10^{-12}$ were chosen. Results were checked with a tenfold smaller tolerance.

Finding a periodic solution is equivalent to finding the zero crossing of the function $g(Y_{0,i}) = Y_{0,i} - f_{\text{num}}(Y_{0,i})$, where $f_{\text{num}}(Y_{0,i})$ is the numerically integrated result for $Y_{0,i+1}$. To identify periodic solutions, a NEWTON-RAPHSON algorithm is utilized. A solution is said to be periodic, if $|g(Y_{0,i})|$, i.e. the difference between consecutive apex heights, does not exceed 10^{-9} .

To determine the effective boundaries of the basin of attraction, a bisection method with the initial interval $[1; Y^*]$, and $[Y^*; K]$ respectively, is used. For the motivation of the latter see Section 2.1.5. The bisections terminate for an interval size below 10^{-9} .

In order to avoid solutions with negative leg stiffness or rest length, termination conditions for vanishing K and L_0 are implemented. The simulation also terminates at ground contact of the point mass.

Simulations are done for leg stiffness $K_{\text{TD}} = 25$ ($k \approx 19.6 \text{ kN m}^{-1}$ for human dimensions, $m = 80 \text{ kg}$ and $l_0 = 1 \text{ m}$). If not mentioned otherwise, solutions are mapped with respect to stiffness rate K' and rest-length rate L'_0 . Increments of 0.3 for K' and 0.002 for L'_0 are used.

2.3. Effects on Hopping

2.3.1. Periodic Solutions

When mapping periodic solutions with respect to rest-length rate L'_0 and stiffness rate K' , two J-shaped areas of periodic solutions are found for the system without additional damping, see Figures 2.4 and 2.5. Surprisingly, all unstable solutions ($|\lambda| > 1$, region Ia in Figure 2.5) lie within the quadrant of negative rest-length rate and positive stiffness rate, all stable ones ($|\lambda| < 1$, region Ib) in the quadrant of

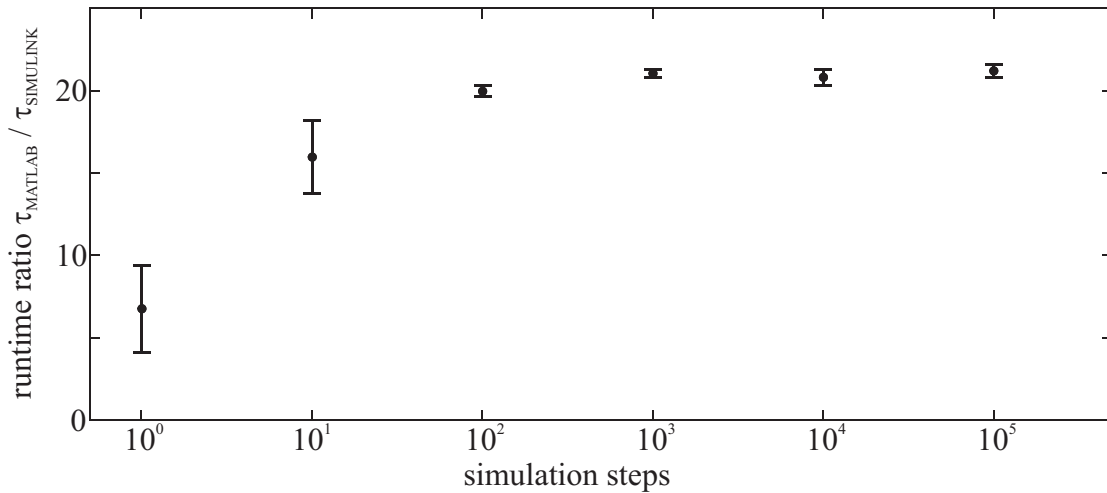


Figure 2.3.: Comparison of runtime for simulation directly in MATLAB, τ_{MATLAB} , and in MATLAB using the SIMULINK toolbox, τ_{SIMULINK} . The ratio of runtimes is displayed over the number of steps of a representative stable SLIP solution (running with $Y_0 = 1$, $Y'_0 \approx 1.6$, $K \approx 25.5$ and $\alpha_0 = 68^\circ$). Mean and standard deviation of five simulations for each number of steps are shown.

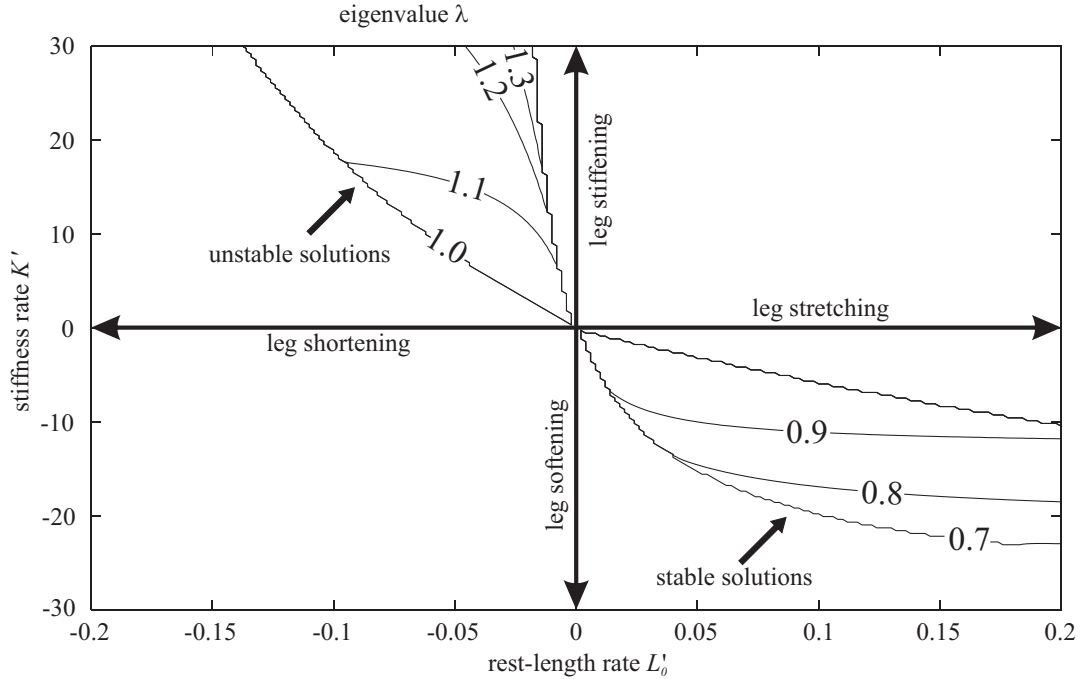


Figure 2.4.: Region of periodic hopping solutions without additional damping for leg stiffness $K_{TD} = 25$. Solutions are mapped with respect to stiffness rate K' and rest-length rate L'_0 . Increments of 0.3 for K' and 0.002 for L'_0 were used. Eigenvalue λ for periodic hopping is shown. Stable solutions require $|\lambda| < 1$.

positive rest-length rate and negative stiffness rate. These areas are connected via the neutrally stable solutions ($|\lambda| = 1$) for $L'_0 = 0$ and $K' = 0$, although they appear to be disconnected because of the resolution of L'_0 and K' . Without additional damping rest-length rate and stiffness rate are required to be of opposite sign in order to allow for periodic hopping. If both parameters are negative only energy withdrawal takes place (region IVa), if both are positive only energy injection (region IVb). Only the combination of extracting energy from the system by reducing one parameter and compensating by increasing the other one ensures that after one step initial energy (equivalent to apex height) can be reached again.

The areas of stable and unstable solutions are both confined between a falling-down barrier and an energy barrier: In the case of the unstable solutions the touch-

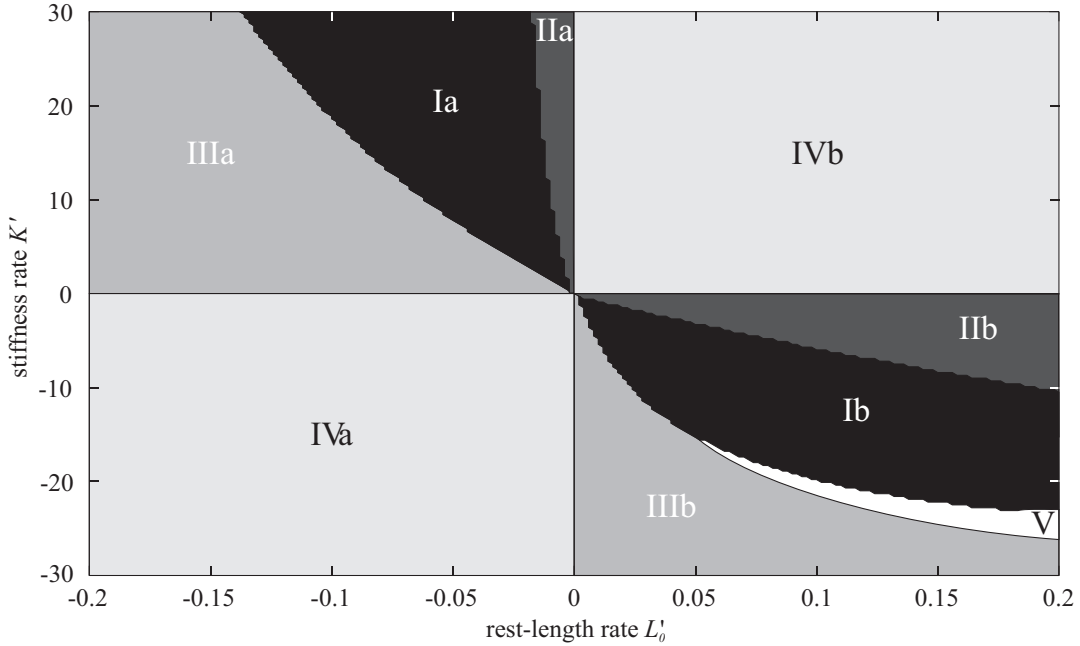


Figure 2.5.: Regions of the investigated parameter space: periodic solutions (I), ground contact within one hopping cycle (II), energy withdrawal cannot be fully compensated (III), unilateral change of energy (IV) and vanishing leg stiffness during contact (V).

down condition, $Y_0 \geq 1$, is violated in region IIa, i.e. the leg is not initialized and the mass point follows a free-fall trajectory until ground contact. For ever faster rest-length declines energy loss due to negative L'_0 exceeds energy injection via positive K' (region IIIa).

In region IIb the spring cannot store sufficient initial energy. Thus, the point mass cannot be supported properly and hits the ground. This is equivalent to the leg being fully compressed, $\Delta L_{\max} = 1$, see Figure 2.6(d). At the lower boundary energy withdrawal via leg softening exceeds energy input by extension of the leg (region IIIb). It should be noted that for fast stiffness declines leg stiffness vanishes during contact (region V), i.e. $K_{\text{TO}} = 0$, see Figure 2.6(f), before the system hits the energy barrier. The simulations are terminated in this area to avoid solutions with negative leg stiffness.

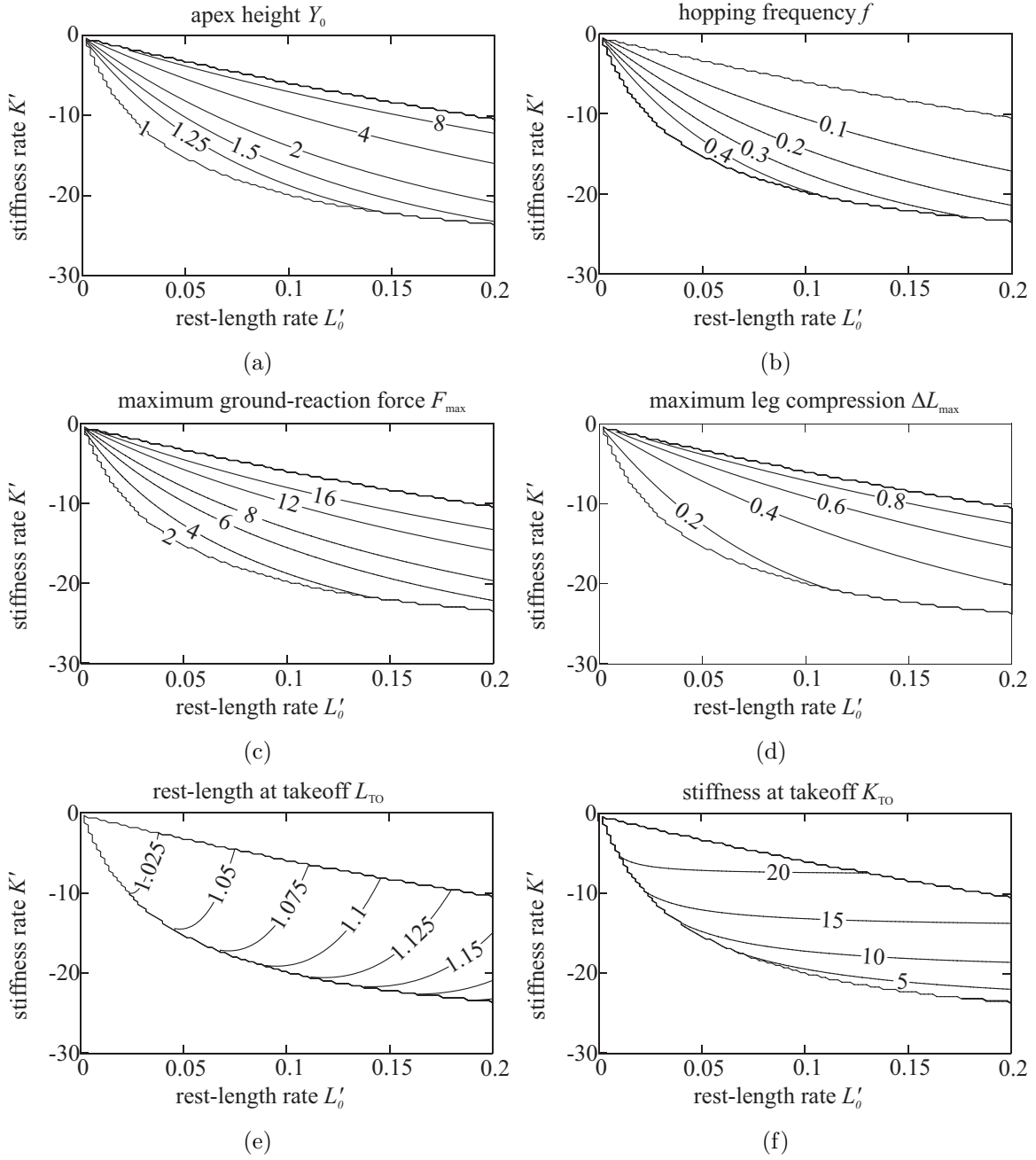


Figure 2.6.: Region of stable hopping solutions ($|\lambda| < 1$, see Figure 2.4) with leg stiffness $K_{\text{TD}} = 25$. Solutions are mapped with respect to stiffness rate K' and rest-length rate L'_0 . (a) Apex height $Y_0 = Y^*$, (b) hopping frequency $f = \tau_{\text{hop}}^{-1}$, (c) maximum ground-reaction force $F_{\max} = Y''_{\max} + 1$, (d) maximum leg compression $\Delta L_{\max} = \max[1 - Y(\tau)/(1 + L'_0\tau)]$, (e) rest-length at takeoff L_{TO} and (f) stiffness at takeoff K_{TO} are shown.

2.3.2. Landing-Takeoff Asymmetry

To illustrate the spatio-temporal behavior of stable and unstable hopping solutions, representative examples are shown in Figure 2.7. Asymmetry of ground-reaction force with respect to instant of half stance time can clearly be seen. Nonetheless, only the stable case corresponds to the experimental findings of Kuitunen et al. (2011) for hopping and Cavagna (2006) for running: Maximum force is reached before the half of stance time, a behavior the SLIP model was unable to reproduce so far. The increase of leg length at takeoff with respect to leg length at touchdown for stable hopping is in agreement with the experimental results as well, e.g. Kuitunen et al. (2011) for hopping and Lipfert (2010) for running. In accordance to the asymmetries observed in ground-reaction force and leg length, the force-length function of the model for both stable and unstable parameter choices deviates from the behavior of a linear spring, Figure 2.7(e,f). Resulting time evolution of total energy and its components during ground contact for the chosen parameter sets is plotted in Figure 2.8. Representative behavior for either stable or unstable solutions can be seen: Stable solutions first exhibit a maximum in total energy followed by a minimum before returning to initial energy (total energy is constant during flight phases) and vice versa for unstable solutions.

Landing-takeoff asymmetry, as observed in human hopping and running (Farley, 1991; Cavagna, 2006; Cavagna and Legramandi, 2009; Kuitunen et al., 2011; Lipfert, 2010), may occur due to numerous reasons. In Cavagna (2006) visco-elasticity of muscles is suggested to be the main contribution. Another potential reason for this kind of asymmetry could be the specific function of the human foot resulting in increases in nominal leg length and decreases in leg stiffness from touchdown to takeoff (Maykranz et al., 2009).

In this thesis, leg segmentation and specific muscle properties were not taken into account. Still, a human-like leg behavior was predicted based on the requirement of

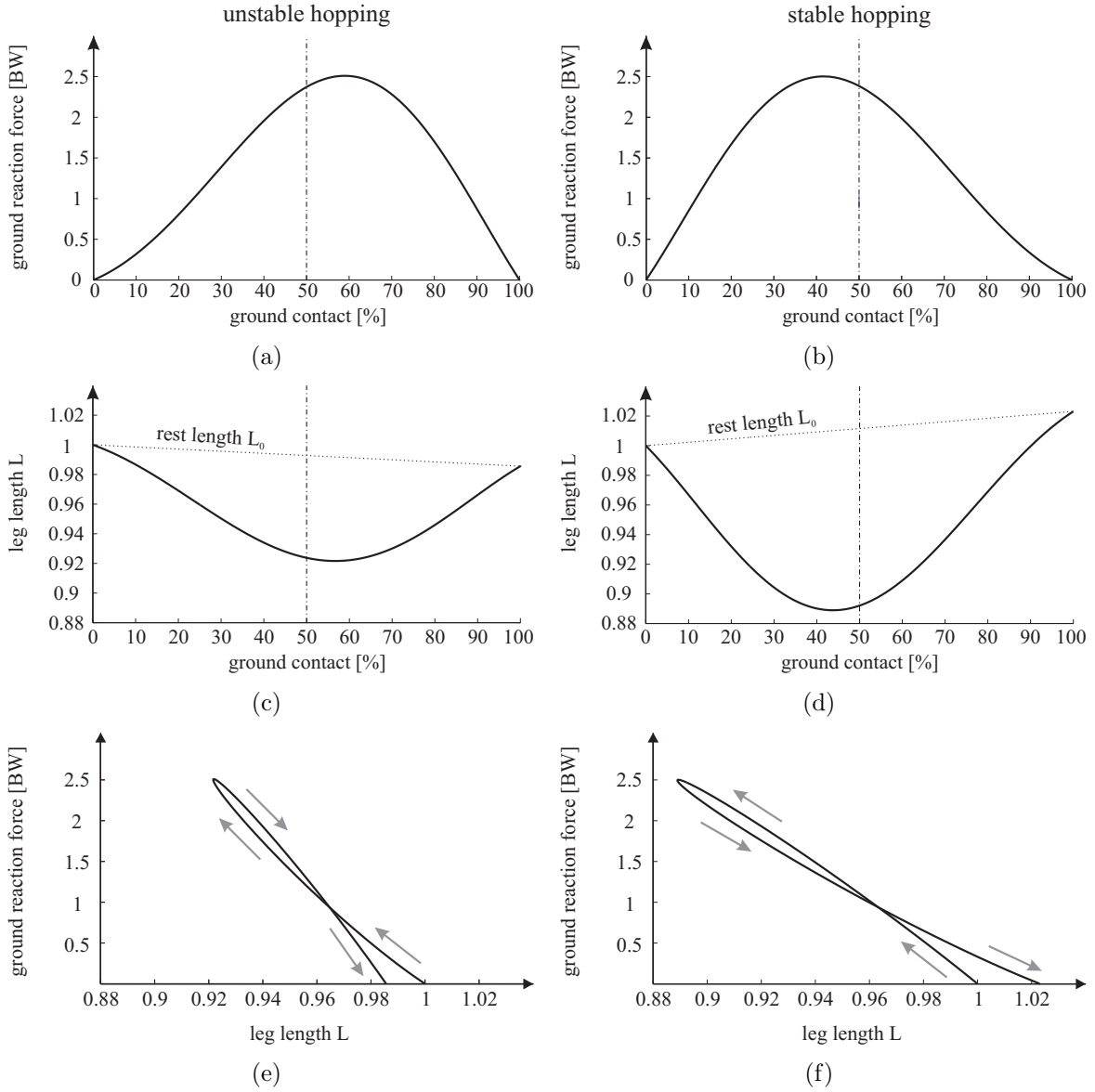


Figure 2.7.: Examples for periodic hopping patterns. In (a,b) ground-reaction forces and in (c,d) leg lengths L are shown for all of stance time using the parameter sets ($L'_0 = -0.018, K' = 23.4$) for unstable and ($L'_0 = 0.022, K' = -9.6$) for stable hopping. (c,d) also show the linear behavior of rest length L_0 during contact (leg stiffness behaves equivalently, but in opposite direction). (e,f) show the resulting force-length functions of the leg spring.

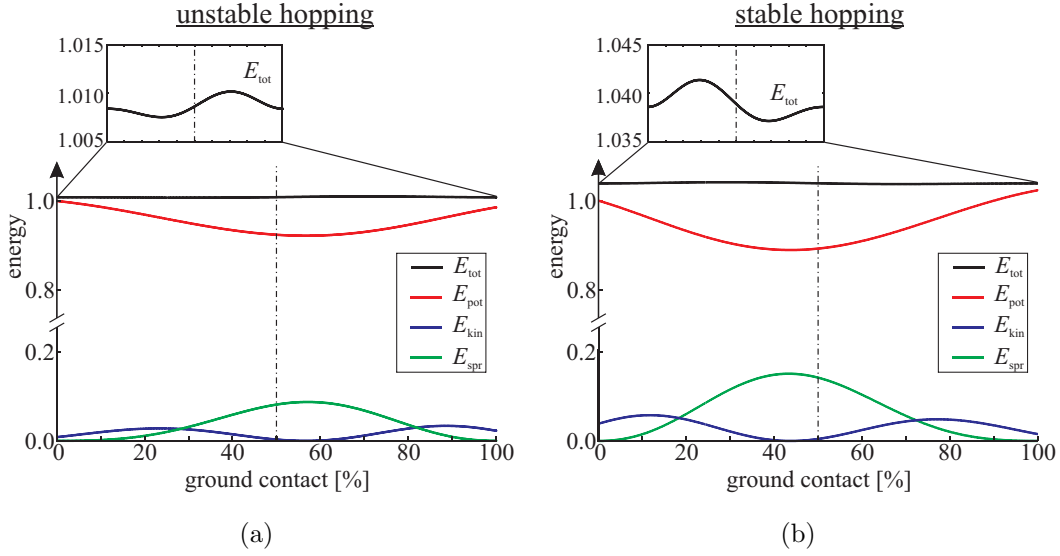


Figure 2.8.: Energy evolution during ground contact for the chosen hopping patterns, see Figure 2.7. Potential energy $E_{\text{pot}} = Y$, kinetic energy $E_{\text{kin}} = \frac{1}{2}Y'^2$, spring energy $E_{\text{spr}} = \frac{1}{2}K(L_0 - Y)^2$ and total energy $E_{\text{tot}} = E_{\text{pot}} + E_{\text{kin}} + E_{\text{spr}}$ are shown over stance time.

stable hopping realized with variable leg-spring properties, Figure 2.7. A decreasing leg stiffness supports stable hopping and shifts the instant of maximum force into the first half of stance, thus reproducing the landing-takeoff asymmetry observed in humans.

2.3.3. Leg Softening and Stretching Ensure Stable Hopping

A clear distinction between the two parameter setups can be made based on stability analysis. Without additional damping, all unstable solutions possess positive stiffness rates and negative rest-length rates (region Ia in Figure 2.5). In contrast, all stable hopping patterns feature negative stiffness rates and positive rest-length rates (region Ib). Therefore, to ensure stable hopping without additional damping, configurations with decreasing leg stiffness and increasing rest length are required.

The decrease of leg stiffness resembles the force-velocity function of muscles. As Blickhan et al. (2003) noted that the negative slope of the force-velocity function

supports stability, a direct connection between stiffness decrease and stability may be drawn. The increase in rest length required to compensate the effects of decreasing leg stiffness may be realized by the foot, with the ankle joint being more extended at takeoff than at touchdown (Lipfert, 2010). This argument also is supported by the findings of Malcolm (2010) showing that the ankle joint is the main contributor of positive work in human walking and running.

It should be noted that a large number of stable solutions found with the numerical model are not physiologically feasible, e.g. in terms of hopping height, amplitude of ground-reaction force, etc. Nevertheless, considering reasonable constraints, e.g. restricting apex height to $Y_0 \leq 1.5$, Figure 2.6(a), and rest-length change to $L_{TO} \leq 1.1$, Figure 2.6(e), a corresponding range of L'_0 and K' for stable hopping can be found. It should be noted that for these hopping solutions the model predictions are in good agreement with human data, e.g. Kuitunen et al. (2011), with hopping frequencies of 1–2 Hz (for $m = 80$ kg and $l_0 = 1$ m), Figure 2.6(b), and ground-reaction forces with amplitudes around three times body weight, Figure 2.6(c).

2.3.4. Additional Damping Is Beneficial for Stable Hopping

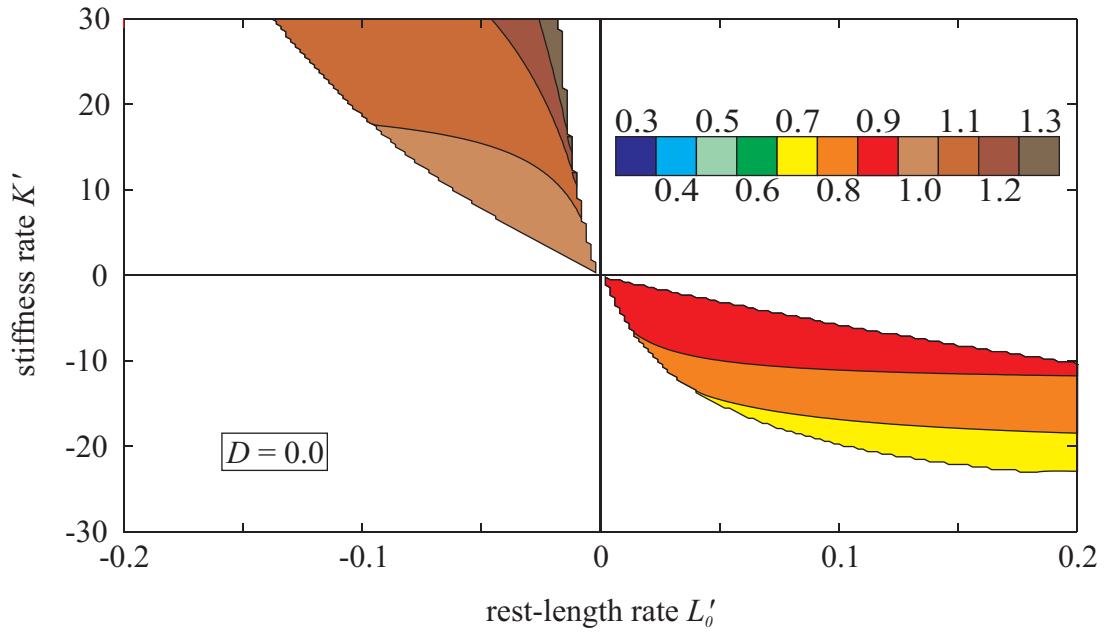
Komsuoglu (2004) stated that in order to achieve stable hopping damping is essential. To compensate for energy losses caused by velocity-dependent damping and plastic ground collision, piecewise-constant modulation of leg stiffness during stance was considered. For simultaneous (linear) variation of rest length and leg stiffness, the results presented here show that additional damping is not required, but beneficial for stable hopping. The functional damping due to leg softening is predicted to be sufficient.

Nonetheless, for increasing damping ever smaller eigenvalues are reached in the stable region. At the same time, the eigenvalues are no longer monotonically distributed. This feature of additional velocity-dependent damping requires further investigation. another advantage of additional damping is the increased range of leg

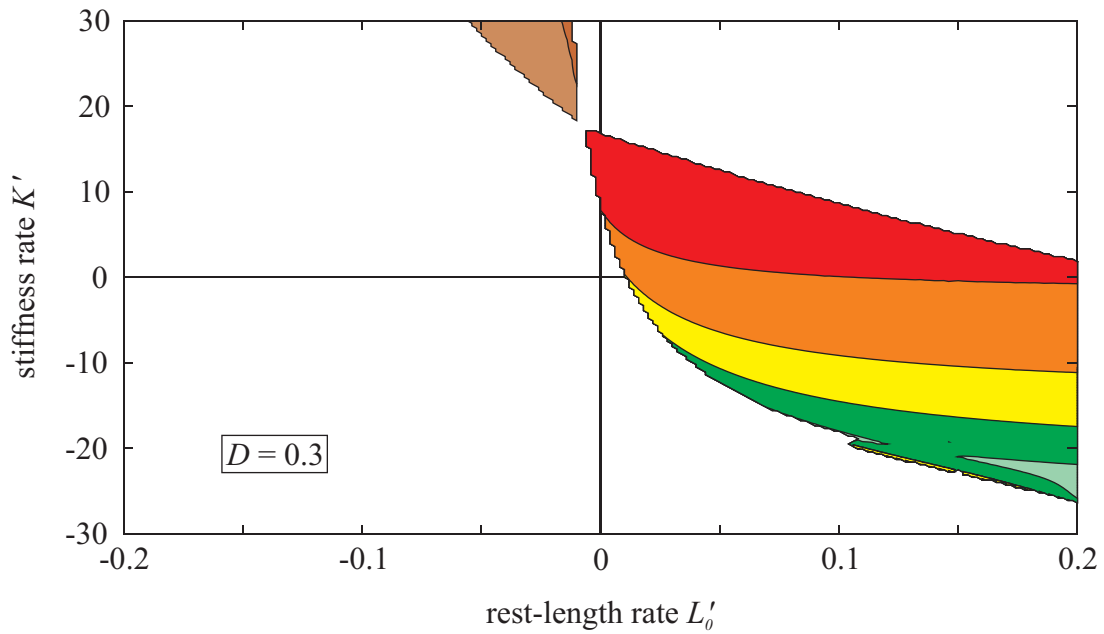
parameter variations resulting in stable hopping, Figure 2.9. For increasing damping coefficients the falling-down barrier is shifted towards higher stiffness rates, see Figure 2.9. Therefore, the stable area broadens considerably and stable solutions also can be found for configurations with positive stiffness rates. Additionally, stable solutions for negative rest-length rates appear. Hence, in combination with positive L'_0 , additional damping does allow for a range of stiffness rates around $K' = 0$, which could be interpreted as hypothetical stiffness perturbations. Thus, it is not required to fine-tune leg stiffness while operating with this parameter setup. Similarly, additional damping combined with positive K' allows for fluctuations of initial rest length. However, such fluctuations of rest length are much more critical than fluctuations of leg stiffness, which is in agreement with the modeling results of Merker et al. (2011) for walking with asymmetric legs.

If additional damping is included the regions confining the area of stable solutions at the lower boundary (regions IIIb and V in 2.5) do not merge smoothly anymore. For certain choices of rest-length rates L'_0 leg stiffness vanishes at the boundary for two distinct stiffness rates K' . Between these points leg stiffness remains non-negative and stable hopping is possible. Thus, a bulge forms, growing more and more prominent for increasing damping.

Both functional and velocity-dependent damping are simplified assumptions and need to be carefully compared to human leg function. Even though the functional damping investigated in this thesis describes the fundamental effects of variable leg-spring parameters, the linear time dependency is still a very coarse approximation of reality. By introducing velocity-dependent damping, additional discrepancies between experiment and model predictions occur. For instance, the model then predicts non-zero landing forces at the instant of touch-down which are not observed in human hopping. Functional damping via variation of leg parameters does not cause such effects, as the damping effect increases with leg compression. Another disadvantage of velocity-dependent damping is that takeoff takes place while leg length

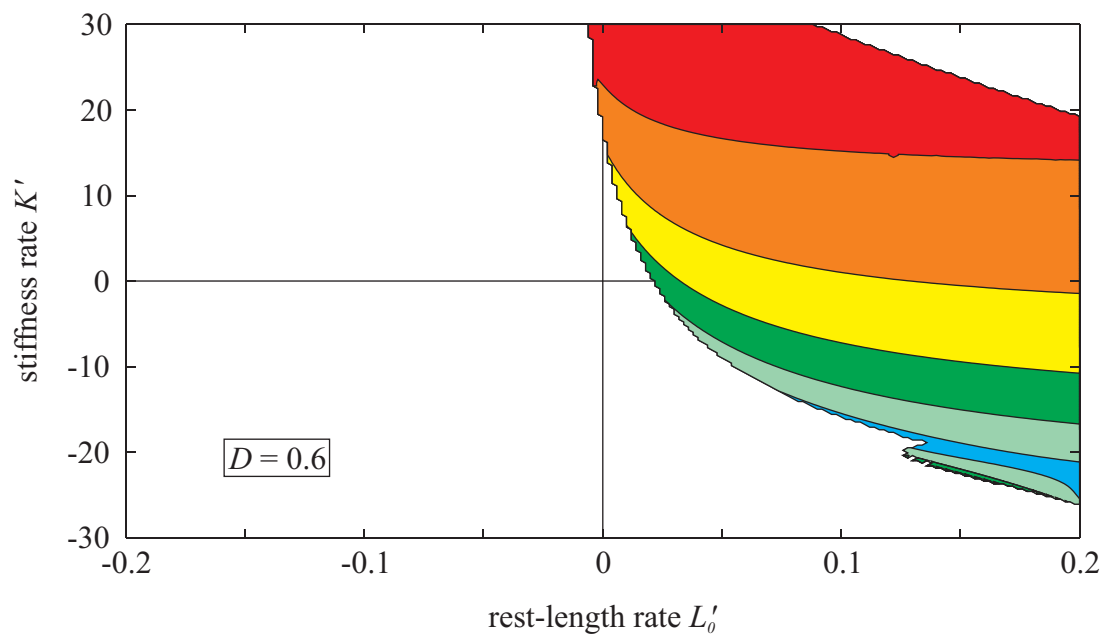


(a)

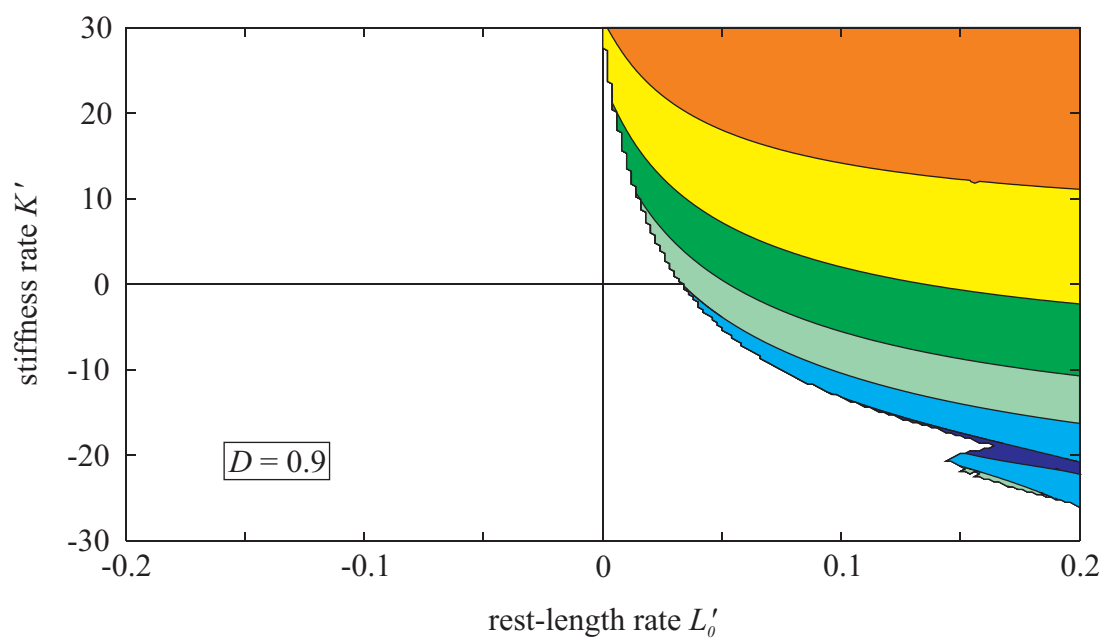


(b)

Figure 2.9.: Influence of damping coefficient D on the area of periodic solutions and stability. Solutions are mapped with respect to stiffness rate K' and rest-length rate L'_0 for leg stiffness $K = 25$. Increments of 0.3 for K' and 0.002 for L'_0 were used. Eigenvalue λ for periodic hopping is shown. Stable solutions require $|\lambda| < 1$.

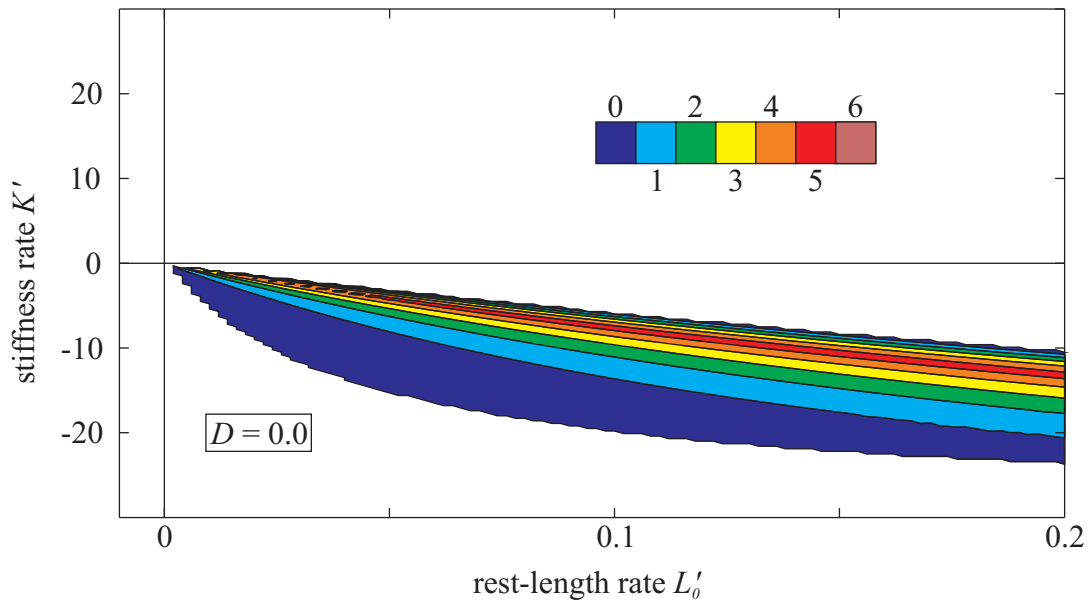


(c)

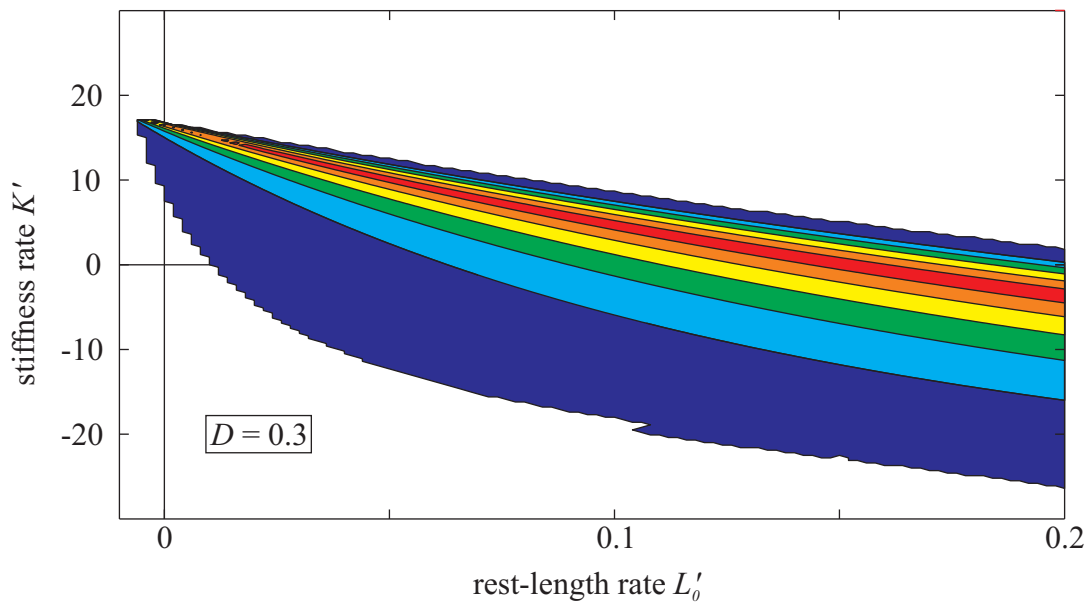


(d)

Figure 2.9.: Influence of damping coefficient D on the area of periodic solutions and stability. Solutions are mapped with respect to stiffness rate K' and rest-length rate L'_0 for leg stiffness $K = 25$. Increments of 0.3 for K' and 0.002 for L'_0 were used. Eigenvalue λ for periodic hopping is shown. Stable solutions require $|\lambda| < 1$.



(a)



(b)

Figure 2.10.: Influence of damping coefficient D on the robustness of stable hopping solutions. Robustness is mapped with respect to stiffness rate K' and rest-length rate L'_0 for leg stiffness $K = 25$. Increments of 0.3 for K' and 0.002 for L'_0 were used.

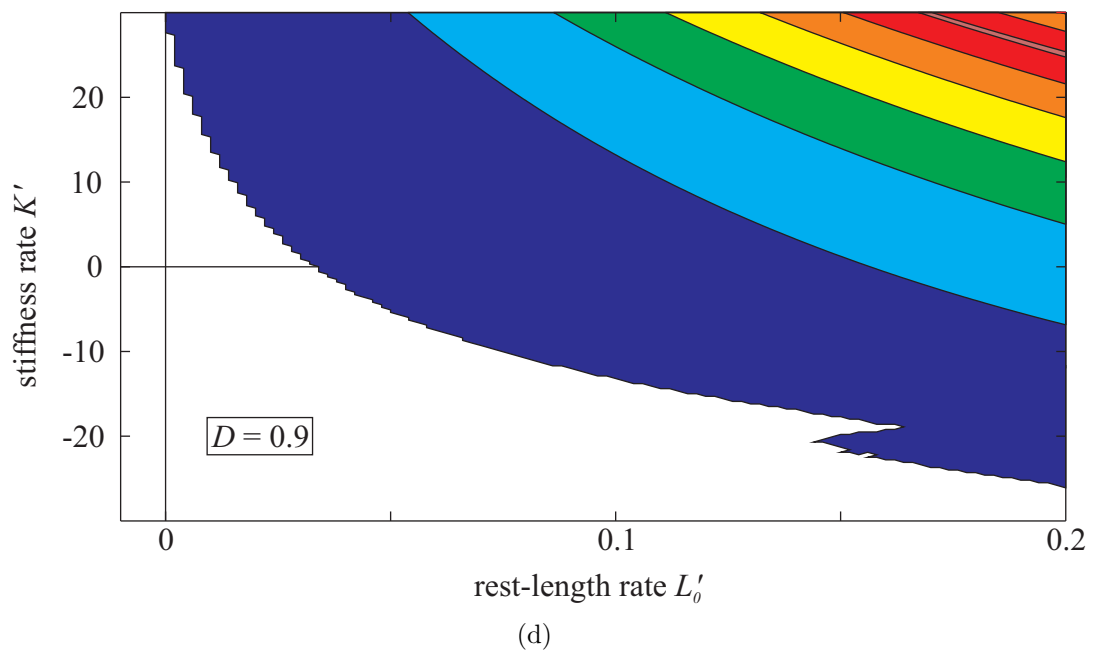
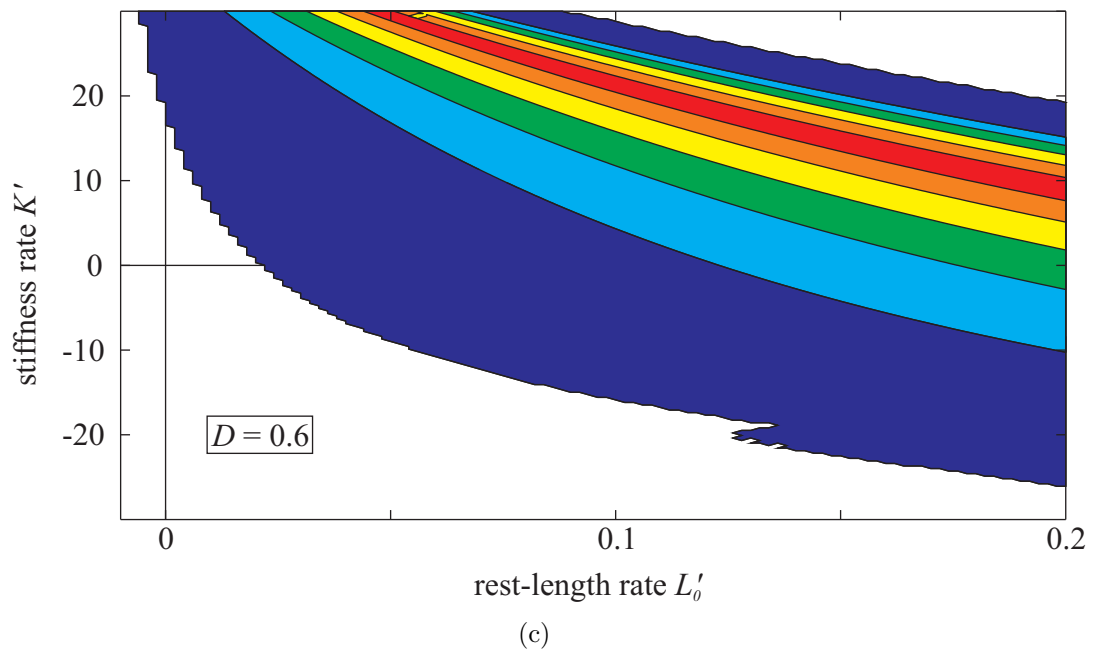


Figure 2.10.: Influence of damping coefficient D on the robustness of stable hopping solutions. Robustness is mapped with respect to stiffness rate K' and rest-length rate L'_0 for leg stiffness $K = 25$. Increments of 0.3 for K' and 0.002 for L'_0 were used.

is still smaller than rest length, i.e. the leg is still compressed.

Here, the strength of the VLS concept becomes clear. Damping, as observed in biological limbs, can be encoded in some non-constant spring stiffness, e.g. $K(\tau)$, as described by the VLS concept. Linear-in-time stiffness changes only represent a first-order approximation of this functional damping. Extensions like functional damping as a function of velocity, $K[Y'(\tau)]$, may be closer to reality (see Section 3).

2.3.5. Trading Stability for Robustness

As in running (Rummel et al., 2010), there is a trade-off between stability and robustness. Stability is maximal for small hopping heights, while robustness is maximal for medium hopping heights, see Figures 2.4, 2.6(a) and 2.10. This is due to the symmetric definition of robustness as the maximum step-up or step-down perturbation the hopper can compensate. Thus, robustness is the minimum distance of the stable fixed point to either boundary of the basin of attraction. For medium hopping heights the stable fixed point is located in the middle of the basin of attraction rather than towards either end, maximizing the distance to both boundaries and therefore robustness.

If reasonable constraints are considered, e.g. restricting apex height to $Y_0 \leq 1.5$ and rest-length change to $L_{TO} \leq 1.1$, see Figure 2.6(a,e), the hopping solutions correspond rather to optimized stability than robustness. However, robustness may still be considerable (up to one half of leg length at touchdown), see Figure 2.10.

Additional velocity-dependent damping shifts the upper falling-down barrier outwards. The hopper is able to achieve larger hopping heights. At the same time, the stable fixed point Y_s^* is not noticeably shifted towards the middle of the basin of attraction. The stable fixed point remains closer to one of the boundaries. Thus, robustness only is marginally increased. Nonetheless, one benefit of additional damping is that the areas for a given level of robustness increase considerably.

2.3.6. Trading Stability for Efficiency

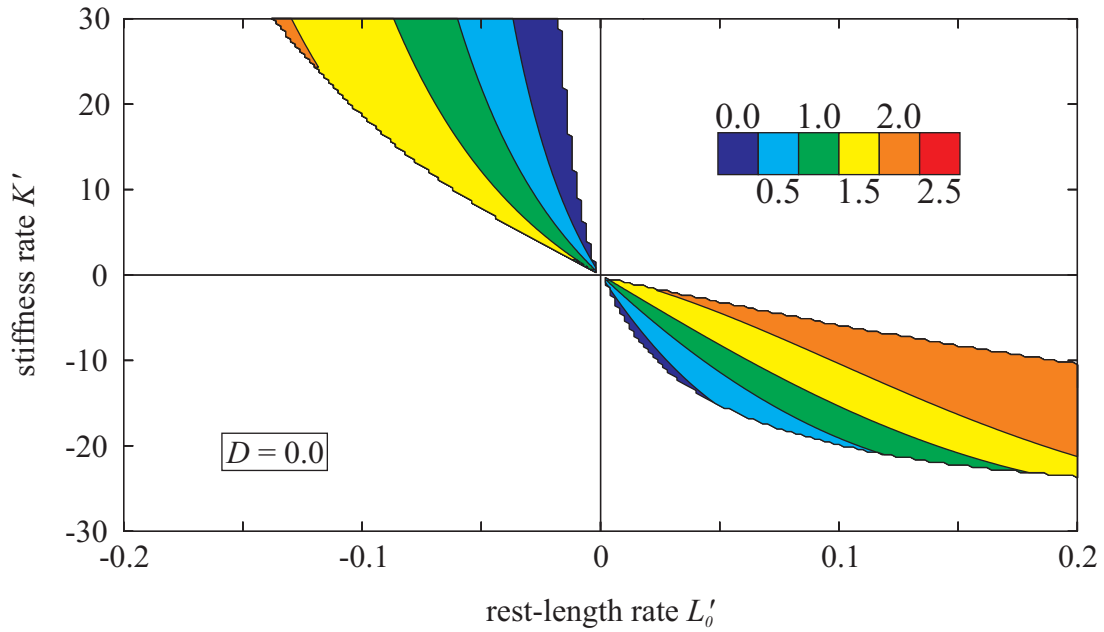
As the model used in this thesis is quite conceptual, it was not attempted to estimate a metabolic or specific cost of transport, e.g. Minetti and Alexander (1997); Collins (2005). Rather the work-based cost of movement C_{Y_0} was applied to calculate the mechanical requirements to achieve the periodic hopping height Y_0 within the variable-leg-spring concept and with additional velocity-dependent damping. Following an argument of Ruina et al. (2005), this simplified approach is valid as long as it is used for comparisons within one model.

Additional velocity-dependent damping only marginally increases the work-based cost of movement with respect to hopping height, while the regions for a given cost level enlarge considerably, see Figure 2.11. This suggests a benefit of additional damping with respect to hopping performance or efficiency.

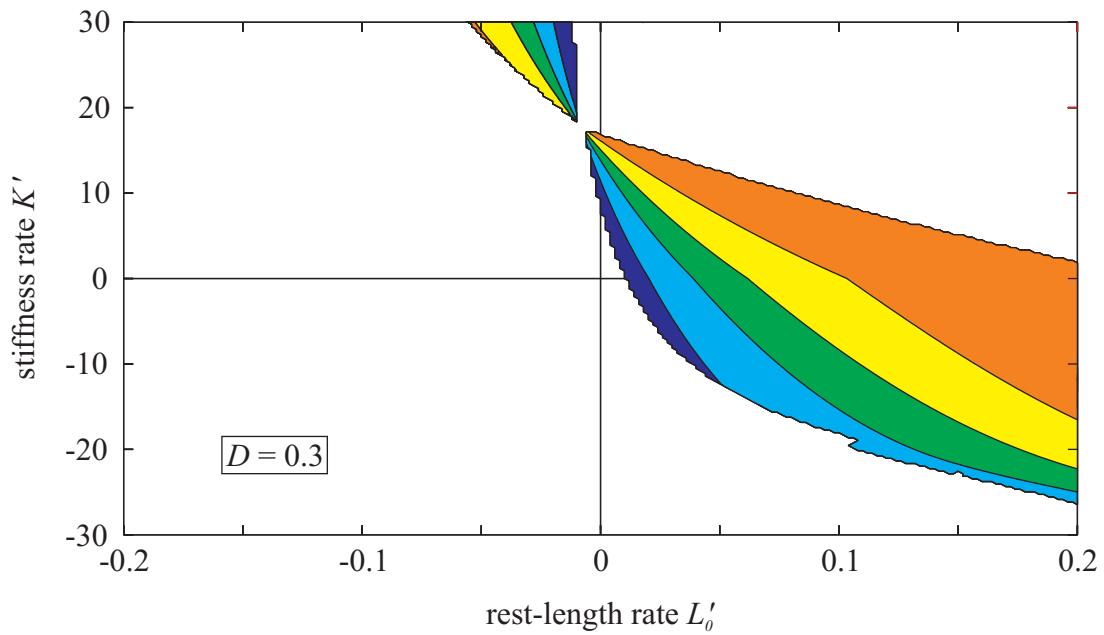
However, the work ratio decreases drastically with additional damping (Fig. 2.12). The work done passively by the spring, so to say “for free”, reduces, whereas the contribution of the damper to support the point mass against gravity increases. Hopping becomes more visco-elastic and less efficient. Thus, from an efficiency point-of-view, the functional damping via leg softening is more beneficial for hopping than the commonly used velocity-dependent damping.

2.4. Application for Robotics

The results of this thesis indicate that with an appropriate combination of L'_0 and K' during contact stable, robust and efficient hopping patterns can be achieved. Within the predicted range of leg parameter variations there is no need for precise parameter tuning. It also is important to note that the change in leg-spring parameters does not require continuous sensory feedback except for the touchdown/takeoff trigger to initiate the parameter variation over time. This indicates that for robotic legs with adjustable leg stiffness successful locomotion could be achieved with little



(a)



(b)

Figure 2.11.: Influence of damping coefficient D on work-based cost of movement C_{Y_0} . Cost of transport is mapped with respect to stiffness rate K' and rest-length rate L'_0 for leg stiffness $K = 25$. Increments of 0.3 for K' and 0.002 for L'_0 were used.

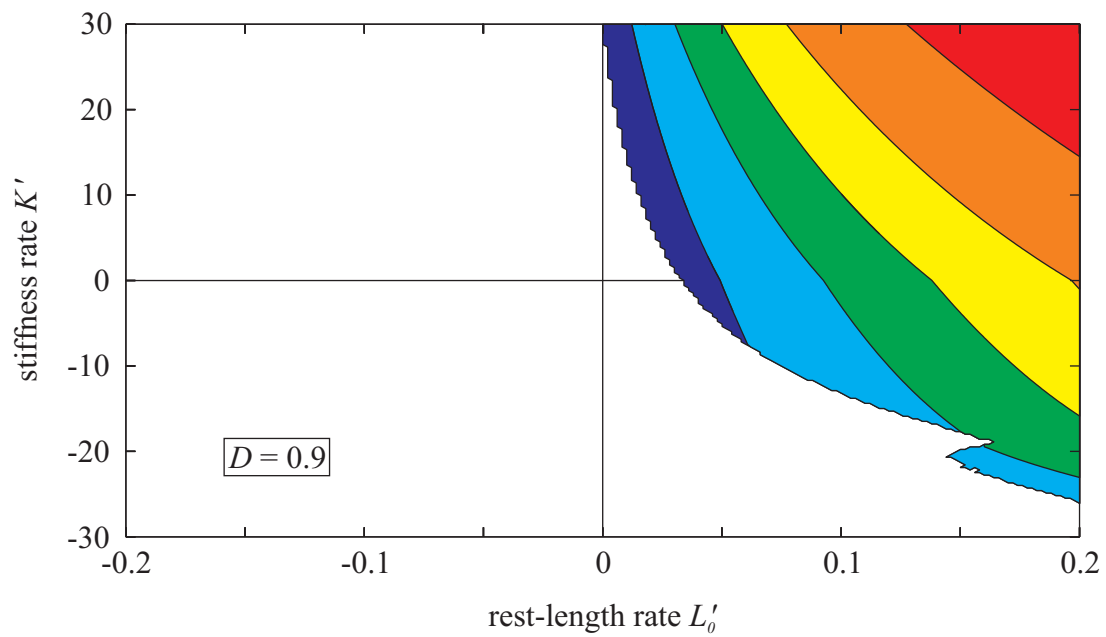
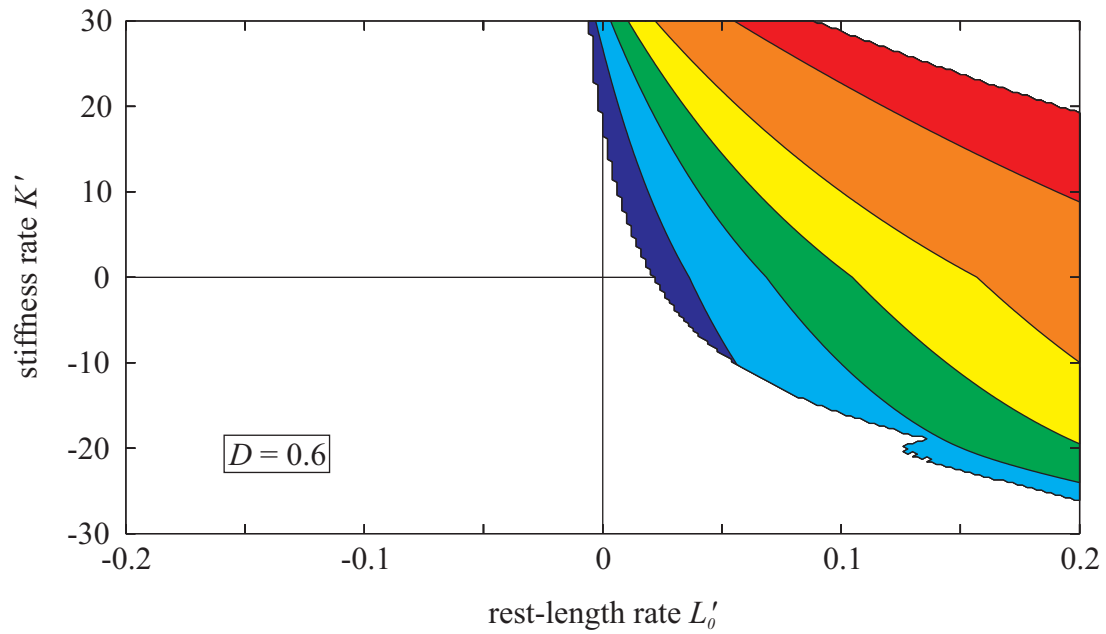


Figure 2.11.: Influence of damping coefficient D on work-based cost of movement C_{Y_0} . Cost of transport is mapped with respect to stiffness rate K' and rest-length rate L'_0 for leg stiffness $K = 25$. Increments of 0.3 for K' and 0.002 for L'_0 were used.

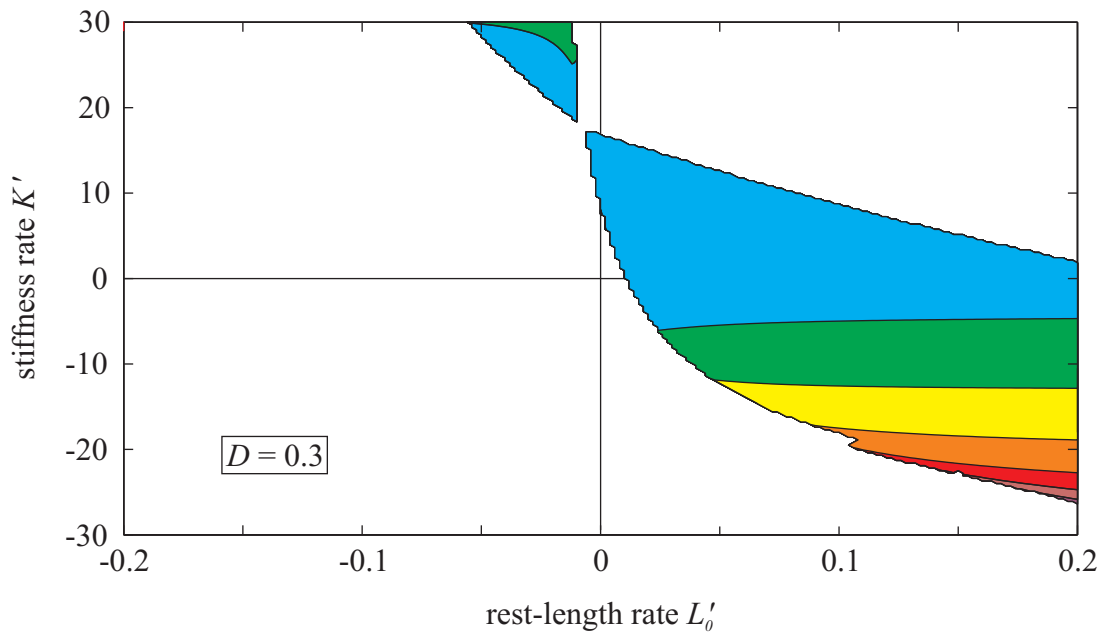
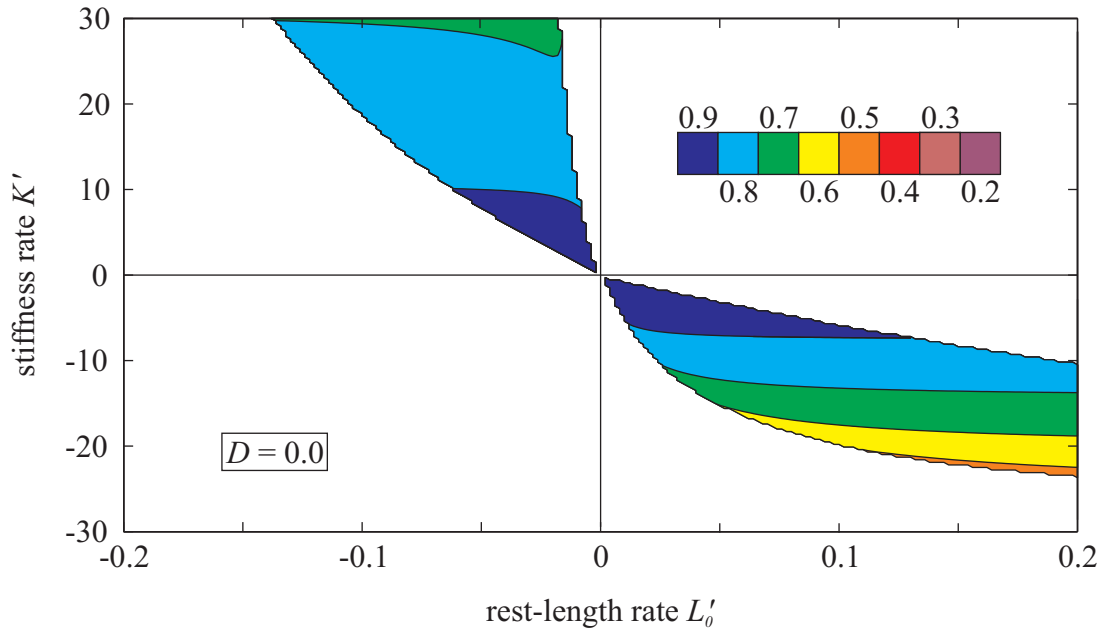
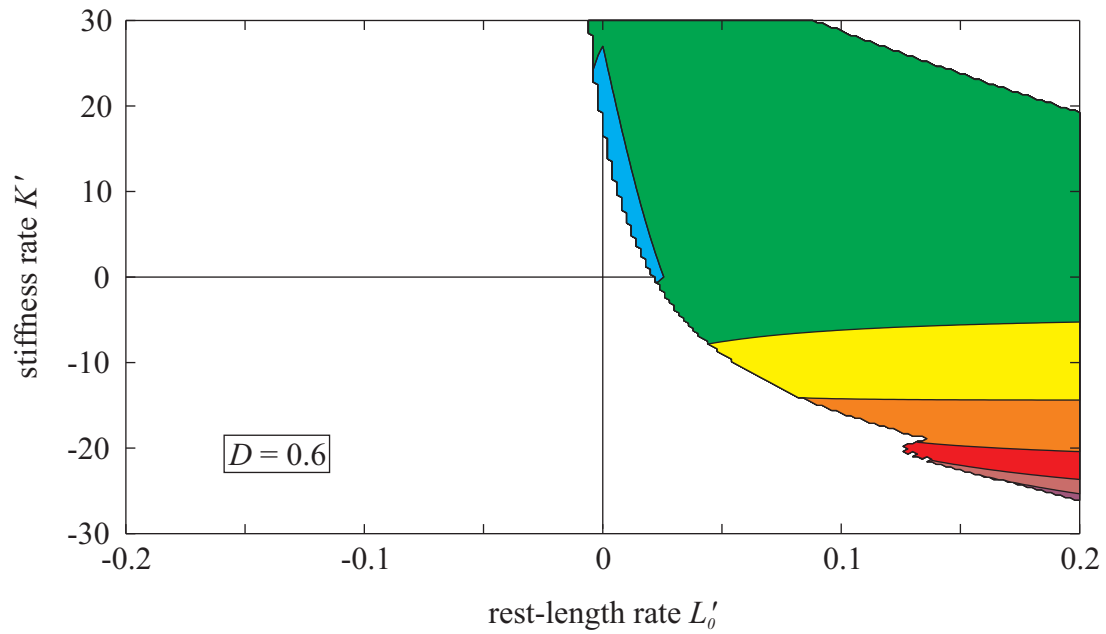
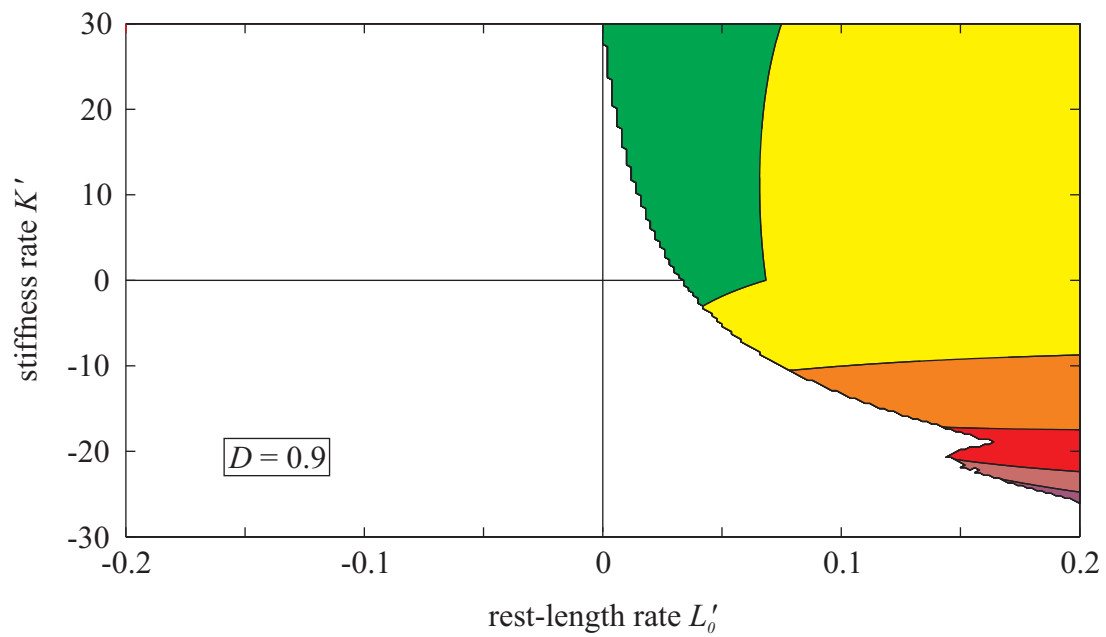


Figure 2.12.: Influence of damping coefficient D on the ratio of elastic and total work η . Work ratio is mapped with respect to stiffness rate K' and rest-length rate L'_0 for leg stiffness $K = 25$. Increments of 0.3 for K' and 0.002 for L'_0 were used.



(c)



(d)

Figure 2.12.: Influence of damping coefficient D on the ratio of elastic and total work η . Work ratio is mapped with respect to stiffness rate K' and rest-length rate L'_0 for leg stiffness $K = 25$. Increments of 0.3 for K' and 0.002 for L'_0 were used.

control effort. Key to this “relaxed control” is the spring-like leg behavior. The underlying elasticity allows to exploit mechanically self-stabilizing effects. Thus, it is not necessary to control the robot at all times. One might even envision some kind of conditional control: The system is allowed to evolve freely for most of the time and control is only enforced in case additional safety measures are required, e.g. certain values for maximum ground-reaction force or leg compression are exceeded.

In the last years, a number of design proposals were presented to actively tune the stiffness of compliant joints (Van Ham et al., 2007; Wolf and Hirzinger, 2008; Jun and Clark, 2009; Galloway, 2009). With this technology it becomes possible to adjust stiffness properties of the legs. This can be done in preparation of or during ground contact. When combined with variation of rest length no additional damping structures in the system may be required to achieve stable locomotion, as suggested by this thesis. The level of damping can be functionally tuned within the variable-leg-spring concept to the required level of stability depending on the system’s or environmental conditions (e.g. inherent damping, compliant ground). In principle, this control scheme would also be applicable if no physical damping was present, even though this is unlikely in engineered systems.

However, additional velocity-dependent damping is beneficial. With additional damping more than 60% disturbance rejection can be achieved (for a damping coefficient of $D = 0.9$), Figure 2.9. Furthermore, the robustness with respect to variation of leg parameters largely increases. This even includes the case of a fixed leg stiffness which may simplify leg design. Robots with telescopic legs based on designs like e.g. *Sprawlita* (Cham et al., 2000) or *Scout II* (Poulakakis et al., 2005) might benefit from the stabilizing properties identified in this thesis. Furthermore, the variable leg-spring concept can be transferred to the operation of a segmented leg (Rummel and Seyfarth, 2008). In a robot with segmented legs, tunable joint stiffness may be useful to ease control of bouncing gaits.

3. The Variable-Leg-Spring Model with Velocity-Dependent Stiffness

3.1. Modification of the VLS Model

3.1.1. Velocity-Dependent Stiffness

In the previous chapter, preplanned time-dependent leg-spring parameters during hopping were investigated. Motivated by the force-velocity relationship of the muscle and its stabilizing effect on hopping (Haeufle et al., 2010), leg-stiffness variation is now considered to be velocity-dependent, i.e. reactive. As asymmetry of the ground-reaction force was found to correlate with stability, see Section 2.3.2, and linear-in-time rest-length variations do not induce any GRF asymmetry, see Section 2.1.2, the control scheme for rest-length changes is inherited from the original VLS model. Therefore, the investigation is focussed on the stabilizing effects of velocity-dependent leg stiffness. Additional damping is neglected in this chapter.

Two models are investigated. In the first model, leg stiffness is allowed to vary only during ground contact and is held constant during flight phases (except of reset to K_{TD} at apex). The second model incorporates the concept of swing-leg control of Blum et al. (2010), in order to analyze whether it is beneficial for stable hopping. The simplest way to introduce this kind of control to the VLS model is to allow leg stiffness to change continuously throughout the whole hopping cycle, rather than

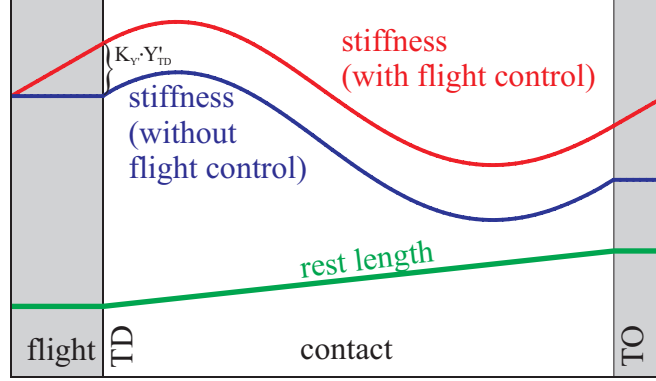


Figure 3.1.: Leg-spring parameters correlating with stable hopping, i.e. rest-length increase and leg-stiffness decrease, are displayed throughout one hopping cycle. Leg-stiffness variation with and without flight control is shown. Rest-length variation coincides for both models.

keeping it constant during flight phases (and resetting at the instant of apex). The model with flight control has the advantage that for parameter setups corresponding with stable hopping, stiffness at touchdown increases with hopping height. Thus, for these parameter choices, the spring is able to better support the point mass. The parameter profiles for the modified models are displayed in Figure 3.1.

The equations for leg-stiffness variation (a) without and (b) with flight control read

$$K(Y') = K_{\text{TD}} + K_{Y'}(Y' - Y'_{\text{TD}}), \quad (3.1a)$$

$$K(Y') = K_{\text{Apex}} + K_{Y'} Y', \quad (3.1b)$$

respectively. $Y'_{\text{TD}} = -\sqrt{2(Y_0 - 1)}$ is calculated at apex via the conservation of energy during flight phase, with initial apex height Y_0 . Thus, touchdown stiffness with and without flight control, $K_{\text{TD,FC}}$ and K_{TD} are related via

$$K_{\text{TD,FC}} = K_{\text{TD}} + K_{Y'} Y'_{\text{TD}} = K_{\text{TD}} - K_{Y'} \sqrt{2(Y_0 - 1)}. \quad (3.2)$$

Rest-length variation during ground contact remains linear in stance time τ ,

$$L_0(\tau) = 1 + L'_0 \tau, \quad (3.3)$$

while rest length is held constant during flight phase and reset at apex to $L_0 = 1$.

3.1.2. Landing-Takeoff Asymmetry

In order to quantify landing-takeoff asymmetry,

$$\varepsilon_{\text{LTO}} := \frac{\tau_{\text{max}} - \tau_{\text{st}}/2}{\tau_{\text{st}}/2} \quad (3.4)$$

is introduced, with $\tau_{\text{max}} = \tau(F_{\text{max}})$ being the time of maximum ground-reaction force and τ_{st} being stance time. By definition, ε_{LTO} is confined to the interval $[-1, 1]$. $\varepsilon_{\text{LTO}} = 0$ is equivalent to the symmetric case, while a negative ε_{LTO} corresponds to a GRF peak in the first half of ground contact and a positive one corresponds to a GRF peak in the second half.

3.1.3. Energy Efficiency

Using the same notions of energy efficiency as in the previous chapter, work-based cost of movement C_{Y_0} and ratio of elastic and total work η need to be adapted to account for velocity-dependent rather than time dependent leg-stiffness variation.

The time derivative of system energy

$$E = Y + \frac{1}{2}Y'^2 + \frac{1}{2}K(Y')(L_0(\tau) - Y)^2. \quad (3.5)$$

now yields

$$E' = \frac{1}{2}(L_0(\tau) - Y)^2 Y'' K_{Y'} + K(Y')(L_0(\tau) - Y) L'_0. \quad (3.6)$$

As Y'' ranges from -1 to $F_{\max} - 1$, Equation 2.3, velocity-dependent leg stiffness will act as damper as well as actuator during one hopping cycle, the main contribution however depending on the sign of $K_{Y'}$.

The work-based cost of movement is now defined as

$$C_{Y_0} := \frac{1}{Y_0} \int_0^{\tau_s} (|P_{\text{spring}}| + |P_{\text{damp}}| + |P_{L'_0}| + |P_{K_{Y'}}|) d\tau, \quad (3.7)$$

with

$$P_{\text{spring}} = K(Y')(L_0(\tau) - Y) Y', \quad (3.8a)$$

$$P_{\text{damp}} = -DY'^2, \quad (3.8b)$$

$$P_{L'_0} = K(Y')(L_0(\tau) - Y) L'_0, \quad (3.8c)$$

$$P_{K_{Y'}} = \frac{1}{2}(L_0(\tau) - Y)^2 Y'' K_{Y'}. \quad (3.8d)$$

Similarly, the work ratio of elastic and total work is defined as

$$\eta := \frac{W_{\text{spring}}}{W_{\text{total}}} = \frac{\int_0^{\tau_s} |P_{\text{spring}}| d\tau}{\int_0^{\tau_s} (|P_{\text{spring}}| + |P_{L'_0}| + |P_{K_{Y'}}| + |P_{\text{damp}}|) d\tau}. \quad (3.9)$$

3.1.4. A Template Muscle-Model

As to further assess the descriptive power of the VLS concept, it is compared to the fundamental muscle model of Haeufle et al. (2010). Containing only an (inverse) contractile element and no elasticity, neither parallel nor serial, it represents the most reduced muscle model capable of vertical hopping. In accordance with Full and Koditschek (1999), it therefore may be seen as a template muscle-model for hopping.

The pulling force of the contractile element is mechanically redirected, hence the

designation “inverse contractile element”, see Figure 1 in Haeufle et al. (2010), and a (pushing) HILL-type leg force (Hill, 1938) is generated,

$$f_{\text{leg}} = A(t) f_l(y) f_v(\dot{y}) f_{\text{iso}}. \quad (3.10)$$

In this model, $A(t)$ is the activation state of the muscle, $f_l(y)$ is the force-length function (FLF), $f_v(\dot{y})$ is the force-velocity function (FVF) and f_{iso} is the maximum contraction force of the muscle generated isometrically, i.e. without change in length. Activation is constrained to $A(t) \in [0, 1] \forall t$. Force-length and force-velocity function only depend on the state variables of the point mass, $f_l(y)$ and $f_v(\dot{y})$ respectively, as during stance y corresponds to momentary leg length and \dot{y} to contraction velocity of the muscle.

In Haeufle et al. (2010), the intrinsic muscle properties correlating to force-length and force-velocity function are each described at three levels of approximation: constant, linear and HILL-type,

$$f_l = \begin{cases} 1 & \text{constant,} \\ \frac{k}{m g} (l_0 - y) & \text{linear,} \\ \exp \left[c_l \left| \frac{y - l_{\text{opt}}}{w} \right|^3 \right] & \text{HILL,} \end{cases} \quad (3.11)$$

and

$$f_v = \begin{cases} 1 & \text{constant,} \\ 1 - \mu \dot{y} & \text{linear,} \\ \begin{cases} \frac{\dot{y}_{\text{max}} + \dot{y}}{\dot{y}_{\text{max}} - c_v \dot{y}}, & \dot{y} > 0 \\ N - (N - 1) \frac{\dot{y}_{\text{max}} - \dot{y}}{\dot{y}_{\text{max}} + 7.56 c_v \dot{y}}, & \dot{y} \leq 0 \end{cases} & \text{HILL.} \end{cases} \quad (3.12)$$

Parameters of the linear force-length function are spring stiffness k and rest length

l_0 , whereas w and c_l describe width and curvature of the bell-shaped HILL-type approximation and l_{opt} denotes optimal muscle length for maximum force, see Geyer et al. (2003).

In the linear approximation the slope of the force-velocity function is described by μ . As μ is chosen to be positive, see Table 3.1, higher leg forces are created during compression of the inverse contractile element, $\dot{y} \leq 0$, than during decompression, $\dot{y} > 0$. Due to mechanical redirecting of muscle force compression and decompression correspond to eccentric and concentric contraction of the muscle, respectively. Thus, force generation within this model is consistent with physiological data, e.g. Cavagna and Legramandi (2009). The non-linear approximation of the force-velocity function is based on HILL'S Equation, (Hill, 1938), for concentric contraction and a relation found by Seyfarth et al. (2000) for eccentric contraction. Here, c_v is the curvature of the force-velocity function and \dot{y}_{max} is the maximum contraction velocity, while N represents the eccentric force enhancement with $N = f_{\text{leg}}/f_{\text{iso}}$ for $\dot{y} = -\dot{y}_{\text{max}}$.

Introducing parameters normalized with respect to g , m and $l_0 \equiv l_{\text{TD}}$, force-length

Parameter		Value
Maximum isometric muscle force	$F_{\text{iso}} = f_{\text{iso}}/(m g)$	3
Stiffness	$K = kl_{\text{TD}}/(m g)$	10
Curvature (FLF)	c_l	-29.96
Width (FLF)	$W = w/l_{\text{TD}}$	0.45
Optimal muscle length	$L_{\text{opt}} = l_{\text{opt}}/l_{\text{TD}}$	0.9
Slope (FVF)	$M = \sqrt{g l_{\text{TD}}} \mu$	0.78
Maximum contraction velocity	$Y'_{\text{max}} = \dot{y}_{\text{max}}/\sqrt{g l_{\text{TD}}}$	-1.1
Curvature (FVF)	c_v	1.5
Eccentric force enhancement	N	1.5

Table 3.1.: Normalized model parameters. Derived from Haeufle et al. (2010).

and force-velocity function now read

$$F_l(Y) = \begin{cases} 1 & \text{constant,} \\ K(1 - Y) & \text{linear,} \\ \exp \left[c_l \left| \frac{Y - L_{\text{opt}}}{W} \right|^3 \right] & \text{HILL,} \end{cases} \quad (3.13)$$

and

$$F_v(Y') = \begin{cases} 1 & \text{constant,} \\ 1 - M Y' & \text{linear,} \\ \begin{cases} \frac{Y'_{\text{max}} + Y'}{Y'_{\text{max}} - c_v Y'} & Y' > 0 \\ N - (N - 1) \frac{Y'_{\text{max}} - Y'}{Y'_{\text{max}} + 7.56 c_v Y'} & Y' \leq 0 \end{cases} & \text{HILL,} \end{cases} \quad (3.14)$$

with the familiar normalization $Y = y/l_{\text{TD}}$, $\tau = \sqrt{g/l_{\text{TD}}}(t - t_{\text{TD}})$ and $'$ being the derivative with respect to τ , see Chapter 2.1.1. Normalized leg force then is

$$F_{\text{leg}} = A(\tau) F_l(Y) F_v(Y') F_{\text{iso}}. \quad (3.15)$$

Normalized model parameters are displayed in Table 3.1. For a physiological motivation of the chosen parameter values see Haeufle et al. (2010) and the references mentioned therein. It should be noted, that the notation of Haeufle et al. (2010) was modified slightly, in order to be consistent with this thesis.

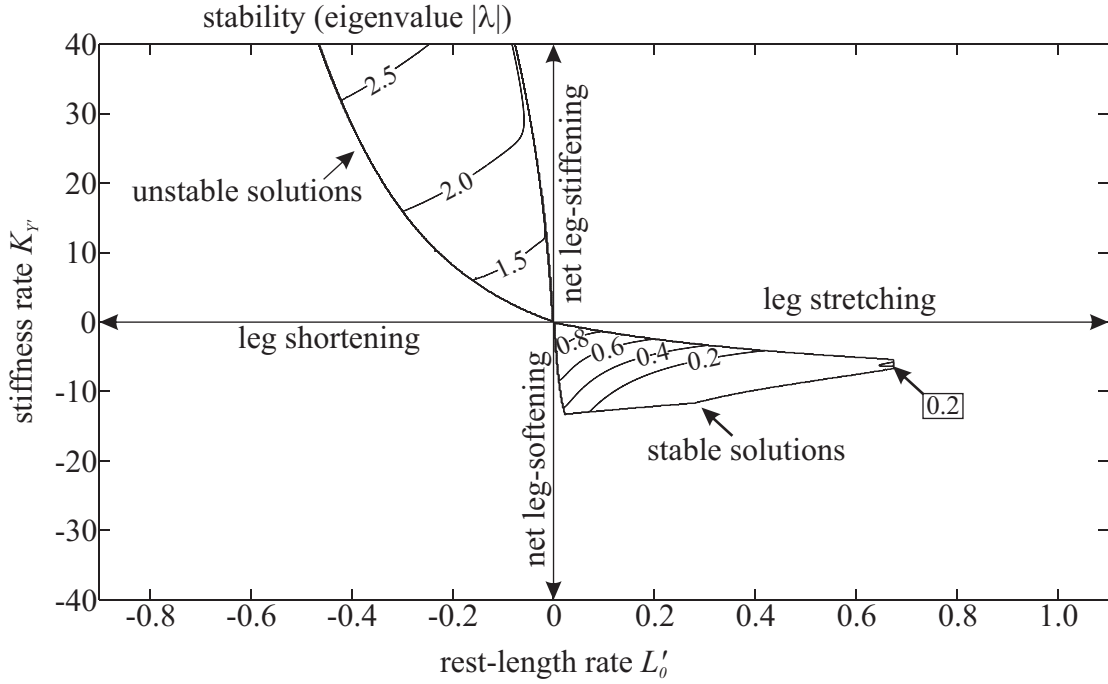


Figure 3.2.: Region of periodic hopping solutions without flight control for leg stiffness $K_{TD} = 25$. Solutions are mapped with respect to stiffness rate $K_{Y'}$ and rest-length rate L_0' . Increments of 0.1 for $K_{Y'}$ and 0.002 for L_0' were used. Eigenvalue λ for periodic hopping is displayed. Stable solutions require $|\lambda| < 1$.

3.2. Effects on Hopping

3.2.1. Basic Stability Properties are Inherited

Clearly separated regions of stable and unstable hopping solutions are inherited from the original VLS model, cf. Figures 2.4 and 3.2 as well as Figures 2.5 and 3.3. Similarly to the model with time-dependent leg stiffness, a net stiffness decrease is needed for stable hopping.

The distribution of unstable periodic hopping still is constrained between a falling-down barrier and an energy barrier, see Figure 3.3. In region II the touchdown condition, $Y_0 \geq 1$, is violated. Thus, the leg is not initialized and the mass point follows a free-fall trajectory until ground contact. Furthermore, for ever faster rest-

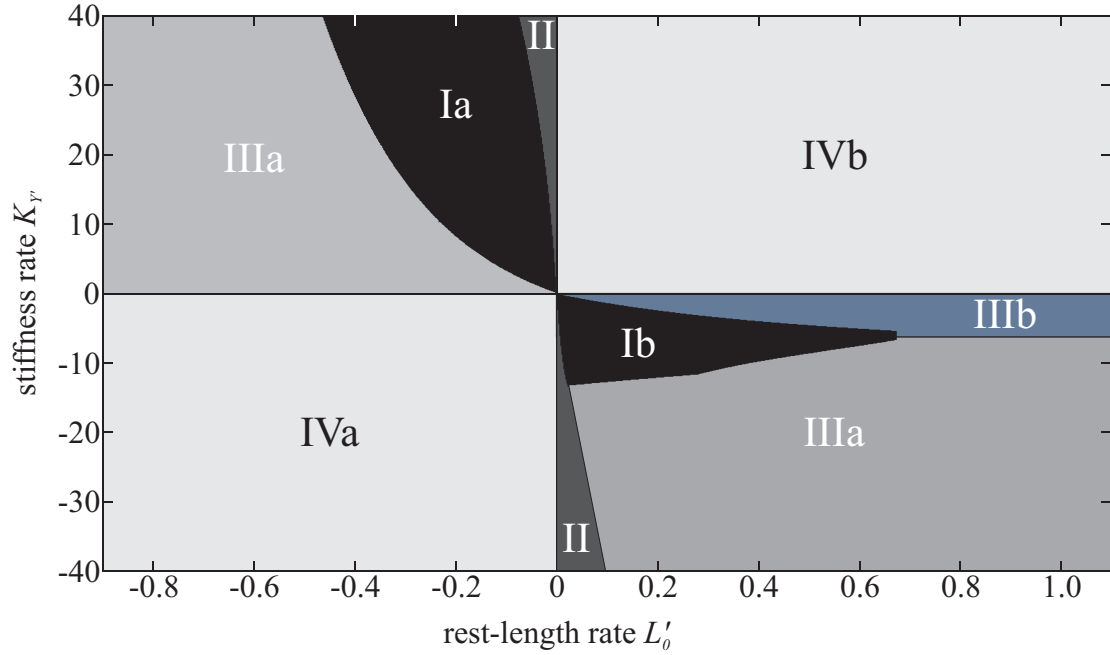


Figure 3.3.: Regions of the investigated parameter space: periodic solutions (I), ground contact within one hopping cycle (II), energy withdrawal/input cannot be fully compensated (III) and unilateral change of energy (IV).

length declines energy loss due to negative L'_0 exceeds energy injection via positive $K_{Y'}$ (region IIIa).

The shape of the domain of stable hopping is no longer J-shaped. Along with a falling-down barrier equivalent to that of the unstable solutions (region II), the area of stable solutions is now confined between regions in which actuation via leg stretching either under- or overcompensates for functional damping via leg softening, regions IIIa and IIIb respectively. Additionally, vanishing leg stiffness no longer occurs.

In any case, rest-length and leg-stiffness variation are still required to be of opposite sign. Otherwise, periodic hopping is not possible at all (regions IVa+b), as only energy input or withdrawal would take place.

However, by introducing a velocity-dependent leg stiffness, stability is increased considerably. Stable hopping requires eigenvalues $|\lambda| < 1$; the smaller $|\lambda|$ the more

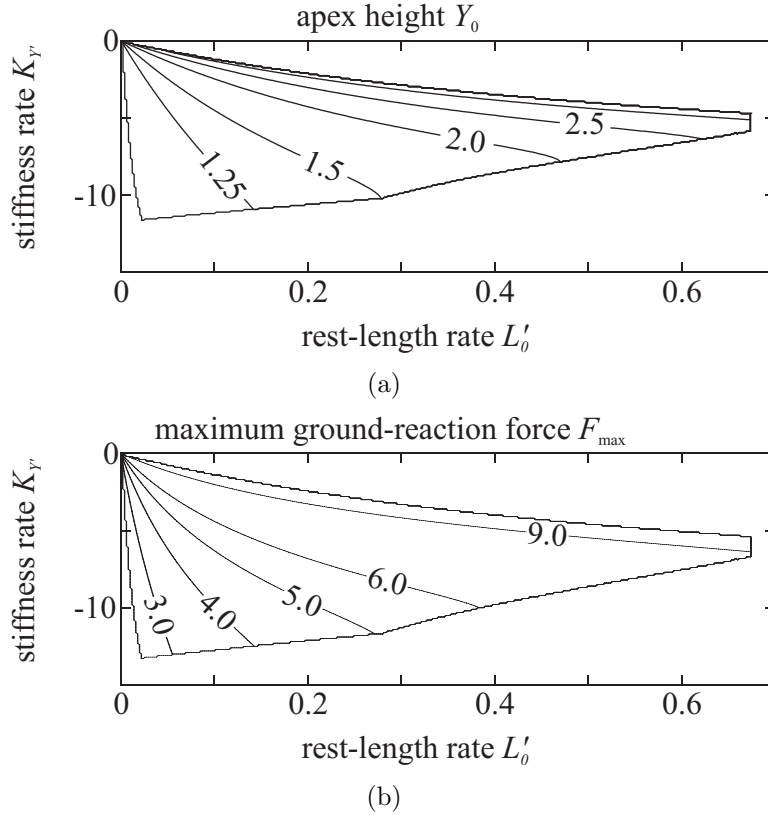


Figure 3.4.: Region of stable hopping solutions without flight control for velocity-dependent leg stiffness, $K_{TD} = 25$. Apex height (a) and maximum ground-reaction force (b) are mapped with respect to stiffness rate $K_{Y'}$ and rest-length rate L'_0 . Increments of 0.1 for $K_{Y'}$ and 0.002 for L'_0 were used.

stable the system. Instead of eigenvalues $\lambda \gtrsim 0.7$ for a time-dependent leg stiffness (without damping) now eigenvalues $\lambda \approx 0$ can be realized and therefore, perturbations can be compensated much faster.

Hopping heights are restricted to a physiologically more reasonable range, e.g. hopping height $Y_{0,\max} \approx 3$ for $K(Y')$ in comparison to $Y_{0,\max} > 10$ for $K(\tau)$, see Figures 2.6(a) and 3.4(a). Ground-reaction forces are only marginally smaller, see Figures 2.6(c) and 3.4(b). Similarly, the values of leg stiffness and rest length at takeoff remain of comparable size, cf. Figures 2.6(e,f) and 3.5.

As a result of this thesis, the VLS model has been validated conceptually also for

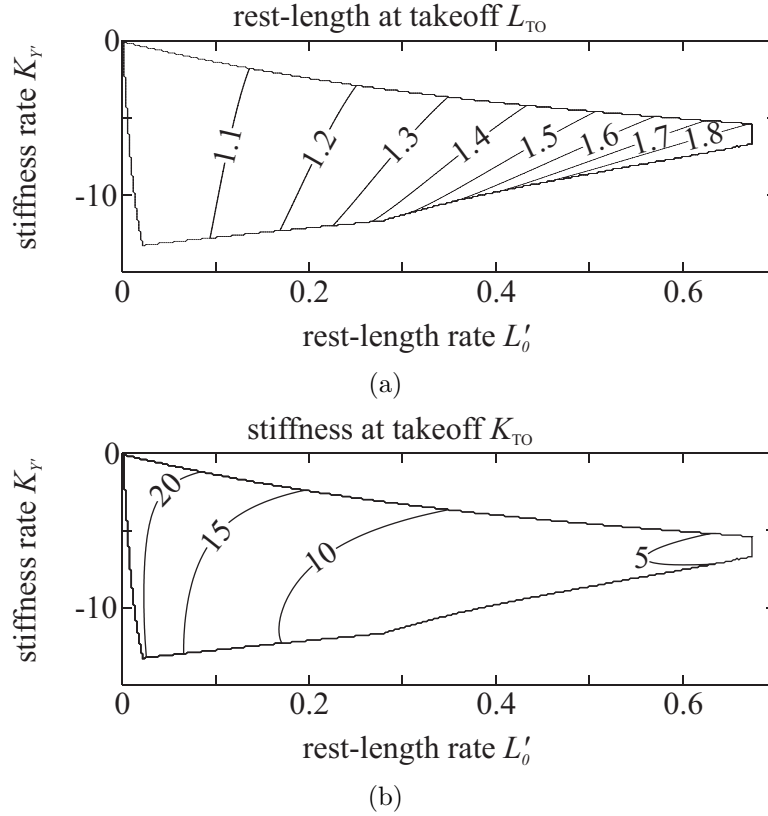


Figure 3.5.: Region of stable hopping solutions without flight control for velocity-dependent leg stiffness, $K_{TD} = 25$. Rest length at takeoff (a) and stiffness at takeoff (b) are mapped with respect to stiffness rate $K_{Y'}$ and rest-length rate L'_0 . Increments of 0.1 for $K_{Y'}$ and 0.002 for L'_0 were used.

non-linear variations of leg stiffness. For a discussion of the muscle-like properties of velocity-dependent leg-stiffness variation see Chapters 3.2.3 and 3.2.4.

3.2.2. Flight Control is Beneficial for Stable Hopping

For the modified VLS hopper with flight control the region of stable hopping considerably increases, cf. Figures 3.2 and 3.6. This is due to a constant stiffness offset during stance as a result of flight control, see Equation 3.2 as well as Figures 3.1 and 3.7: As stiffness $K(Y')$ influences the magnitude of energy changes within the system, see Equations 3.7 and 3.8, it also affects the equilibrium of energy input

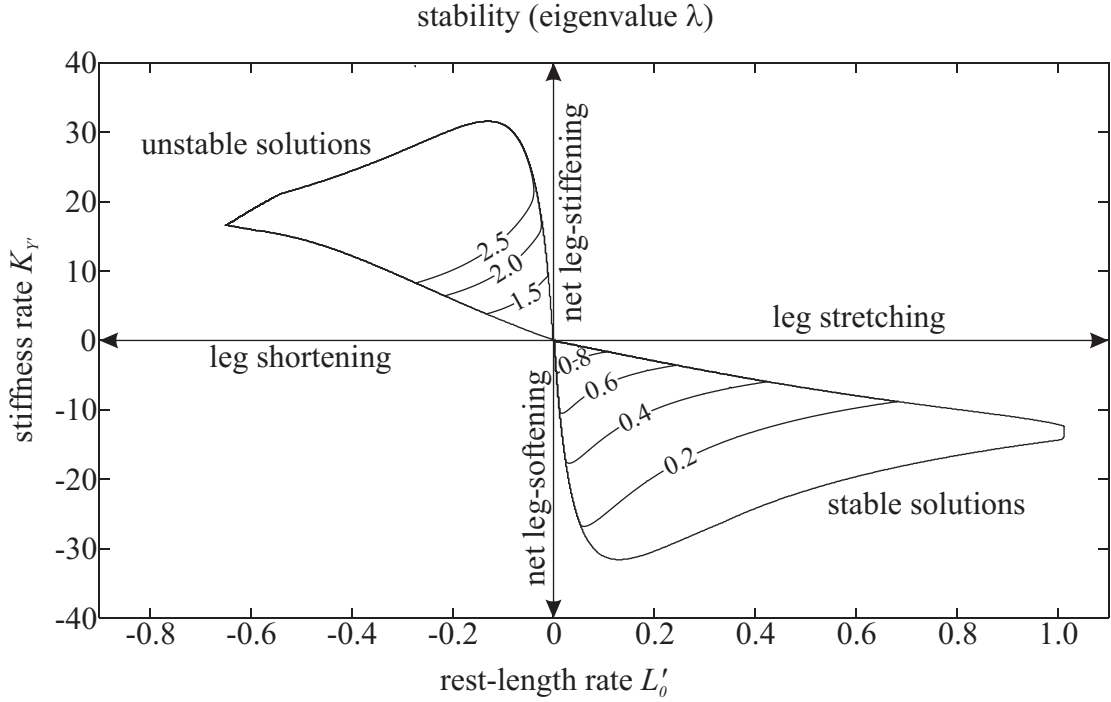


Figure 3.6.: Region of periodic hopping solutions with flight control for leg stiffness $K_{\text{Apex}} = 25$. Eigenvalue λ for periodic hopping is shown. Stable solutions require $|\lambda| < 1$. Results are mapped with respect to stiffness rate $K_{Y'}$ and rest-length rate L'_0 . Increments of 0.1 for $K_{Y'}$ and 0.002 for L'_0 were used.

and withdrawal necessary to allow for periodic hopping. Hopping heights Y_0 and maximum ground-reaction forces F_{max} do not change considerably, cf. Figures 3.4 and 3.8.

As eigenvalues of the modified VLS hopper without flight control already reach $\lambda \approx 0$, i.e. perfect stability with perturbations being dissipated within one hopping cycle, the potential effect of flight control on hopping stability is less obvious than could be expected by the results of Blum et al. (2010). However, the accessible control space is spread substantially, as well the areas of a given level of stability. Hence, in order to maintain a certain level of stability at a certain hopping height, a wider range of control parameters is applicable, i.e. less precise, “relaxed” control

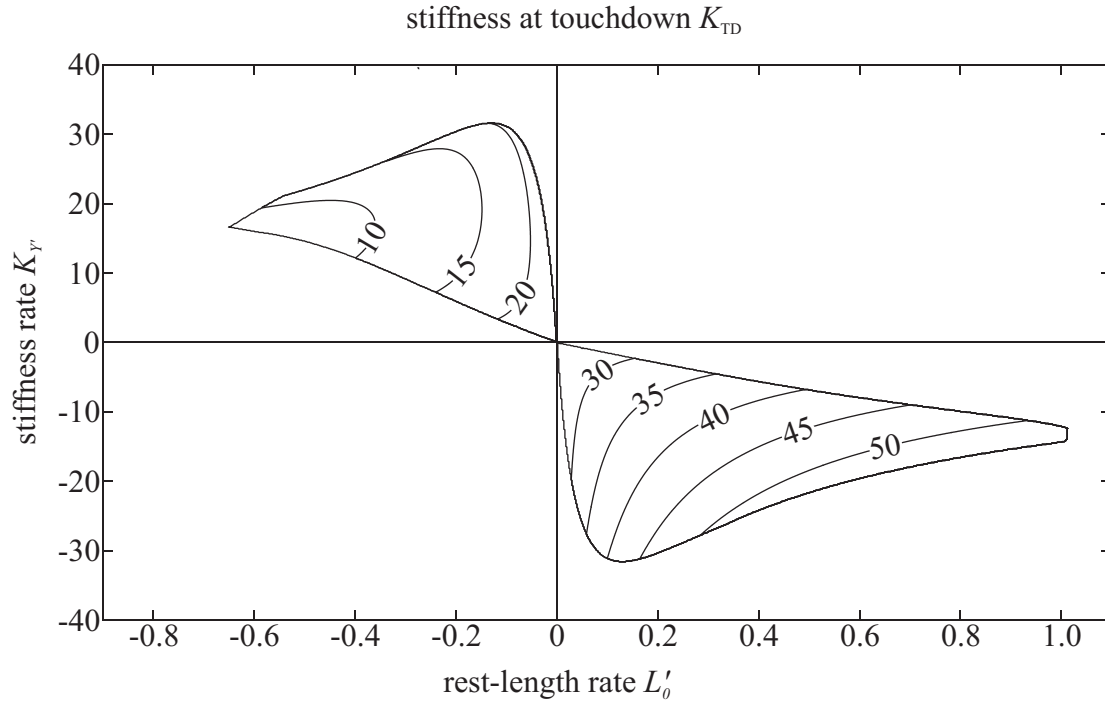


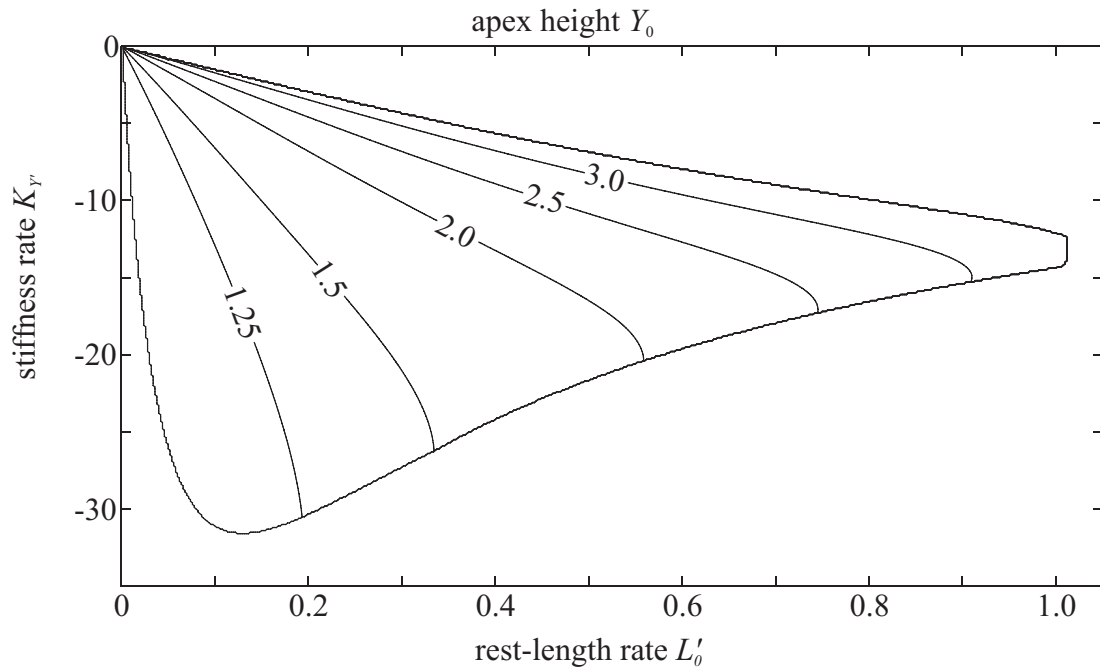
Figure 3.7.: Region of periodic hopping solutions with flight control for velocity-dependent leg stiffness, $K_{\text{Apex}} = 25$. Stiffness at touchdown K_{TD} is shown. Results are mapped with respect to stiffness rate $K_{Y'}$ and rest-length rate L'_0 . Increments of 0.1 for $K_{Y'}$ and 0.002 for L'_0 were used.

suffices, see Figures 3.6 and 3.8(a).

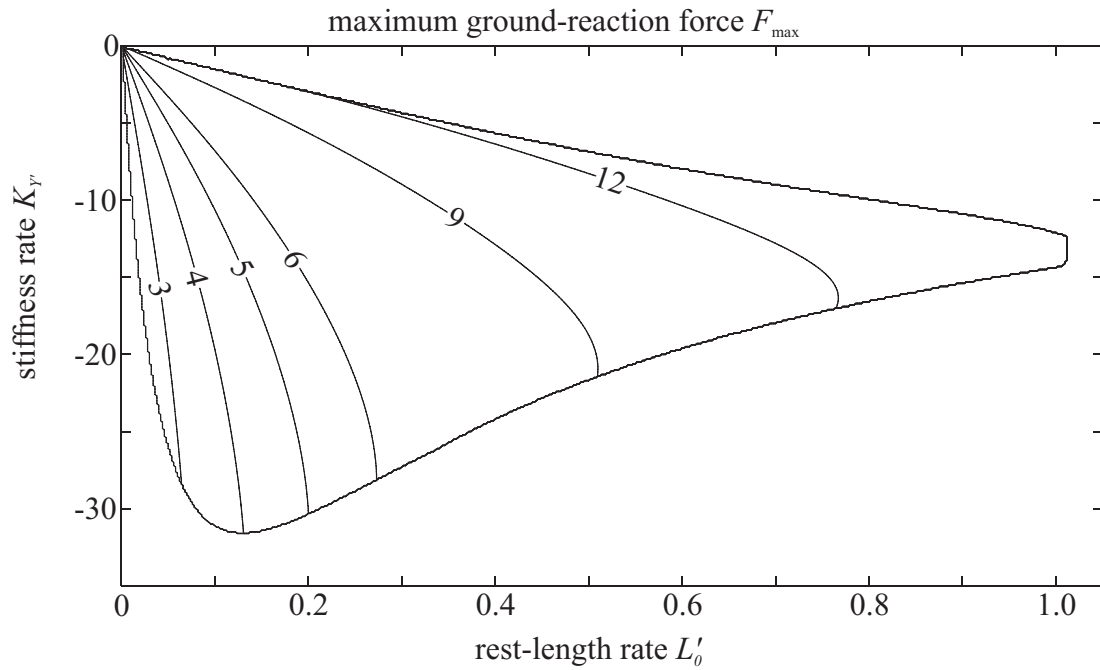
3.2.3. Muscle-like Properties are Beneficial for Stable Hopping

Increasing landing-takeoff asymmetry is associated with increasing stability, see Figure 3.9. The more the model deviates from a perfect spring, with the peak in ground-reaction force closer to touchdown, the more stable the movement is. Deviation from elastic behavior also decreases work ratio η , Figure 3.10(b), with roughly only one third of all work in the system done elastically for solutions with eigenvalues $\lambda \approx 0$.

Unlike in the VLS model with time-dependent leg stiffness, the tradeoff between robustness and cost of movement is less pronounced, see Figure 3.11. Hopping solutions with maximum robustness may be achieved at low to medium cost of

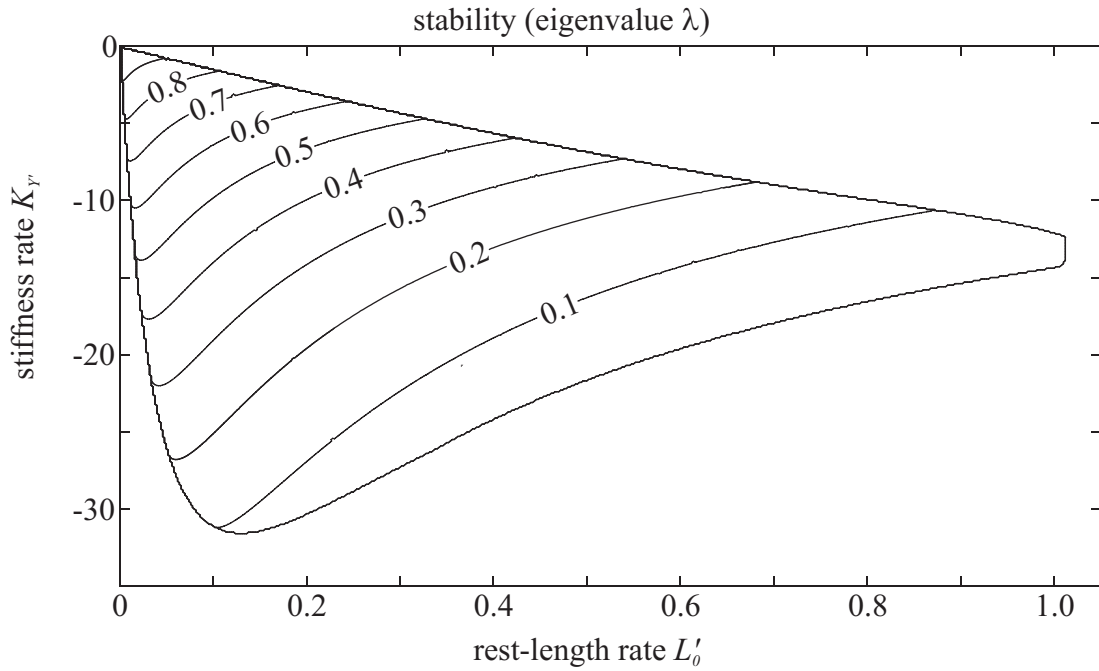


(a)

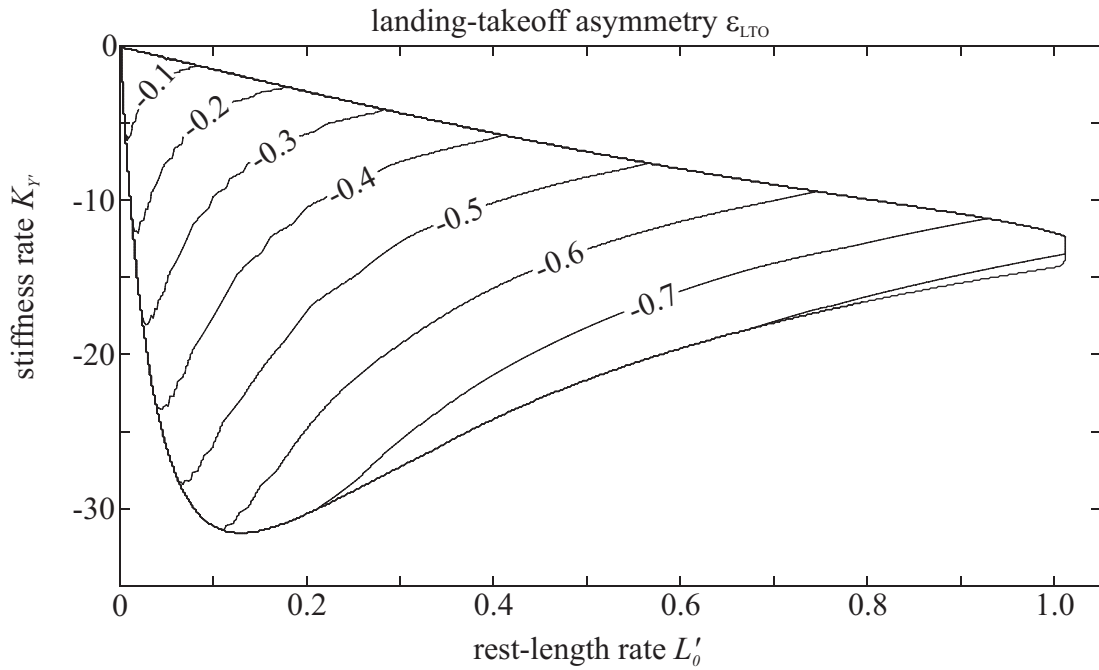


(b)

Figure 3.8.: Region of stable hopping solutions with flight control for velocity-dependent leg stiffness, $K_{\text{Apex}} = 25$. Apex height (a) and maximum ground-reaction force (b) are shown. Results are mapped with respect to stiffness rate $K_{Y'}$, and rest-length rate L'_0 . Increments of 0.1 for $K_{Y'}$, and 0.002 for L'_0 were used.

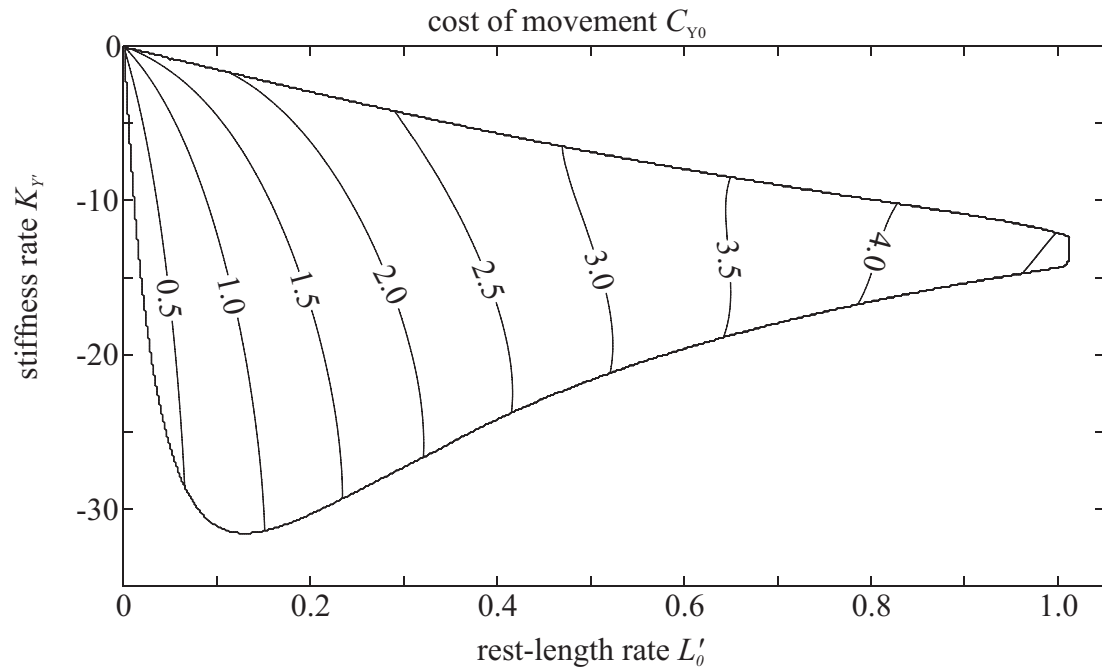


(a)

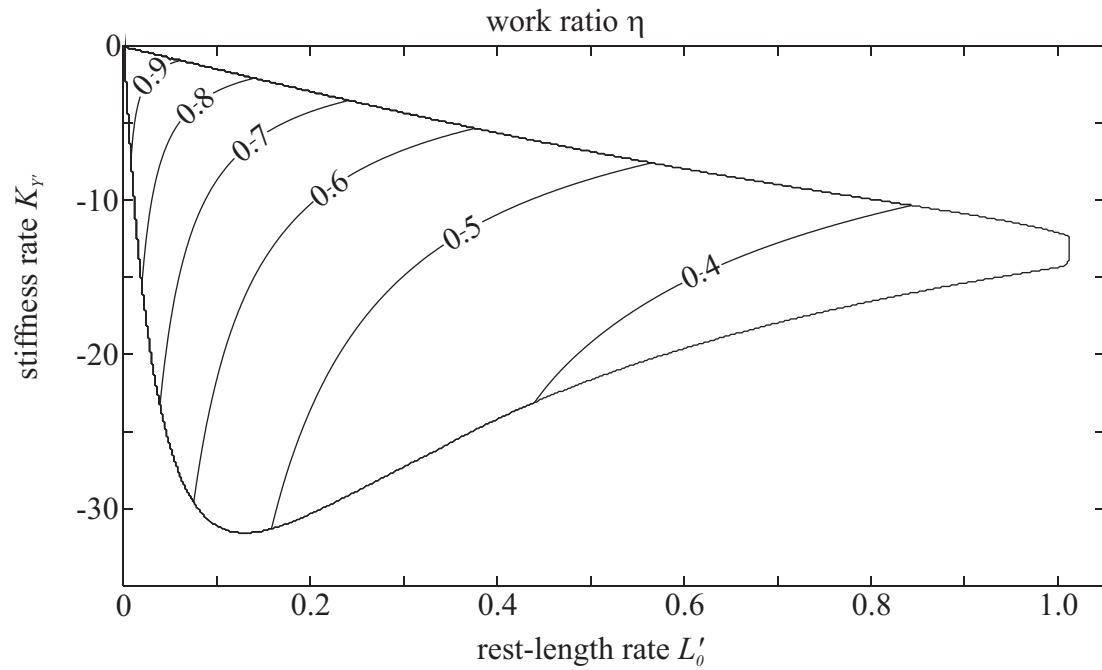


(b)

Figure 3.9.: Region of stable hopping solutions with flight control for velocity-dependent leg stiffness, $K_{\text{Apex}} = 25$. Stability (eigenvalue λ) (a) landing-takeoff asymmetry ε_{LTO} (b) are mapped with respect to stiffness rate K_y and rest-length rate L'_0 . Increments of 0.1 for K_y and 0.002 for L'_0 were used.



(a)



(b)

Figure 3.10.: Region of stable hopping solutions with flight control for velocity-dependent leg stiffness, $K_{\text{Apex}} = 25$. Cost of Movement C_{Y_0} (a) and work ratio η (b) are mapped with respect to stiffness rate K_Y' and rest-length rate L'_0 . Increments of 0.1 for K_Y' and 0.002 for L'_0 were used.

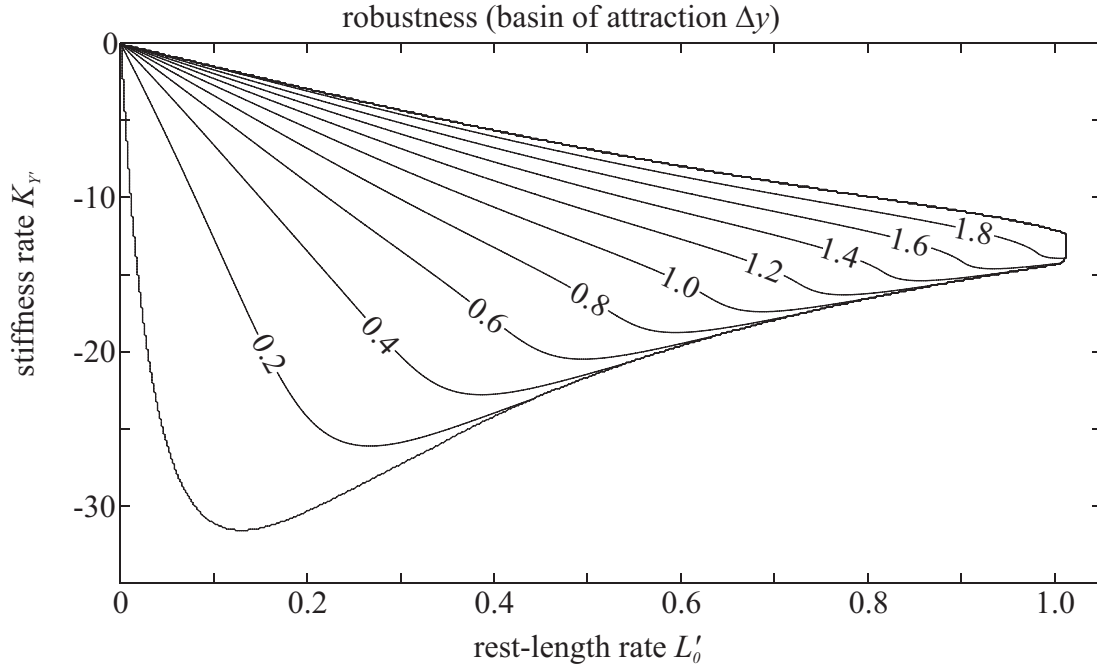


Figure 3.11.: Region of stable hopping solutions with flight control for velocity-dependent leg stiffness, $K_{\text{Apex}} = 25$. Robustness is mapped with respect to stiffness rate K' and rest-length rate L'_0 . Increments of 0.1 for $K_{Y'}$ and 0.002 for L'_0 were used.

movement. Furthermore, in the modified VLS model there are areas with optimal stability and robustness.

As aforementioned, the VLS model has been validated conceptually for non-linear stiffness variation. Muscle-like properties have proven to be beneficial for stable and robust hopping movements. Stability arises due to reflexes, i.e. zero-time-delay control based on mechanical properties of the system (Brown and Loeb, 1997; Haeufle et al., 2010). Here, mimicking the negative slope of the force-velocity function via velocity-dependent stiffness declines during stance, “functional” damping, is key. Energy dissipated by functional damping is compensated for via time-dependent rest-length increases.

Such combinations of reflexes and feedforward motor patterns reflect recent approaches in robotics, e.g. Cham et al. (2000). With usage of actuators with built-in

muscle-like properties mimicking the force-velocity relationship of HILL-type muscle models, e.g. Haeufle et al. (2010), control effort could be highly facilitated: Muscle-like properties improve hopping stability and robustness at cost of energy efficiency. Neural control enables the muscle to behave more spring-like. The level of stability and energy efficiency can be tuned on demand, with completely elastic behavior as one extreme (perfect efficiency, no hopping stability).

3.2.4. Comparison with a Template Muscle-Model

In order to compare the VLS hopper with the muscle model of Haeufle et al. (2010), the following hybrid approach was employed: At first, center-of-mass trajectory Y , center-of-mass velocity Y' and ground-reaction force F_{leg} for all parameter combinations $(L'_0, K_{Y'})$ resulting in periodic hopping for the modified VLS model with flight control were normalized to stance time. Secondly, force-length function $F_l(Y)$

$A(\text{const.}, \text{const.})$	$A(\text{const.}, \text{lin.})$	$A(\text{const.}, \text{Hill})$
$Y_0 = 1.072$	$Y_0 = 1.089$	$Y_0 = 1.051$
$F_{\text{max}} = 3.000$	$F_{\text{max}} = 3.214$	$F_{\text{max}} = 2.720$
$\lambda = 0.172$	$\lambda = 0.141$	$\lambda = 0.233$
$L'_0 = 0.064$	$L'_0 = 0.078$	$L'_0 = 0.046$
$K_{Y'} = -28.1$	$K_{Y'} = -29.6$	$K_{Y'} = -25.0$
$A(\text{lin.}, \text{const.})$	$A(\text{lin.}, \text{lin.})$	$A(\text{lin.}, \text{Hill})$
–	–	–
$A(\text{Hill}, \text{const.})$	$A(\text{Hill}, \text{lin.})$	$A(\text{Hill}, \text{Hill})$
$Y_0 = 1.072$	$Y_0 = 1.089$	$Y_0 = 1.051$
$F_{\text{max}} = 2.997$	$F_{\text{max}} = 3.214$	$F_{\text{max}} = 2.718$
$\lambda = 0.170$	$\lambda = 0.141$	$\lambda = 0.230$
$L'_0 = 0.064$	$L'_0 = 0.078$	$L'_0 = 0.046$
$K_{Y'} = -28.2$	$K_{Y'} = -29.6$	$K_{Y'} = -25.1$

Table 3.2.: Maximum hopping height for stable VLS hopping corresponding to a feasible solution for the muscle model, i.e. muscle activation satisfying $0 \leq A(F_Y, F_{Y'}) \leq 1$. Furthermore, maximum ground-reaction force F_{max} , eigenvalue λ and the control parameters, L'_0 and $K_{Y'}$, corresponding to that solution are shown.

and force-velocity function $F_v(Y')$ were calculated each at all three levels of approximation (constant, linear and HILL-like). Thus, there are nine combinations of force-length and force-velocity function. Finally, Equation 3.15 was solved for activation state $A(\tau)$ and parameter combinations violating $0 \leq A(\tau) \leq 1, \forall \tau$ were omitted. The region of periodic hopping that is consistent with the modified VLS hopper as well as the template muscle-model, is displayed in Figure 3.12 for all combinations of $F_l(Y)$ and $F_v(Y')$.

As can be seen in Figure 3.12, there are no stable solutions (color-coded blue) for a linear force-length function. This is due to the fact, that for stable VLS hopping the leg needs to be stretched. Thus, momentary leg length necessarily exceeds touchdown leg-length during decompression, $Y > 1$. Therefore, F_l would become negative, see Equation 3.13 (linear), resulting in a negative muscle activation $A(\tau)$ and violating the activation constraint.

Due to the parameter choices for the muscle model, maximum leg force is roughly constrained to maximum isometric force of the muscle, $F_{\text{leg,max}} \approx F_{\text{iso}} = 3$, see Table 3.2. Thus, only a fraction of the periodic hopping solutions for the modified VLS model are also accessible for the muscle model. The only exceptions are some combinations with linear force-length function. As there is substantial leg compression for the modified VLS model and as the muscle model is assumed to generate the same center-of-mass movement, force amplification via the force-length function allows for maximum ground-reaction forces up to $F_{\text{max}} \approx 9$ for linear F_l and constant F_v or $F_{\text{max}} \approx 5.5$ for both linear F_l and F_v . For linear force-length function and HILL-type force-velocity function however, there is no overlap of periodic hopping for the modified VLS hopper and the muscle model.

In the case of linear force-length function and constant force-velocity function, the maximum periodic hopping height also considerably exceeds the results of Haeufle et al. (2010), $Y_{0,\text{max}} \approx 2.3$ as opposed to $Y_{0,\text{max}} \approx 1.1$. In all other cases, maximum hopping heights are slightly smaller, see Table 3.2. In accordance with the results

of Haeufle et al. (2010), the overlap region of both models decreases for an increase in complexity of the force-velocity function, see 3.12. However, with respect to hopping height the constant F_v is outperformed by the linear one. The differences for an increasingly more complex force-length function are marginal, see Table 3.2. Maximum hopping heights are the same for constant and HILL-type force-length function, while the HILL-type F_l is slightly more stable. Furthermore, activation patterns hardly differ in these cases, see Figure 3.12.

The landing-takeoff asymmetry of the calculated activation patterns is related to the asymmetry of the ground-reaction forces of the VLS model. All activation patterns resulting in unstable hopping share the feature of maximum activation during decompression. This is in contradiction to physiological data, e.g. Cavagna and Legramandi (2009), showing higher activation during compression, as more support of the body weight is needed during that phase in order to avoid falling down. Accordingly, for constant F_v , stable hopping requires maximum activation during compression. For increasing complexity of the force-velocity function, activation is more or less symmetric. As activation patterns for HILL-type force-length function resemble those for $F_l = 1$, it may be argued that, in the muscle model, the force-velocity function mimics viscous, muscle-like properties of the leg, while activation corresponds to elastic, spring-like properties.

The results show the close relationship between the modified VLS hopper and the template muscle-model of Haeufle et al. (2010) for hopping. In fact, if the muscle model with linear force-length and force-velocity function would be extended to incorporate linear-in-time variations of rest length, the models would be equivalent. Both models emphasize the supporting effects of muscle-like properties for stable hopping as reported in other studies, e.g. Van der Krogt et al. (2009).

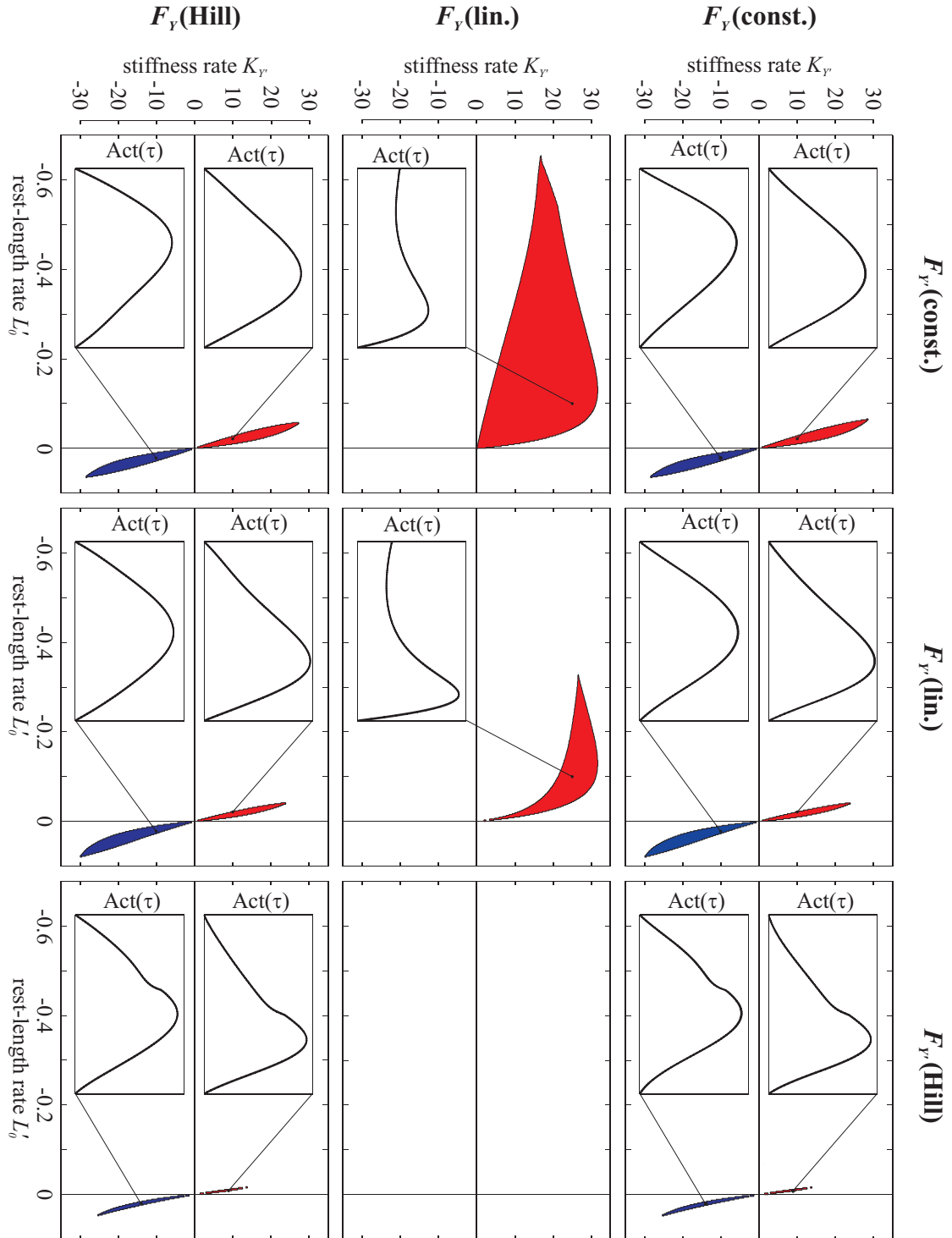


Figure 3.12.: Region of periodic hopping corresponding to a feasible solution for the muscle model, i.e. muscle activation satisfying $0 \leq A(F_Y, F_{Y'}) \leq 1$. Red corresponds to unstable and blue to stable hopping. Additionally, representative activation pattern normalized to stance time are displayed.

4. Variable Leg-Spring Properties in Human Hopping

The following chapter is based on Riese et al. (2012). The analyses and results in this chapter are the contribution of the author of this thesis. Discussions with A. Seyfarth and S. Grimmer were appreciated. The experiments were conducted by S. Grimmer.

4.1. Extraction of Leg-Spring Properties from the Data

4.1.1. Experimental Setup

Six healthy male subjects (76.5 ± 8.4 kg) participated in the study. Prior to the measurements, the experiment was approved by the ethics review board of the University of Jena, as laid out in the Declaration of Helsinki, and all subjects gave their written informed consent.

The subjects were asked to perform vertical jumps on both legs. Initially, each subject was instructed to jump with self-selected frequency (and height). Then, following Farley (1991), the hopping frequencies 1.2 Hz, 1.8 Hz, 2.8 Hz and 3.6 Hz were prescribed with a metronome. The sequence of hopping frequencies was randomized for each subject.

Each trial was of 30 seconds length. At the beginning and end of each trial, the subjects were asked to stand quiet for five seconds, leaving 20 seconds of vertical hopping, resulting in approximately 20 – 50 hopping cycles depending on subject and frequency.

4.1.2. Kinematics and Kinetics

In order to obtain kinematics, 17 reflective markers were placed on each subject. Spatial positions of the markers were measured with 1 kHz using a ten-camera infrared system (Proflex MCU240, Qualisys, Gothenburg, Sweden). From this data, the center-of-mass (CoM) position was calculated in accordance to Dempster’s body segment parameter data (Dempster, 1955; Winter, 2009).

Ground-reaction forces (GRF) were measured directly with 1 kHz using a Kistler force platform. Furthermore, using a custom MATLAB routine, the center-of-pressure (CoP) position was extracted from GRF data.

4.1.3. Estimation of stiffness and rest length

In order to estimate global leg properties, the SLIP model was used: All mass was assumed to be located in the center of mass and the leg was approximated as a massless spring, connecting center of mass and center of pressure, see Figure 4.1. As this thesis is focused on vertical hopping, ground-reaction forces and center-of-mass movement were projected into leg direction. Therefore, in the coordinate system aligned with the leg the three-dimensional data set is reduced to one-dimensional (“vertical”) hopping.

Additionally, ground-reaction forces were normalized to body weight and momentary leg length to initial center-of-mass height l_{init} . Thus, estimated stiffness and rest length are non-dimensional. As the GRF and leg-length data is noisy, both data sets were smoothed using a lowpass Butterworth filter of 5th order, with a cut-off

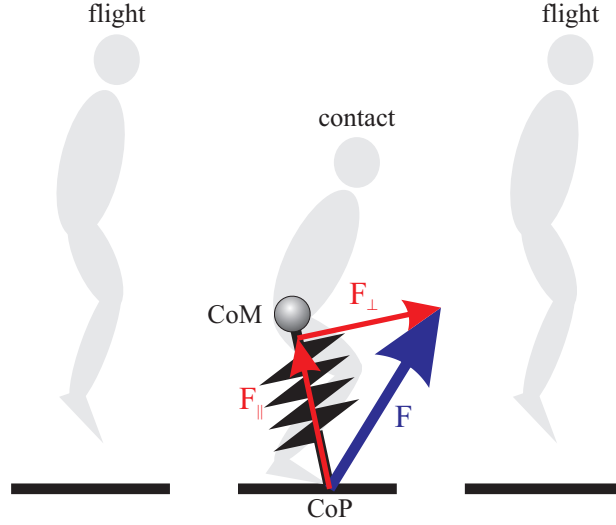


Figure 4.1.: Underlying SLIP model during human hopping. All mass is located in the center of mass (CoM) and the leg length is assumed to be the distance between center of mass and center of pressure (CoP). The misalignment of the ground-reaction force (GRF) and the leg was exaggerated to illustrate the GRF contributions parallel and perpendicular to the leg direction, F_{\parallel} and F_{\perp} respectively.

frequency of 25 Hz.

For each trial, stance phases ($F_{\parallel} \geq 0.01 \text{ BW} \approx 5 - 10 \text{ N}$) were extracted and normalized to 100% stance time. Ground-reaction forces F_{\parallel} and leg length L were interpolated accordingly. Following Rozendaal and van Soest (2008); Peter et al. (2009) and assuming a linear spring at each time step $i = 1, 3, \dots, 99$, the equation

$$\begin{pmatrix} F_{\parallel}(i) \\ F_{\parallel}(i+1) \end{pmatrix} = K(i) \cdot \begin{pmatrix} L_0(i) - L(i) \\ L_0(i) - L(i+1) \end{pmatrix} \quad (4.1)$$

had to be solved. As there are two unknowns per time step i , $K(i)$ and $L_0(i)$, it was assumed that $K(i) \equiv K(i+1)$ and $L_0(i) \equiv L_0(i+1)$. Even though in this approach the spring is linear for two consecutive time steps, resulting parameter profiles may be non-constant, leading to a non-linear spring throughout stance. To

ensure physically meaningful solutions, stiffness is constrained to values $K > 0$. Accordingly, during stance rest length has to satisfy $L_0 > L$, as $L_0 = L$ denotes the transition from flight to stance phases and vice versa.

As a first approach, stiffness and rest length were calculated directly by solving Equation 4.1 analytically for $K(i)$ and $L_0(i)$. However, the constraints for stiffness and rest length were violated for a considerable amount of time steps, especially for frequencies below the preferred frequency f_p . Thus, Equation 4.1 was solved numerically with the least-squares method *lsqcurvefit* implemented in MATLAB (R2010a, The MathWorks Inc., Natick, MA, USA) using the constraints for K and L_0 as lower boundaries.

4.2. Results

Except at 1.2 Hz, results presented here for a given frequency are means over all trials of all six subjects at that frequency. At 1.2 Hz, behavior of half the subjects distinctively differs from that of the other half, thus denoted in the figures as “1.2 Hz I” and “1.2 Hz II”, respectively. Furthermore, at each frequency there is some variability between trials of each subject. However, these data sets show a similar qualitative behavior and no relevant information is lost by averaging.

4.2.1. Measured data

Center-of-mass movement during stance, i.e. momentary leg length $L(i)$, for frequencies from f_p to 3.6 Hz corresponds to running-like spring-mass dynamics, whereas at 1.2 and 1.8 Hz also walking-like center-of-mass trajectories were measured, see Figure 4.2(a). While at 1.2 Hz there are two distinct subsets of behavior, “1.2 Hz I” and “1.2 Hz II”, at 1.8 Hz the quantities estimated from the data exhibit a similar qualitative behavior for all subjects. Thus, at 1.8 Hz means over all subjects are displayed. center-of-mass height at touchdown decreased with frequency (except

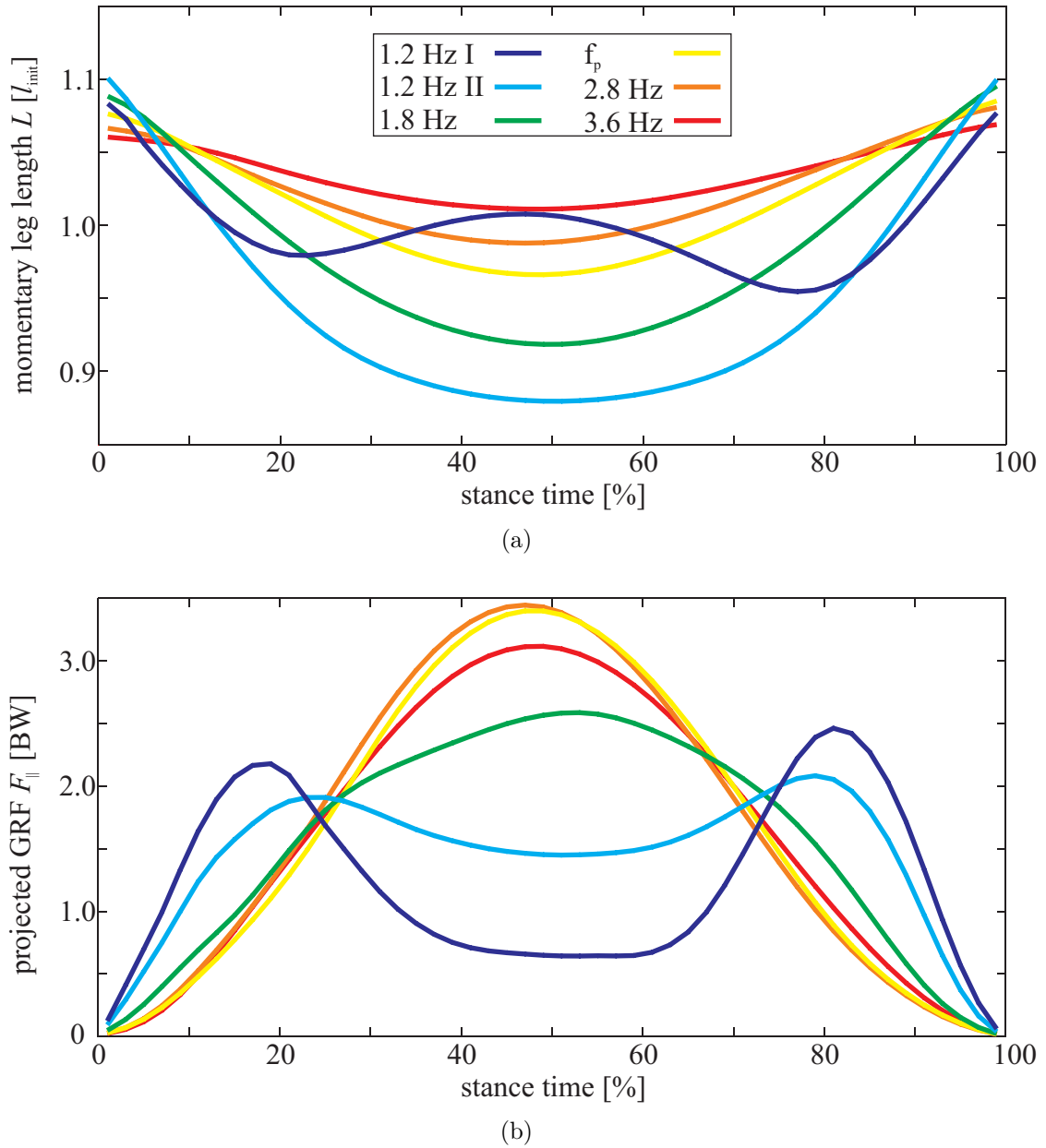


Figure 4.2.: Human hopping data. Center-of-mass movement projected into leg direction, (a), and the projected ground-reaction forces, (b), are shown over stance time. Human hopping was investigated for five different hopping frequencies (ranging from 1.2 to 3.6 Hz). Results are means over all trials of all subjects at a given frequency (at 1.2 Hz there are two distinct subsets consisting of half the subjects each).

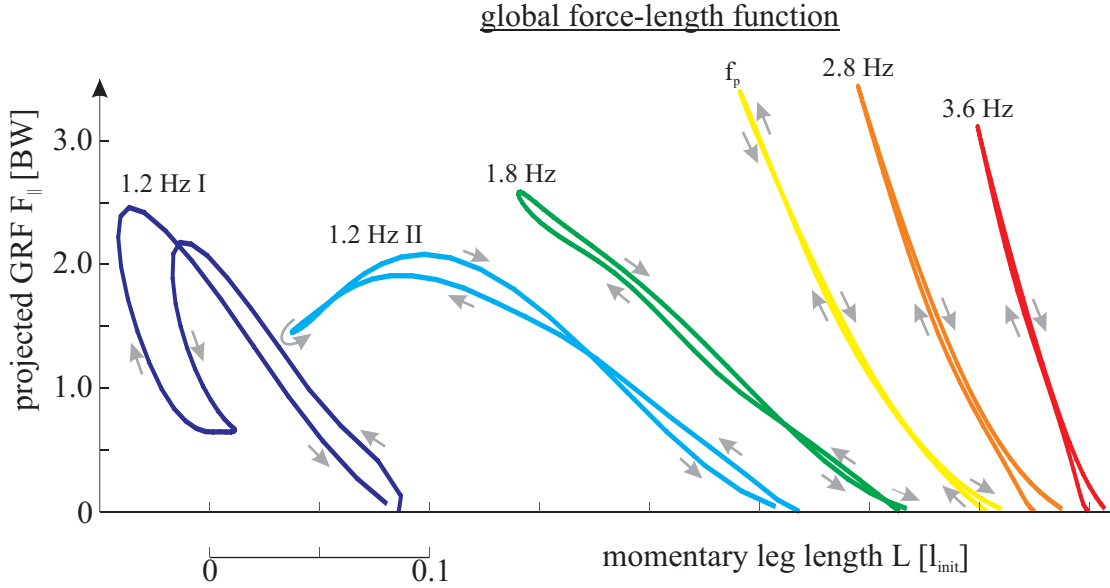


Figure 4.3.: Human hopping data. The global force-length function (FLF) resulting from center-of-mass movement and ground-reaction force is displayed. Human hopping was investigated for five different hopping frequencies (ranging from 1.2 to 3.6 Hz). Results are means over all trials of all subjects at a given frequency (at 1.2 Hz there are two distinct subsets consisting of half the subjects each).

at “1.2 Hz I”), so did center-of-mass displacement and center-of-mass position at take-off.

Accordingly, GRF profiles $F_{||}(i)$ for hopping ranging from f_p up to 3.6 Hz feature only a single peak, as expected from spring-mass hopping, see Figure 4.2(b). Impacts were not observed; this is true for all trials and not an averaging effect. For 1.2 Hz walking-like double-peak patterns were observed (even though half the subjects exhibit running-like center-of-mass trajectories). As this frequency is quite low, subjects avoided premature takeoff by decreasing leg force around midstance, resulting in a second compression-decompression phase. For 1.8 Hz two of the subjects mostly exhibit double-peak hopping, while the rest mostly features single-peak GRF patterns. Thus, hopping at this frequency is of transitory behavior. In the mean, however, single-peak hopping takes place.

Resulting from ground-reaction forces and center-of-mass movement, the global force-length function (FLF) is fairly linear down to 1.8 Hz, see Figure 4.3. However, at 1.2 Hz it is highly non-linear.

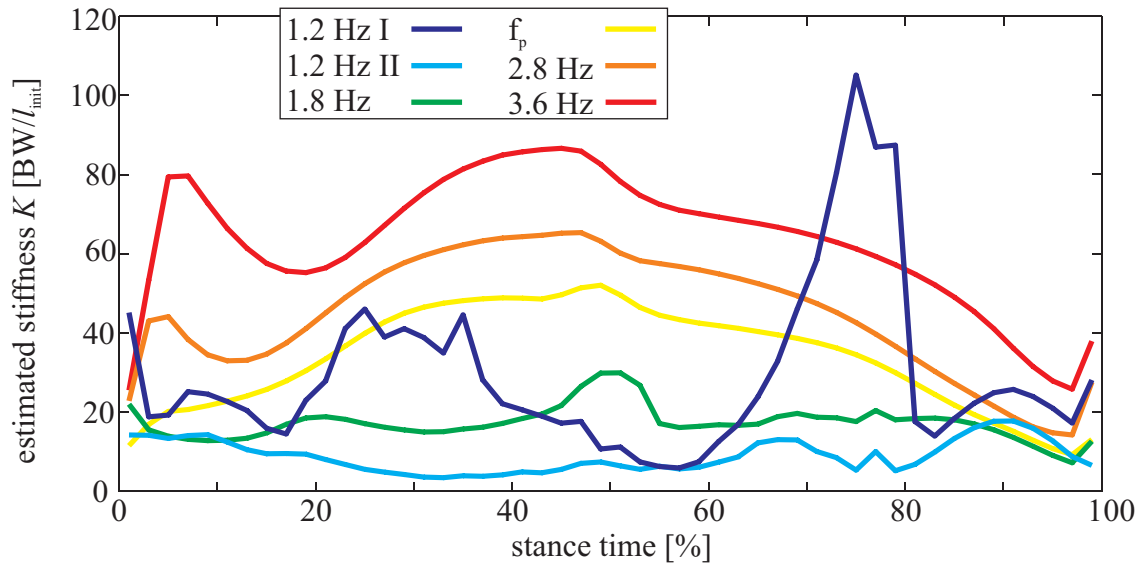
4.2.2. Estimation results

For hopping within f_p -3.6 Hz the stiffness profiles $K(t)$ are roughly bell-shaped, with increasing maximum stiffness for increasing frequency, see Figure 4.4(a). At 2.8 and 3.6 Hz also an additional impact-like maximum is present in the stiffness pattern. However, in the force profiles no impacts were observed. This deviation from the bell shape may be a result of muscle activation in anticipation of touchdown for these rapid hopping movements (Seyfarth et al., 2000). At 1.2 and 1.8 Hz there are considerable stiffness fluctuations over stance time. Most prominently, for “1.2 Hz I” there is a clear maximum during the second GRF peak, indicating an active push-off. This assumption also is supported by the energy profiles displayed in Figures 4.6 and 4.7. At 1.2 and 1.8 Hz considerably more energy is stored in the spring than at higher frequencies, resulting in substantial fluctuations of total energy, with maximum spring energy coinciding with maximum stiffness for “1.2 Hz I”.

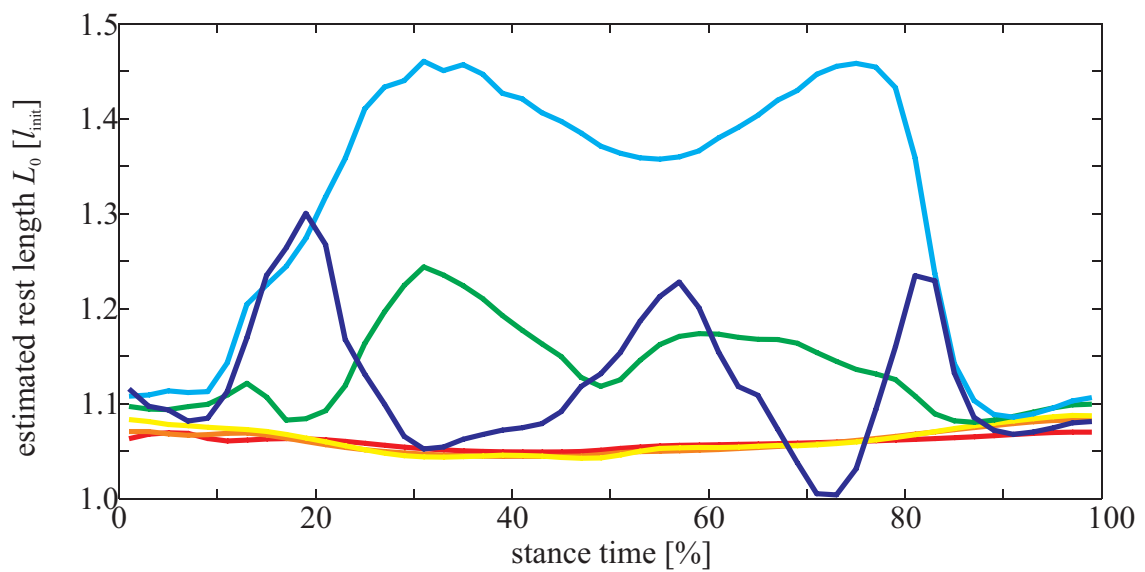
Rest-length profiles $L_0(i)$ at f_p to 3.6 Hz resemble the center-of-mass movement, cf. Figures 4.4(b) and 4.2(a), while leg displacement $\Delta L(i) = L_0(i) - Y(i)$ resembles the ground-reaction forces, cf. Figures 4.5 and 4.2(b). At 1.2 Hz, rest length $L_0(i)$ and displacement $\Delta L(i)$ for half of the subjects feature a plateau with an indent around midstance, “1.2 Hz II”, while the other half exhibits a triple-peak pattern, “1.2 Hz I”. At 1.8 Hz, again transitory behavior is observed.

In Figure 4.8 the corrected force-length functions are shown for all measured frequencies, using the leg compression $\Delta L(i)$ instead of the actual leg length $L(i)$. Due to the estimated rest-length profile $L_0(i)$, non-linearity of the corrected force-length function at 1.2 Hz considerably increased with respect to the uncorrected case. At 1.8 Hz the corrected force-length function now is non-linear, also due to

the estimated $L_0(i)$ pattern. For all other measured hopping frequencies a linear approximation of the force-length function is still applicable.



(a)



(b)

Figure 4.4.: Estimated leg parameters, stiffness K and rest length L_0 , over stance time. Results are means over all trials of all subjects at a given frequency (at 1.2 Hz there are two distinct subsets consisting of half the subjects each).

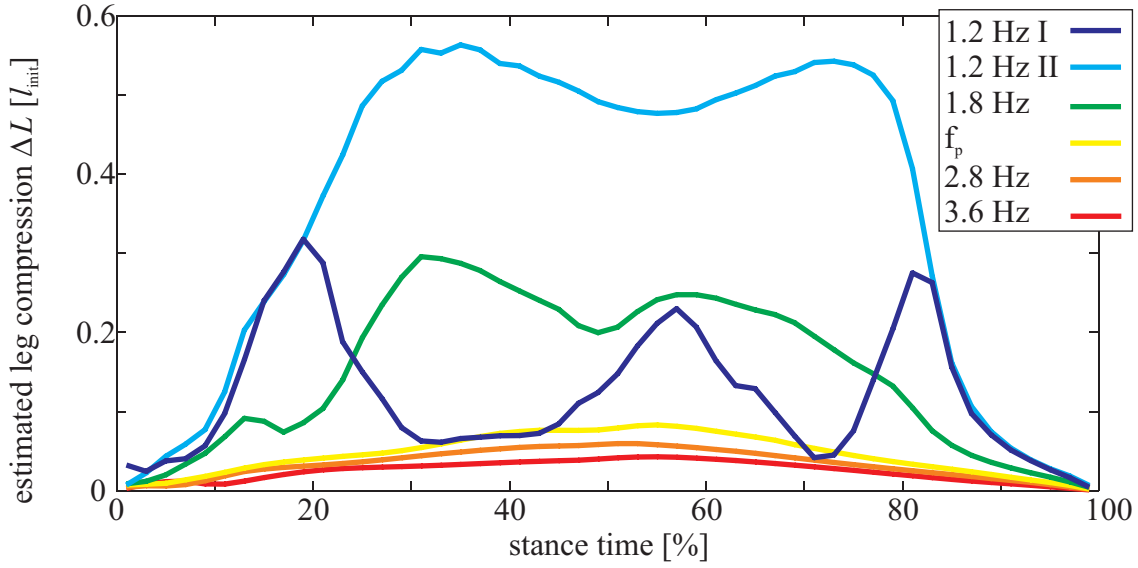


Figure 4.5.: Estimated leg compression $\Delta L = L_0 - L$ over stance time is shown. Results are means over all trials of all subjects at a given frequency (at 1.2 Hz there are two distinct subsets consisting of half the subjects each).

4.3. Variable Leg-Spring Properties

It was found that for vertical human hopping stiffness and rest length change during stance, see Figure 4.4. These findings contradict the well-established assumption that due to its linear force-length function hopping features constant spring parameters. On the contrary, the results are in better agreement the VLS concept. In order to achieve orbital stability, stiffness decreases were key. As a first-order approximation for parameter variability, stiffness and rest length were assumed to change linearly with stance time. The stiffness and rest-length profiles estimated from experimental data are much more complex than this simple approximation. Even though there is no general trend between touchdown and takeoff, simultaneous variation of stiffness and rest length in the model could now be validated based on experimental data.

It is still an open question how global leg properties relate to properties on joint

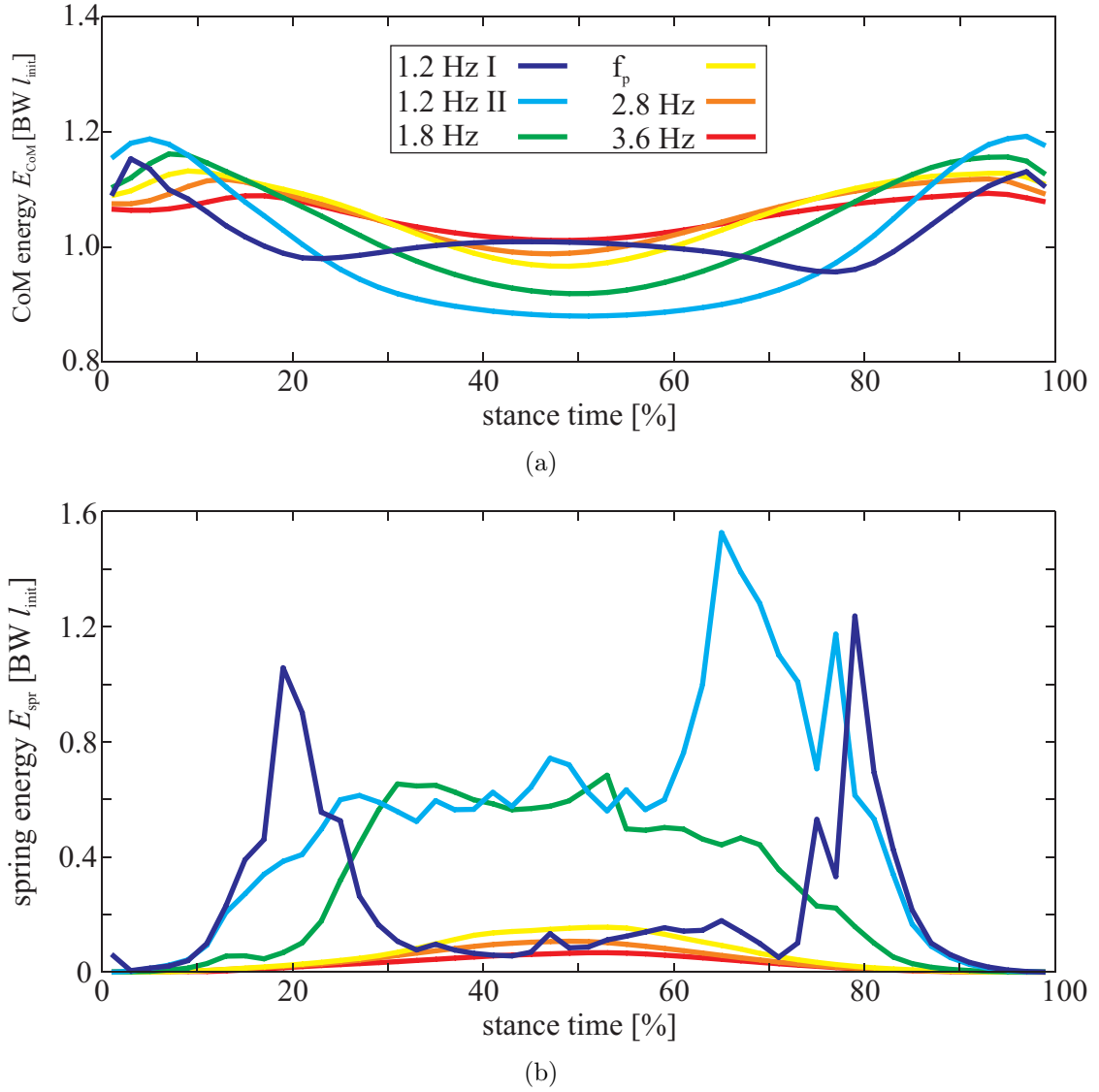


Figure 4.6.: Energy contributions over stance time. (a) CoM energy $E_{\text{CoM}} = E_{\text{kin}} + E_{\text{pot}}$ and (b) spring energy $E_{\text{spr}} = \frac{1}{2}K(\Delta L)^2$ are shown. Energies are normalized to $E_0 = mgl_{\text{init}}$. Results calculated from means over all trials of all subjects at a given frequency (at 1.2 Hz there are two distinct subsets consisting of half the subjects each).

level. Amazingly though, the bell-shaped stiffness profiles, found here for the better part of the investigated hopping frequencies, Figure 4.4(a), correspond directly to the results of Rapoport (2003) on joint level. Using a segmented sagittal-plane

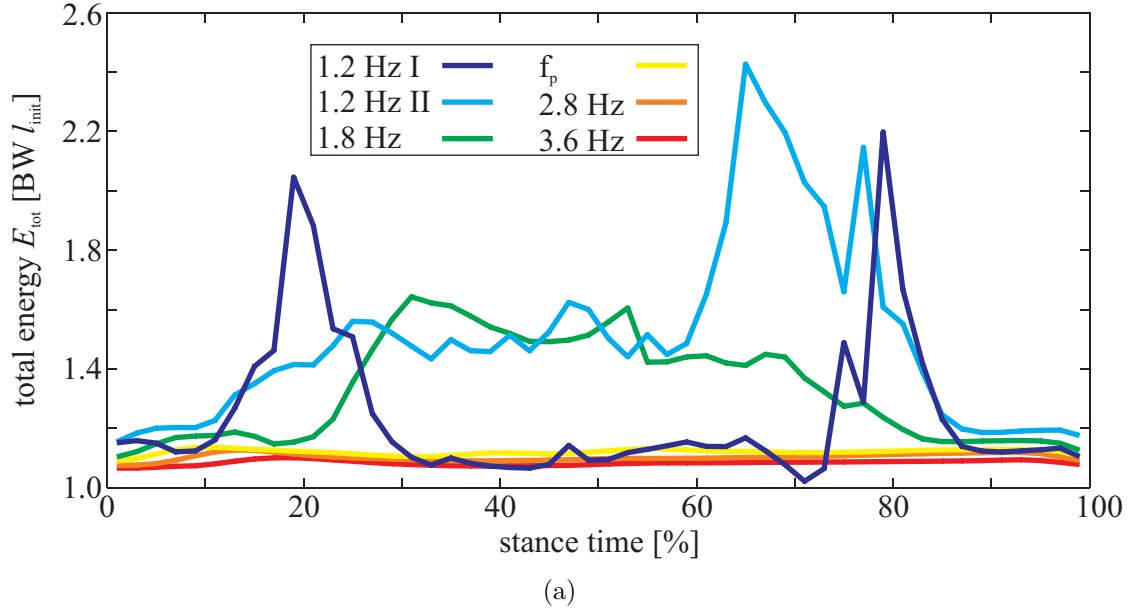


Figure 4.7.: Total energy $E_{\text{tot}} = E_{\text{CoM}} + E_{\text{spr}}$ over stance time. Energy is normalized to $E_0 = mgl_{\text{init}}$. Results calculated from means over all trials of all subjects at a given frequency (at 1.2 Hz there are two distinct subsets consisting of half the subjects each).

hopping model Rapoport (2003) found that joint stiffness increases with angular deflection, resulting in bell-shaped stiffness profiles over stance time.

4.4. Non-linear Parameters vs. Linear Dynamics

There is overwhelming evidence that human legs behave like linear springs during bouncy gaits, e.g. Farley (1991); Kim and Park (2011). Even in the presence of severe perturbations, such as compliant surfaces (Moritz and Farley, 2005) or an elastic exoskeleton (Ferris, 2006; Grabowski and Herr, 2009), humans maintain spring-like center-of-mass dynamics. As spring-mass systems have been proven to possess self-stabilizing properties, e.g. Seyfarth et al. (2002), it has been suggested, that emulating linear spring-mass dynamics may ease control and thus “may be a primary neuromuscular control strategy during bouncing gait” (Grabowski and Herr, 2009).

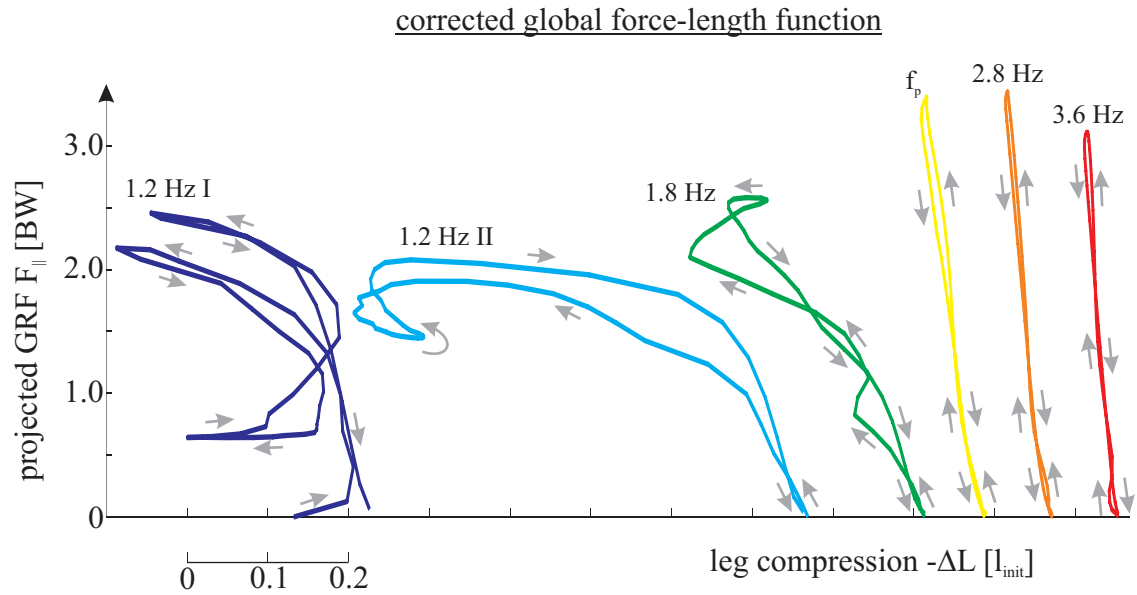


Figure 4.8.: Corrected global force-length function, using leg compression ΔL instead of leg length L . Results are means over all trials of all subjects at a given frequency (at 1.2 Hz there are two distinct subsets consisting of half the subjects each).

However, in Ferris (2006) and Bobbert and Casius (2011) it was stressed that spring-like behavior should not be confused with actual mechanical springs.

The results presented here support this argument. Even though the global force-length function, i.e. the relationship between ground-reaction force and momentary leg length, is (in good approximation) linear for hopping frequencies down to 1.8 Hz, Figure 4.3, neither stiffness nor rest length are constant. However, the actual variation of rest length and stiffness is masked by the interaction of both parameter profiles. Rest length and stiffness vary in such a way that in the resulting ground-reaction forces and center-of-mass trajectories the non-linearities compensate each other. This also holds if the corrected force-length function is used, the only major difference being that linear force-length functions now are only found for frequencies ranging from f_p to 3.6 Hz, see Figure 4.8.

The non-linearity of the stiffness profile also is in qualitative agreement with

findings of Karssen and Wisse (2011). There, the effect of non-linear leg springs on disturbance rejection during running was investigated using optimization techniques. It was shown that the optimal stiffness profile is highly non-linear, with considerably better disturbance rejection than the optimal linear stiffness (up to a factor of seven). However, the predicted force-length function resulting from the optimal stiffness profile for running becomes non-linear beyond a certain leg compression.

4.5. Frequency-dependent Control

At hopping frequencies of f_p and above, stiffness and rest length exhibit a similar qualitative behavior. Stiffness and rest-length profiles are smooth, even for rapid movements (up to 3.6 Hz). This uniform parameter variation across different hopping frequencies may be due to reflexes, i.e. zero-time-delay control based on mechanical properties of the system (Brown and Loeb, 1997; Haeufle et al., 2010). The fact that variability between trials decreases for higher frequencies further supports this reasoning. The parameter profiles themselves are bell-shaped, what might reflect the bell-shaped stiffness profiles found on joint level in Rapoport (2003). The impact-like peaks at 2.8 and 3.6 Hz may be due to pre-activation of the muscles prior to touchdown (Seyfarth et al., 2000).

At 1.2 Hz however, stiffness and rest-length profiles are quite rugged, Figure 4.4, implying active neural control. Two distinct control schemes can be observed at this frequency. While for “1.2 Hz II” control is mainly reflected by rest-length variation, for “1.2 Hz I” stiffness and rest length oscillate phase-shiftedly, with a dramatic stiffness increase in preparation of takeoff. In accordance with Farley (1991), this suggests an active push-off to compensate for energy dissipated in the first half of contact. Similar actuation schemes with stiffness increases during the second half of contact were proposed in e.g. Koditschek and Buehler (1991); Kalveram et al. (2010).

Hopping with 1.8 Hz shows a transitory behavior between slow and fast hopping. Recent findings of Kim and Park (2011) support the statement that humans employ different control strategies to stabilize bouncy gaits, and that the chosen strategy depends on the rate of movement. Surprisingly, the results presented here resemble a gait transition from walking to running, Figure 4.2, even though there is no locomotion. For the “1.2 Hz II” data set even hybrid gaits with running-like center-of-mass trajectories and walking-like ground-reaction forces were observed.

In accordance with Bobbert and Casius (2011); Hobara et al. (2011), linear spring-like behavior was found for hopping with a smaller frequency than f_p , Figure 4.3, contradicting findings of Farley (1991). However, this is only true if the global force-length function is based on momentary leg length. Though, this approach implicitly assumes a constant rest length of the leg and may limit the interpretation of leg-spring behavior, as substantial changes in rest length (up to $0.4L_{TD}$ for “1.2 Hz II”) were found here. Changes in rest length were not taken into account by the aforementioned studies. However, doing so significantly changes the patterns of the FLF on leg level during hopping, Figures 4.3 and 4.8, and facilitates interpretation of leg function and control.

5. Conclusion and Outlook

5.1. Conclusion

Adjustable spring systems are widely developed and used in engineering, e.g. Van Ham et al. (2007); Wolf and Hirzinger (2008); Jun and Clark (2009); Galloway (2009). In order to apply these systems, clear guidelines how to tune system stability are required. This thesis presents a theoretical framework for applying variable leg stiffness in locomotion, the variable-leg-spring (VLS) concept. A clear relationship between rest-length and leg-stiffness variation is required for stable hopping (rest-length increase, leg-stiffness decrease). Nevertheless, different individual leg adjustments for a given stability level may be selected. Thus, additional goals and constraints (e.g. robustness, energy efficiency, range of ground-reaction force, range of leg compression) can be taken into account. However, practical considerations for implementation in engineered systems need to be integrated into these concepts.

The key feature of the VLS control scheme is functional damping via leg softening during contact. Additional viscous damping improves stability and eases control, but is less energy-efficient than functional damping. Such control resembling the VLS concept may be encoded in biological musculo-skeletal systems via neural programs, e.g. the λ -model describing actuation of the ankle joint (Micheau et al., 2003). Experimental data suggest that the visco-elasticity of bouncy gaits is not fully described by a parallel arrangement of linear elasticity and additional velocity-dependent damping: For instance, velocity-dependent damping predicts non-zero

ground-reaction forces at the instant of touch-down. These are not observed in human hopping, e.g. Kuitunen et al. (2011). Secondly, takeoff would take place while the leg is still compressed. Functional damping as investigated here avoids these discrepancies with respect to experimental data.

Muscle-like properties improve hopping stability and robustness at cost of efficiency. Neural control enables the muscle to behave more spring-like. The level of stability and energy efficiency can be tuned on demand, with completely elastic behavior as one extreme (perfect efficiency, neutral hopping stability).

Combining stance-leg control, as described by the VLS concept, and swing-leg control of Blum et al. (2010), provides additional advantages.

During human hopping, leg-spring parameters, i.e. leg stiffness and rest length, evolve in a non-linear way during stance, even though center-of-mass dynamics resemble that of a linear spring-mass system. Non-linearity of the leg-spring parameters was no prerequisite, but a result of data analysis. Furthermore, leg-stiffness and rest-length profiles differ distinctively for slow and fast hopping, implying that control may depend on the rate of movement.

5.2. Future Work

In order to translate leg protocols proposed in this thesis to an engineered system, a number of important considerations have to be made. For example, stable, robust and efficient hopping can be achieved by appropriate parameter strategies. However, the differences resulting from linear-in-time and velocity dependent leg stiffness suggest that these properties may be influenced by the used actuation protocol, which relies on continuous parameter variations throughout the whole contact. Variation of spring parameters only during part of ground contact may allow for more beneficial combinations of gait stability, robustness and energy efficiency, but was not addressed here. Alternative protocols have been proposed, e.g. actuation at the in-

stant of maximum leg compression (Raibert, 1986), actuation starting before and ending after the instant of maximum leg compression (“actuator phasing”; Cham and Cutkosky 2003), or actuation between maximum leg compression and takeoff (Kalveram et al., 2010). The question remains open which time window is most beneficial to achieve stable and robust locomotion. The insights on the variability of leg properties in human hopping presented here may serve as a stepping stone in answering this question.

Vertical hopping may be interpreted as running with vanishing horizontal velocity, $v_{\text{hor}} \equiv 0$, and thus as a subset of running gaits. Hence, the VLS concept can be generalized to include non-zero horizontal velocity, i.e. running gaits, in a natural way. From there, also double support of the point mass with two legs, like in walking, may be included.

Variable leg properties during stance can also be caused by leg segmentation (Rummel and Seyfarth, 2008). Therefore, a more detailed analysis on how changed joint stiffness affects leg stiffness and thus orbital stability during locomotion would be of interest. Together with leg segmentation, the effects of leg segment masses could be investigated. This would allow to investigate impacts which have been neglected in this thesis.

Following the approach of interpreting natural gait variability not as perturbations, but rather incorporating it as a fundamental property into biomechanical models, it is straight-forward to combine the VLS concept with left-right asymmetries of the locomotory system (Merker et al., 2011). Especially understanding and dealing with the energetic requirements induced by asymmetric legs is of great importance for the development of artificial legged systems.

For cyclic locomotion, stance-leg control can naturally be complemented by a matching swing-leg control (Blum et al., 2010). The results presented in Section 3.2.2 suggest benefits with respect to the control effort. With combinations of stance- and swing-leg control, more general and realistic control schemes based on the VLS

concept may be derived, generating gait patterns that are stable against kinematic as well as energetic perturbations.

Finally, the VLS concept may serve as a tool to guide the development of artificial muscles as a composition of mechanical structures which can be tuned by control schemes (Haeufle et al., 2012). In return, muscle models may help to answer the question how variable stiffness can be understood in terms of muscle-like properties. Thus, it is important to compare these different approaches in more detail. For instance, here a hybrid strategy was used to calculate activation states in the template muscle-model of Haeufle et al. (2010) corresponding to hopping trajectories predicted by the VLS model. In a next step, these activation patterns have to be reapplied to the template muscle-model in order to check if they actually generate stable hopping. Following this approach, it may be possible to construct building blocks which could be combined to more complex systems, e.g. with multiple joints or biarticular coupling, capable of accomplishing a multitude of complex tasks, e.g. bouncing, balancing, kicking and so on.

Bibliography

- R. McN. Alexander. Elastic energy stores in running vertebrates. *American Zoologist*, 24(1):85–94, 1984.
- R. Blickhan. The spring-mass model for running and hopping. *Journal of Biomechanics*, 22(11-12):1217–1227, 1989. DOI:10.1016/0021-9290(89)90224-8.
- R. Blickhan and R. J. Full. Similarity in multilegged locomotion: Bouncing like a monopode. *Journal of Comparative Physiology A: Neuroethology, Sensory, Neural, and Behavioral Physiology*, 173:509–517, 1993.
- R. Blickhan, H. Wagner, and A. Seyfarth. Brain or muscles? *Recent Research Developments in Biomechanics*, 1:215–245, 2003.
- Y. Blum, . W. Lipfert, J. Rummel, and A. Seyfarth. Swing leg control in human running. *Bioinspiration & Biomimetics*, 5(2):026006 (11pp), 2010. DOI:10.1088/1748-3182/5/2/026006.
- M. F. Bobbert and L. J. R. Casius. Spring-like leg behaviour, musculoskeletal mechanics and control in maximum and submaximum height human hopping. *Philosophical Transactions of the Royal Society B: Biological Sciences*, 366(1570):1516–1529, 2011.
- I.E. Loeb Brown and G.E. Loeb. *Biomechanics and Neural Control of Posture and Movement*, chapter: A reductionist approach to creating and using neuromusculoskeletal models. Springer, 1997.

- G. A. Cavagna. The landing–take-off asymmetry in human running. *Journal of Experimental Biology*, 209(20):4051–4060, 2006. 10.1242/jeb.02344.
- G. A. Cavagna and M. A. Legramandi. The bounce of the body in hopping, running and trotting: different machines with the same motor. *Proceedings of the Royal Society B: Biological Sciences*, 276(1677):4279–4285, 2009. 10.1098/rspb.2009.1317.
- J. G. Cham, S. A. Bailey, and M. R. Cutkosky. Robust dynamic locomotion through feedforward-preflex interaction. In *ASME IMECE Proceedings*, pages 5–10, 2000.
- J. G. Cham and M. R. Cutkosky. Adapting work through actuator phasing in running. In *International Symposium on Adaptive Motion of Animals and Machines (AMAM)*, (8pp), 2003.
- S. H. Collins, A. Ruina, R. L. Tedrake, and M. Wisse. Efficient bipedal robots based on passive-dynamic walking. *Science*, 307(5712):1082–1085, 2005.
- M. A. Daley, A. Voloshina, and A. A. Biewener. The role of intrinsic muscle mechanics in the neuromuscular control of stable running in the guinea fowl. *Journal of Physiology*, 587(11):2693–2707, 2009.
- W. Dempster. *WADC Technical Report 55159 (WADC-55-159, AD-087-892)*, chapter Space requirements of the seated operator, pages 55–159. 1955.
- J. B. Dingwell, H.G. Kang, and L. C. Marin. The effects of sensory loss and walking speed on the orbital dynamic stability of human walking. *Journal of Biomechanics*, 40(8):1723–1730, 2007.
- C. T. Farley, R. Blickhan, J. Saito, and C. R. Taylor. Hopping frequency in humans: a test of how springs set stride frequency in bouncing gaits. *Journal of Applied Physiology*, 71(6):2127–2132, 1991.

- D. P. Ferris, Z. A. Bohra, J. R. Lukos, and C. R. Kinnaird. Neuromechanical adaptation to hopping with an elastic ankle-foot orthosis. *Journal of Applied Physiology*, 100(1):163–170, January 2006.
- R. J. Full and D. E. Koditschek. Templates and anchors: neuromechanical hypotheses of legged locomotion on land. *Journal of Experimental Biology*, 202(23):3325–3332, 1999.
- K. C. Galloway, J. E. Clark, and D. E. Koditschek. Design of a tunable composite leg for dynamic locomotion. In *ASME 2009 International Design Engineering Technical Conferences & Computers and Information in Engineering Conference (IDETC/CIE)*, (8pp), 2009.
- H. Geyer, A. Seyfarth, and R. Blickhan. Positive force feedback in bouncing gaits? *Proceedings of the Royal Society of London. Series B: Biological Sciences*, 270(1529):2173–2183, 2003.
- H. Geyer, A. Seyfarth, and R. Blickhan. Compliant leg behaviour explains basic dynamics of walking and running. *Proceedings of the Royal Society B: Biological Sciences*, 273(1603):2861–2867, 2006.
- A. M. Grabowski and H. M. Herr. Leg exoskeleton reduces the metabolic cost of human hopping. *Journal of Applied Physiology*, 107(3):670–678, September 2009.
- S. Grimmer, M. Ernst, M. Guenther, and R. Blickhan. Running on uneven ground: leg adjustment to vertical steps and self-stability. *Journal of Experimental Biology*, 211(18):2989–3000, 2008. 10.1242/jeb.014357.
- M. Guenther and R. Blickhan. Joint stiffness of the ankle and the knee in running. *Journal of Biomechanics*, 35(11):1459 – 1474, 2002.
- D. F. B. Haeufle, S. Grimmer, and A. Seyfarth. The role of intrinsic muscle properties for stable hopping - stability is achieved by the force-velocity relation.

- Bioinspiration & Biomimetics*, 5(1):016004 (11pp), 2010. doi: 10.1088/1748-3182/5/1/016004 1748-3190
- D. F. B. Haeufle, M. Günther, R. Blickhan, and S. Schmitt. Can Quick Release Experiments Reveal the Muscle Structure? A Bionic Approach. *Journal of Bionic Engineering*, 9(2):211—223, 2012. doi: 10.1016/S1672-6529(11)60115-7
- A. V. Hill. The heat of shortening and the dynamic constants of muscle. *Proceedings of the Royal Society of London. Series B - Biological Sciences*, 126(843):136–195, 1938.
- H. Hobarra, K. Inoue, K. Omuro, T. Muraoka, and K. Kanosue. Determinant of leg stiffness during hopping is frequency-dependent. *European Journal of Applied Physiology*, 111:2195–2201, 2011.
- P. Holmes, D. Koditschek, and J. Guckenheimer. The dynamics of legged locomotion: Models, analyses, and challenges. *Dynamics*, 48(2):207–304, 2006.
- J. W. Hurst, J. E. Chestnutt, and A. A. Rizzi. An actuator with physically variable stiffness for highly dynamic legged locomotion. In *Proceedings of the IEEE International Conference on Robotics and Automation*, volume 5, pages 4662–4667, New Orleans, Louisiana, 2004.
- J. Y. Jun and J. E. Clark. Dynamic stability of variable stiffness running. In *IEEE International Conference on Robotics and Automation (ICRA) 2009*, pages 1756–1761, 2009.
- K. T. Kalveram, D. F. B. Haeufle, S. Grimmer, and A. Seyfarth. Energy management that generates hopping. comparison of virtual, robotic and human bouncing. In *Simulation, Modelling and Programming for Autonomous Robots (SIMPAN) 2010 (Darmstadt, Germany)*, pages 147–156, 2010.

- J. G. D. Karszen and M. Wisse. Running with improved disturbance rejection by using non-linear leg springs. *The International Journal of Robotics Research*, 30(13):1585–1595, 2011.
- S. Kim and S. Park. Leg stiffness increases with speed to modulate gait frequency and propulsion energy. *Journal of Biomechanics*, 44(7):1253 – 1258, 2011.
- D. E. Koditschek and M. Buehler. Analysis of a simplified hopping robot. *The International Journal of Robotics Research*, 10(6):587–605, 1991.
- H. Komsuoglu. *Toward a Formal Framework for Open-Loop Stabilization of Rhythmic Tasks*. PhD thesis, Ann Arbor: University of Michigan, 2004.
- S. Kuitunen, K. Ogiso, and P. V. Komi. Leg and joint stiffness in human hopping. *Scandinavian Journal of Medicine & Science in Sports*, 21(6):e159–e167, 2011.
- S. W. Lipfert. *Kinematic and dynamic similarities between walking and running*. Verlag Dr. Kovac, Hamburg, 2010. ISBN:978-3-8300-5030-8.
- P. Malcolm. *Influence of intrinsic and extrinsic determinants on the transition from walking to running*. PhD thesis, Ghent University, 2010.
- H. M. Maus, S. W. Lipfert, M. Gross, J. Rummel, and A. Seyfarth. Upright human gait did not provide a major mechanical challenge for our ancestors. *Nature Communication*, 1(70), 2010.
- D. Maykranz, S. Grimmer, S. Lipfert, and A. Seyfarth. Foot function in spring mass running. In Rüdiger Dillmann, Jürgen Beyerer, Christoph Stiller, J. Marius Zöllner, and Tobias Gindele, editors, *Autonome Mobile Systeme 2009*, Informatik aktuell, pages 81–88. Springer Berlin Heidelberg, 2009.
- T. A. McMahon and G. C. Cheng. The mechanics of running: How does stiffness couple with speed? *Journal of Biomechanics*, 23, Supplement 1(0):65 – 78, 1990.

- A. Merker, J. Rummel, and A. Seyfarth. Stable walking with asymmetric legs. *Bioinspiration & Biomimetics*, 6(4):045004, 2011.
- P. Micheau, A. Kron, and P. Bourassa. Evaluation of the lambda model for human postural control during ankle strategy. *Biological Cybernetics*, 89(3):227–236, 2003.
- A. E. Minetti and R. McN. Alexander. A theory of metabolic costs of bipedal gaits. *Journal of Theoretical Biology*, 186(4):467–476, 1997.
- C. T. Moritz and C. T. Farley. Human hopping on very soft elastic surfaces: implications for muscle pre-stretch and elastic energy storage in locomotion. *Journal of Experimental Biology*, 208(5):939–949, 2005.
- S. Peter, S. Grimmer, S. W. Lipfert, and A. Seyfarth. Variable joint elasticities in running. In *Autonome Mobile Systeme 2009*, pages 129–136, Karlsruhe, Germany, Dec 3-4 2009. Springer.
- I. Poulakakis, J. A. Smith, and M. Buehler. Modeling and experiments of untethered quadrupedal running with a bounding gait: The Scout II robot. *The International Journal of Robotics Research*, 24(4):239–256, 2005.
- M. H. Raibert. *Legged robots that balance*. MIT Press, Cambridge, Massachusetts, 1986.
- S. Rapoport, J. Mizrahi, E. Kimmel, O. Verbitsky, and E. Isakov. Constant and variable stiffness and damping of the leg joints in human hopping. *Journal of Biomechanical Engineering*, 125(4):507–514, 2003.
- S. Riese and A. Seyfarth. Stance leg control: variation of leg parameters supports stable hopping. *Bioinspiration & Biomimetics*, 7(1):016006, 2012.

-
- S. Riese and A. Seyfarth. Robustness and efficiency of a variable-leg-spring hopper. In *The Fourth IEEE RAS/EMBS International Conference on Biomedical Robotics and Biomechatronics Roma, Italy. June 24-27, 2012*, 2012.
- S. Riese, A. Seyfarth, and S. Grimmer. Linear center-of-mass dynamics emerge from non-linear leg-spring properties in human hopping. *Journal of Biomechanics*, (submitted), 2012.
- L. A. Rozendaal and A. J. “Knoek” van Soest. Stabilization of a multi-segment model of bipedal standing by local joint control overestimates the required ankle stiffness. *Gait & Posture*, 28(3):525 – 527, 2008.
- A. Ruina, J. E. A. Bertram, and M. Srinivasan. A collisional model of the energetic cost of support work qualitatively explains leg sequencing in walking and galloping, pseudo-elastic leg behavior in running and the walk-to-run transition. *Journal of Theoretical Biology*, 237(2):170–192, 2005. DOI:10.1016/j.jtbi.2005.04.004.
- J. Rummel, Y. Blum, and A. Seyfarth. Robust and efficient walking with spring-like legs. *Bioinspiration & Biomimetics*, 5(4):046004 (13pp), 2010.
- J. Rummel and A. Seyfarth. Stable running with segmented legs. *The International Journal of Robotics Research*, 27(8):919–934, 2008.
- J. Schmitt and J. Clark. Modeling posture-dependent leg actuation in sagittal plane locomotion. *Bioinspiration & Biomimetics*, 4(4):046005, 2009. 1748-3182.
- J. Schuy, P. Beckerle, J. Wojtusich, S. Rinderknecht, and O. von Stryk. Conception and evaluation of a novel variable torsion stiffness for biomechanical applications. In *The Fourth IEEE RAS/EMBS International Conference on Biomedical Robotics and Biomechatronics Roma, Italy. June 24-27, 2012*, 2012.

- A. Seyfarth, R. Blickhan, and J. L. Van Leeuwen. Optimum take-off techniques and muscle design for long jump. *Journal of Experimental Biology*, 203(4):741–750, 2000.
- A. Seyfarth, H. Geyer, M. Guenther, and R. Blickhan. A movement criterion for running. *Journal of Biomechanics*, 35(5):649 – 655, 2002.
- M. Srinivasan and A. Ruina. Computer optimization of a minimal biped model discovers walking and running. *Nature*, 439(7072):72–75, 2006.
- S. H. Strogatz. *Nonlinear dynamics and chaos: With applications to physics, biology, chemistry, and engineering*. Westview Press, Cambridge, Massachusetts, 1994.
- M. M. van der Krogt, W. W. de Graaf, C. T. Farley, C. T. Moritz, L. J. Richard Casius, and M. F. Bobbert. Robust passive dynamics of the musculoskeletal system compensate for unexpected surface changes during human hopping. *Journal of Applied Physiology*, 107(3):801–808, 2009.
- R. Van Ham, B. Vanderborght, M. Van Damme, B. Verrelst, and D. Lefeber. Mac-cepta, the mechanically adjustable compliance and controllable equilibrium position actuator: Design and implementation in a biped robot. *Robotics and Autonomous Systems*, 55(10):761–768, 2007.
- R. Van Ham, T. G. Sugar, B. Vanderborght, K. W. Hollander, and D. Lefeber. Compliant actuator designs review of actuators with passive adjustable compliance/controllable stiffness for robotic applications. *IEEE Robotics & Automation Magazine*, 16(3):81–94, 2009.
- D. A. Winter. *Biomechanics and Motor Control of Human Movement*. Wiley, 2009.
- S. Wolf and G. Hirzinger. A new variable stiffness design: Matching requirements of the next robot generation. In *IEEE International Conference on Robotics and Automation (ICRA) 2008*, 2008.

Danksagung

Zunächst möchte ich Prof. Dr. Bernd Brüggemann danken, ohne dessen Unterstützung diese Promotion so nicht möglich gewesen wäre.

Ebenso gilt mein Dank Prof. Dr. André Seyfarth für die Möglichkeit, in seiner Arbeitsgruppe zu lernen und zu forschen, für die vielen fachlichen Diskussionen, die daraus resultierende Vertiefung meines Verständnisses der Biomechanik im Allgemeinen und des Federmassemodells im Besonderen und schließlich die Möglichkeit, Konferenzen zu besuchen und mich mit interessanten Menschen auszutauschen. Auch den vielen Mitgliedern des Lauflabors, gegenwärtigen wie ehemaligen, danke ich für ihre Hilfe während der Erstellung dieser Arbeit.

Für weitere nützliche Kommentare und Ratschläge danke ich außerdem meinen Freunden Dr. David Hilditch, Dr. Christian Vitense, Björn Oetzel und Uwe Schinkel.

Sehr wichtig waren auch das Verständnis und die Unterstützung meiner Familie und Freunde während dieser akademisch, wie privat sehr anspruchsvollen Zeit. Alle diese mir sehr teuren Menschen hier zu nennen, würde den Rahmen sprengen; und anstatt einige, in jedem Fall zu wenige Beispiele herauszupicken, möchte ich ihnen allen zusammen danken.

Schließlich danke ich der Deutschen Forschungsgesellschaft (DFG), der Bundesagentur für Arbeit und **jenarbeit** (Jobcenter der Stadt Jena) für die finanzielle Förderung dieser Arbeit.

Ehrenwörtliche Erklärung

Ich erkläre hiermit ehrenwörtlich, dass ich die vorliegende Arbeit selbstständig, ohne die unzulässige Hilfe Dritter und ohne die Benutzung anderer als der angegebenen Hilfsmittel und Literatur angefertigt habe. Die aus anderen Quellen direkt oder indirekt übernommenen Daten und Konzepte sind unter Angabe der Quelle gekennzeichnet. Personen, die an der inhaltlich-materiellen Erstellung der vorliegenden Arbeit beteiligt waren, sind am Anfang des jeweiligen Kapitels erwähnt. Weitere Personen waren nicht beteiligt. Insbesondere habe ich hierfür nicht die entgeltliche Hilfe von Vermittlungs- und bzw. Beratungsdiensten (Promotionsberater oder andere Personen) in Anspruch genommen. Niemand hat von mir unmittelbar oder mittelbar geldwerte Leistungen für Arbeiten erhalten, die im Zusammenhang mit dem Inhalt der vorgelegten Dissertation stehen.

Die Arbeit wurde bisher weder im In- noch im Ausland in gleicher oder ähnlicher Form einer anderen Prüfungsbehörde vorgelegt.

Die geltende Promotionsordnung der Physikalisch-Astronomischen Fakultät ist mir bekannt. Ich versichere ehrenwörtlich, dass ich nach bestem Wissen die reine Wahrheit gesagt und nichts verschwiegen habe.

Jena, den 17. Dezember 2012

Sebastian Riese

Lebenslauf

Name	Sebastian Riese
Geburtsdatum	10.06.1982
Geburtsort	Stralsund
Schulbildung	1989 - 1991 Ferdinand-von-Schill-Schule, Stralsund 1991 - 1993 Fröbel-Grundschule, Stralsund 1993 - 2000 Herder-Gymnasium, Stralsund 2000 - 2002 Hansa-Gymnasium, Stralsund Abitur: „Sehr Gut“ (1,4)
Wehrdienst	01.10.2002 - 30.06.2003 Grundwehrdienst
Hochschulstudium	WS 2003/2004 bis WS 2008/2009 Diplom-Studiengang Physik an der Friedrich-Schiller-Universität Jena Gesamtnote: „Gut“ (1,8) Diplomthema: <i>Bewegung rotierender Körper unter gravitativer Spin-Bahn-Kopplung</i>

Jena, den 17. Dezember 2012

Sebastian Riese